THEORETICAL STUDIES OF IMPURITIES IN MOTT-HUBBARD AND CHARGE-TRANSFER INSULATORS

by

PRASENJIT SEN

DEPARTMENT OF PHYSICS

INDIAN INSTITUTE OF TECHNOLOGY KANPUR

JULY, 1997

THEORETICAL STUDIES OF IMPURITIES IN MOTT-HUBBARD AND CHARGE-TRANSFER INSULATORS

A Thesis Submitted

in Partial Fulfillment of the Requirements

for the Degree of

Doctor of Philosophy

by

PRASENJIT SEN

to the

DEPARTMENT OF PHYSICS

INDIAN INSTITUTE OF TECHNOLOGY KANPUR

JULY 1997

CERTIFICATE

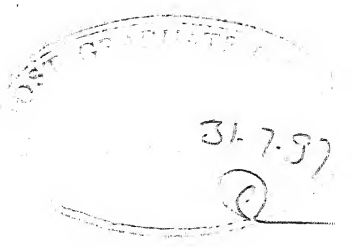

It is certified that the work contained in this thesis entitled "*Theoretical Studie Impurities in Mott-Hubbard and Charge-Transfer Insulators*", by *Prasenjit Sen*, has b carried out under my supervision and that this work has not been submitted elsewhere any degree.

Avinash Singh

Dr. Avinash Singh
Associate Professor
Department of Physics
Indian Institute of Technology
Kanpur

July 1997

To my parents,

for whom all this has been possible.

Acknowledgments

It is a rather difficult task to acknowledge all the help – small and big – that I have received over the years from so many people, which have, in various ways, helped me write this thesis or have made my stay here a memorable one. Yet it is a sacred duty and I should at least make an attempt.

First of all I would like to thank my thesis supervisor Dr. Avinash Singh. But for his able and friendly guidance and constant encouragement it would not have been possible for me to do whatever is there in this volume. I would, at the same time, thank Dr. Vijay Singh and Dr. Y. N. Mahapatra – the two other semester evaluation committee members – for their valuable advice from time to time.

In the department I have had the good luck of interacting with and getting help from so many of my colleagues – senior, contemporary and junior. The weekly graduate students seminar was one occasion where I had the opportunity of having some lively and interesting discussions with them, and, needless to say, was greatly benefited. Special mention must be made of Sayan, Shanti, Sujay, Aloke, Rajan, Bhabani, Abir, Sudhansu, Sanju, George Saurabh, Gaurav, and Tapan Nath and Sandeep Singh.

During five long years of my stay here, there was lot more to life than just academics and here also I had some very good friends and companions who made my days enjoyable. But for their support, it would have been difficult for me to withstand the occasional academic pressure. Although they are no longer in IIT-K, I still remember the help I got from BC or the good time I spent with Dinuda and Co. With a sort of nostalgic feeling I remember

the happy times I spent with the erstwhile C-mid group – Shobhit, Mouli, Shubhankar and specially Asif, who was always a great support. The C-top group also demands some special mention for giving me the opportunity of spending some wonderful moments in their jovial company. Memories of all the good time I spent with Debada, Tapan Khan, Tapo, Deba, Subit, Sumanata, Ani, Aloke and Manoj will remain fresh in my mind forever.

But the most satisfying moments I spent in my IIT-K life was surely in the company of Kishore, Arnab, Srabani, Ali, Sandeep, Anirban and Biswajit. Be it the regular tea-sessions in the evening or the occasional visits to the restaurants in the city, the book-shop in Lucknow, enjoying movies at the *Le Montage* shows – sweet memories of all that will remain permanently etched in my mind. I'll particularly miss the 'intellectually stimulating' discussions, ranging from Beethoven-Freud-Illyas-Ray to the functioning of a cinema projector, that we used to have that opened up new vistas of knowledge and information in front of me and also indirectly provided me with the motivation to continue with my academic work.

The most trying time for me during the whole of my Ph. D. life was the period when I was finally writing this thesis. The long hours in the CC or the sleepless nights that I had to spend demanded a good amount of mental and physical endurance; and I must admit that during all these days my young friends – Kamalesh, Kaushik Basak and Koushik Biswas – were of invaluable support to me. After long hours of hard work I could relax and shed my tension in their youthful company. But for their caring support things would have been much more difficult for me.

There must have been many more people during these five years who have been of help and support to me. It is difficult to recall all of them, but a few names deserve separate mention. I can always recall the good time I spent with Amlan, Senda, Tapasda and Gaurda; the lighter moments I spent with Akhilesh or the support I had from Manish.

Lastly, I must thank my wife, Kakali, for the extreme patience she has shown during the last one and a half years.

Prasenjit Sen

List of Published/Submitted Papers

1. Collective and Single-particle Excitations in a Hubbard Antiferromagnet, P. Sen, and A. Singh, Phys. Rev. B **48**, p-15 792, (1993)[1].
2. Gap states in a Doped Mott-Hubbard Insulator, P. Sen, S. Basu and A. Singh, Pramana, Jl. of Phys. **44**, p-L77, (1995).
3. Gap states, Local moments, and Magnetic dynamics in a Mott-Hubbard Antiferromagnet Doped with Static Impurities, P. Sen, S. Basu and A. Singh, Phys. Rev. B **50**, p-10 381 (Rapid Comm.), (1994).
4. Impurity Scattering of Spin Waves in a doped Mott-Hubbard Antiferromagnet, P. Sen, and A. Singh, Phys. Rev. B **53**, p-328, (1996).
5. Self-consistent Numerical Study of Pure and Impurity-Doped Three-band Hubbard Model, P. Sen, and A. Singh, (Submitted to Pramana, Jl. of Physics).
6. Magnetic Impurities in Antiferromagnets and Superconductors, A. Singh, and P. Sen, (Submitted to Phys. Rev. B).

[1]This paper does not pertain to the topic of this thesis.

Synopsis

From the very early days of high-T_c superconductivity it has been believed that substitutional studies in cuprates can help in understanding superconducting and magnetic properties of these materials [1]. In view of this, a number of experimental studies have been done on these systems doped with impurities – both magnetic, *e.g.* Fe^{+3}, Ni^{+2}, Co^{+3} and nonmagnetic, *e.g.* Zn^{+2}, Al^{+3}, Ga^{+3} – that substitute copper in the copper oxide planes. Some of the most interesting effects of doping these materials is that irrespective of the magnetic nature of the dopant, local moments are formed in the system, T_c is drastically reduced, and nonmagnetic impurities reduce Néel temperature T_N. As the parent compounds of all these materials are antiferromagnets (AF) and the antiferromagnetic correlations persist even in the superconducting phase, formation of local moments in presence of nonmagnetic impurities can be naively understood as due to removal of copper spins from a compensated spin system. But this picture of AF plus spin-hole becomes simplistic in view of the recent NMR measurements by Mahajan *et al.* [2] which suggest that the moment resides mainly on the four copper sites neighbouring the impurity. So a more detailed picture is called for. In this thesis we try to develop a deeper understanding of the formation of moment and to gain insight into other effects of impurity-doping in high-T_c cuprates.

The thesis begins with Chapter 1 giving a general introduction to the high-T_c cuprates and to the particular questions about the impurity-doped systems that we address. This leads us to the problem of nonmagnetic impurities in a Mott-Hubbard AF in Chapter 2. A formalism for Hartree-Fock (HF) mean-field treatment of the Hubbard AF had already been

loped [3]. We study the effects of impurities in this state within a T-matrix analysis. It is d that such impurities give rise to energy-states within the Hubbard gap (defect states). ng amplitude mainly on the four sites neighbouring the impurity. These, if occupied by :rons, give rise to local moments as seen in experiments. Moments are seen to form even ıe superconducting and 'metallic' phases when there is no AF long-range-order (LRO) ıe system (although short-range-order persists). So in Chapter 3 we address the problem nonmagnetic impurity in a small cluster of Hubbard model having short-range-order. find that the existence of the defect state is robust with respect to the range of order in system.

The next question to ask is how these impurities affect the magnetic dynamics in the system and thereby the Néel temperature. Chapter 4 of the thesis deals with impurity- :tering of spin waves in an impurity-doped Hubbard AF. In a two-dimensional (2D) system find a logarithmically diverging correction to the long wavelength magnon energies. In e of an anisotropic (layered) 3D system this divergence is cutoff by the interlayer hopping. use linear spin-wave theory to calculate the reduction in sublattice magnetisation due :hermal excitation of spin waves at finite temperature and find the dependence of T_N on ɔurity concentration, which agrees well with neutron-scattering experiments of Keimer *et* [4].

If a hole is added to the system having an impurity, it will go in the defect state as that is : lowest energy state available for a hole and the moment will be lost. But fluctuations can nsfer some of the spectral weight of the hole from the defect state to the upper Hubbard ıd so that part of the moment can be recovered. In Chapter 5 we study how the local ment is recovered due to thermal and quantum fluctuations.

Few questions still remain unanswered. For example, how the moment survives at low ıperatures in presence of impurities, why do all nonmagnetic impurities, irrespective of :ir electronic structure, produce the same moment and why is this moment less than

what one would expect for an $S = \frac{1}{2}$ spin-hole in an $S = \frac{1}{2}$ AF. We try to answer these by studying the effects of nonmagnetic impurities in a charge-transfer insulator(CTI). Chapter 6 of the thesis contains the results of our self-consistent numerical HF calculations on pure and impurity-doped CTI described by a three-band Hubbard model. In absence of direct oxygen-oxygen hopping (t_{pp}), the system shows nesting property and goes into an AF state for any non-zero positive Coulomb repulsion on the copper sites (U_d). The nesting, however, is lost in presence of a finite t_{pp} and the system becomes AF only above a certain critical value of U_d, which increases with t_{pp}. The transverse spin excitations in the system have a gapless Goldstone mode. Each nonmagnetic impurity in a CTI produces two defect states. The upper defect state remains occupied by electrons even in presence of finite concentration of mobile holes and the local moment is robust. Density of the occupied defect state on the copper sites is less than 1 and this density decreases for a larger copper-oxygen hopping. This clearly shows that part of the local moment escapes to the oxygen sites because of Cu3d–O2p hybridisation. The local magnitude of the local moment is also found to be quite insensitive to the impurity potential V suggesting that the observed moment is independent of the detailed nature of the impurity.

In Chapter 7 we develop a formalism to treat magnetic impurities in a Mott-Hubbard AF describing 3d electrons in the copper-oxide planes of high-T_c superconductors. In the case the impurity spin (S') equal to the host spin (S), represented via modification in the local hopping strength around the impurity, we get a momentum independent non-diverging renormalisation of the magnon energies. In the long wavelength limit, our result agrees with that of Wan *et al.* [5] on a Heisenberg AF. We also present our study – using exact eigenstates method – on the effects of magnetic impurities on magnon wave functions and density of states. When $S' \neq S$, we develop a representation of such impurities in terms of multiple orbitals on the impurity site and examine their effects on the magnon spectrum via a scaling study.

Contents

List of Figures

Chapter 1

Introduction

The revolutionising discovery of high-temperature superconductivity in cuprates by Bednorz and Müller [6] generated tremendous amount of interest and enthusiasm, and attracted the attention of physicists and material scientists from all over the world. So powerful was the wave that the first few years of high-T_c superconductivity saw tens of thousands of publications on the subject. But the period of initial euphoria is over and the task of understanding these materials is proving to be more and more difficult and challenging. Ten years after Bednorz and Müller's discovery, it seems that although some of the basic properties of these compounds have been unambiguously ascertained, there is till some time before the mechanism of superconductivity is understood properly.

One of the many techniques used to study high-T_c cuprates is substitution of Cu in the CuO_2 planes of these materials by different impurities like Fe, Ni, Co, Zn, Al, Ga *etc.* Even nonmagnetic impurities like Zn^{+2}, Al^{+3}, Ga^{+3} induce local moments in these systems. They also have drastic effects on superconducting transition temperature (T_c) and reduce Néel temperature (T_N) of these materials. Some theoretical studies have been done to understand the magnetic effects of these impurities. For example, Wan *et al.* have done a detailed study on the effects of impurities on the magnetic dynamics in a Heisenberg antiferromagnet (AF). But to our knowledge, no attempt has been made to understand the formation of

l moments because of nonmagnetic impurities in the CuO_2 planes, how they affect T_N why all nonmagnetic impurities, irrespective of their electronic structure, give the same nent. In this thesis we address these key questions and other related problems involving urity-doping in high-T_c cuprates within an electronic model such as a one-band or a ee-band Hubbard model wherein electronic and magnetic properties can be examined on equal footing.

Before we go on to discuss our work, we give a brief introduction to the class of materials are interested in, some of their basic properties and the particular questions we are dressing.

.1 Structure

The first high-T_c cuprate compound discovered by Bednorz and Müller, $La_{2-x}Ba_xCuO_4$, s the quasi two dimensional (2D) structure of K_2NiF_4 (Figure 1.1). It has a series of CuO_2 anes with charge reservoirs in between (LaO layers in this case). The parent compound a_2CuO_4 and also other derivatives, such as $La_{2-x}Sr_xCuO_4$, possess this structure with elon- ted Cu-O octahedra. The Cu-O distance is rather short, ~ 1.9Å. La_2CuO_4 is orthorhombic room temperature and becomes tetragonal at $\sim$ 500K. The temperature at which this ructural phase transition from an orthorhombic to a tetragonal phase occurs depends on ie doping concentration x in $La_{2-x}M_xCuO_4$ (M=Sr, Ba) [7].

The superconducting Y-Ba-Cu-O also has a series of CuO_2 sheets in the 'ab' plane (as is usually referred to in literature). There are two sheets per unit cell, ~ 3.2Åapart. These vo planes are 8.2Åapart from the next two planes. In addition it has Cu-O chains along ie b-axis. The orthorhombic lattice parameters of $YBa_2Cu_3O_{6+\delta}$ (1-2-3) vary with oxygen ontent and when $\delta \sim 0.6$Å, the structure becomes tetragonal. In $YBa_2Cu_3O_6$ ($\delta = 0.0$) iere are no chain oxygens and Cu in the chains are in the +1 state. Structural studies uggest that oxygen vacancies may be ordered when $\delta = 0.5$ and $\delta = 0.25$. In $\delta = 0.5$

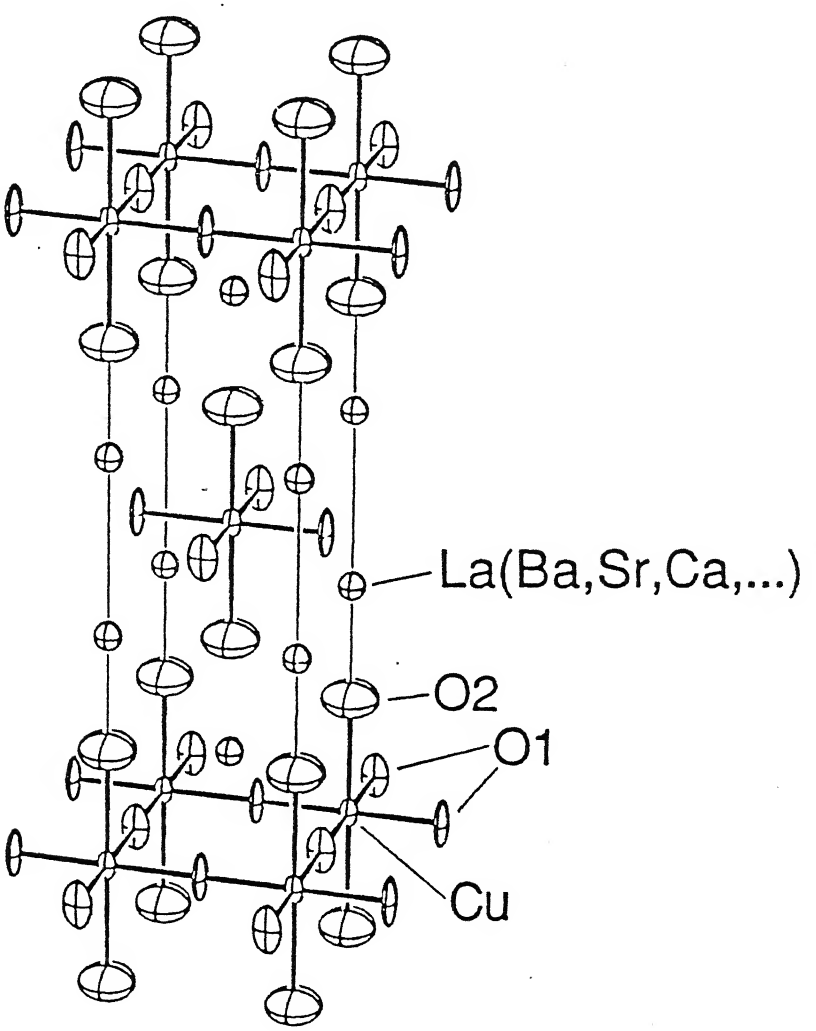

Figure 1.1: The structure of $La_{2-x}A_xCuO_4$, where A=Ba, Sr, Ca, ... Figure taken from Reference 7.

position, fully oxygenated CuO chains are present along the b-axis alternately with fully ɜen deficient chains. Because of orthorhombic structure these compounds show extensive ıning. Across the twin boundary there is a 90^0 rotation of the a- and b-axes.

All the Bi- and Tl- based high-T_c compounds discovered later possess CuO_2 planes as an ɜntial structural unit. These CuO_2 planes dominate the high-T_c material from magnetic l electrical points of view and also, to a large extent, from the structural point of view. It enerally accepted that superconductivity in these materials occur in the CuO_2 planes and ood understanding of the CuO_2 planes is required for an explanation of superconductivity these materials. Since the in-plane and out-of-plane structure, Cu-O distance *etc.* are ıstically different, one can expect these materials to be anisotropic. In fact, the ab plane d c-axis (perpendicular to the ab plane) properties in the compound are, in some cases, alitatively different (see discussions below).

.2 Phase diagram

The parent compounds of the cuprates are 'doped' which ultimately leads to metallic haviour and superconductivity. Doping is achieved either by heterovalent substitution as $La_{2-x}Sr_xCuO_4$, in $Nd_{2-x}Ce_xCuO_4$ and in $Bi_2Sr_2Ca_{1-x}Y_xCu_2O_8$ or by a variation of the tal oxygen content as in $YBa_2Cu_3O_{6+\delta}$. Doping introduces additional charge carriers into e CuO_2 planes [8]. In $La_{2-x}Sr_xCuO_4$ the formal valency of strontium is +2. To maintain ıarge neutrality in this case, the in-plane oxygen atoms change from an $O2p^6$ to an $O2p^5$ ate leaving additional holes in the planes. In $Nd_{2-x}Ce_xCuO_4$ the neodymium Nd^{+3} state replaced by a cerium Ce^{+4} yielding an electron which enters the planes. The sign of ıe measured Hall coefficient supports the picture of hole carriers in $La_{2-x}Sr_xCuO_4$ and of ectron carriers in $Nd_{2-x}Ce_xCuO_4$ [9].

In $YBa_2Cu_3O_{6+\delta}$ doping amounts to the addition of oxygen atoms in between the out-of-lane Cu atoms. This leads to the formation of Cu-O chains. It is believed that these oxygen

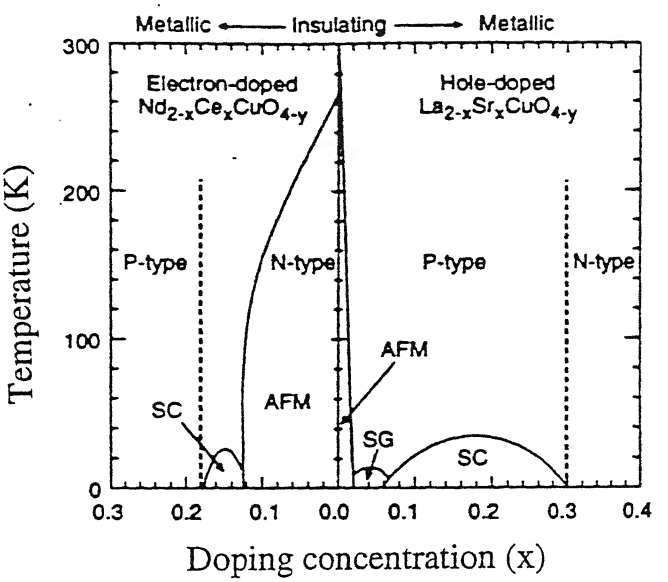

Figure 1.2: Temperature vs. doping concentration phase diagram for $YBa_2Cu_3O_{7-\delta}$ (left panel) and of $La_{2-x}Sr_xCuO_4$ combined with $Nd_{2-x}Ce_xCuO_4$ (right panel). Figure taken from Reference 46.

atoms form O^{-2} states by absorbing electron from the rest of the material and, to a certain extent, from out of the CuO_2 planes. This process is controversial. If true, it introduces the possibility of hole type carriers in the CuO_2 planes and it is certainly responsible for the non-linear relation between the dopant concentration and the in-plane carrier density in $YBa_2Cu_3O_{6+\delta}$ [10].

In Figure 1.2 we have shown the phase diagrams of $La_{2-x}Sr_xCuO_4$, $Nd_{2-x}Ce_xCuO_4$ and of $YBa_2Cu_3O_{6+\delta}$ in the temperature (T) vs. doping concentration (x) plane. Depending on T and x the cuprate superconductors can be varied continuously between an antiferromagnetic insulator, a spin-glass phase, a high-temperature superconductor and a 'normal' metal. In $La_{2-x}Sr_xCuO_4$, for example, upon doping, antiferromagnetism vanishes rather rapidly ($\sim 2\%$ of hole). It becomes superconducting at about $\sim 6\%$ of hole doping. In the intermediate-

ing range, it shows a spin-glass behaviour. Above T_c it behaves like a 'strongly correlated al'. Upon further doping more standard metallic behaviour shows up [10].

3 Properties of high-T_c cuprates

3.1 Superconducting properties

These copper-oxide superconductors share all the basic properties of ordinary superıductors like Meissner effect, zero resistance and pairing of quasiparticles with charge 2e. iring is seen in Shapiro steps displayed by Josephson tunnel junctions biased with both and dc voltages. These steps have voltage spacing $h\nu/2e$ which is expected if quasipartis of charge e are bound into pairs [11, 12, 13]. Also, the flux-quantum has been directly ıasured and is $hc/2e$, indicating pairing [14, 15]. Moreover Andreev scattering experiment /eals pairing of particles with opposite momenta. Also, Josephson tunneling has been served to occur between a Pb-Sn alloy and $YBa_2Cu_3O_{6+\delta}$ [16]. Such an effect is thought be impossible between a singlet-paired and a triplet-paired superconductor [17]. Since, a)-Sn alloy is singlet-paired, $YBa_2Cu_3O_{6+\delta}$ is also thought to be singlet-paired.

In measurements of electron tunneling and electromagnetic absorption, an energy gap s been observed in the distribution of the energy levels available to the system, and it of the same order of magnitude at temperatures $T \ll T_c$ as that predicted by the BCS eory. The observed values initially extended over a range from about 2 to $14k_BT_c$, later periments put the value in the range $4 - 8k_BT_c$. Recently there have come mounting idence for an anisotropic gap and a d-wave pairing in the high-T_c superconductors [18].

.3.2 Some unusual properties

The high-T_c superconductors have three most unusual fundamental properties — large , short coherence lengths and large spatial anisotropy. The large T_c values open the

way for many new applications which were not previously attractive economically. From a fundamental viewpoint, T_c values of the order of 90K or higher are probably too high to be explained by BCS theory unless one assumes that some interaction much stronger that electron-phonon interaction is at work [19]. When T_c is large, many types of excitations, such as phonons, are present in the upper temperature ranges of superconductivity. The presence of these excitations, if they break Cooper-pairs, is expected to affect some of the properties of these compounds, such as, T_c and the critical current density J_c [20, 21, 22].

In these new materials ξ_{GL}, the Ginzberg-Landau coherence length at $T \ll T_c$ is typically between 0.5 and 30Å, depending on the crystallographic direction of the electron momentum, the substance, the type of experiment *etc.* [7]. In the conventional superconductors, $\xi_{GL}(0)$ is typically a few thousand Angstroms, unless it is decreased by alloying or defects. Because $\xi_{GL}(T)$ is much shorter than electromagnetic penetration depth λ in high-T_c materials, they are all type II superconductors with extremely high values of the upper critical field H_{c2}. Also associated with the short coherence length is a weak pinning of fluxoids in the mixed phase [23], compared with pinning in the conventional superconductors. This decreased flux-pinning diminishes the size of J_c.

The high-T_c cuprates have a high spatial anisotropy. For Y-Ba-Cu-O the least anisotropic among the high-T_c superconductors, one finds $\xi_{ab} = 14 \pm 2$Å, $\xi_c = 1.4 \pm 3$Å, $\lambda_{ab} = 1400$Åand $\lambda_c \sim 7000$Å. In the 'normal state', the electrical resistivity data show similar anisotropy. In Y-Ba-Cu-O, resistivity in the c-direction, ρ_c, is typically larger by a factor of 50 or more than the planar resistivity ρ_{ab}. For a Bi-Sr-Ca-Cu-O sample (with $T_c \sim 81$K) this anisotropy is extremely large, nearly 10^5 [24]. For homogeneous single-phase samples which are superconducting, the following general differences are seen — a) ρ_{ab} is 'metallic' with $\frac{d\rho_{ab}}{dT}$ positive and comparable to $\frac{\rho_{ab}}{T}$. b) ρ_c is usually 'non-metallic' ($\frac{d\rho_c}{dT} < 0$) [24].

One of the basic questions about the normal state of the high-T_c cuprates is whether they are standard Fermi liquids or not. On the one hand, there is a well-defined Fermi

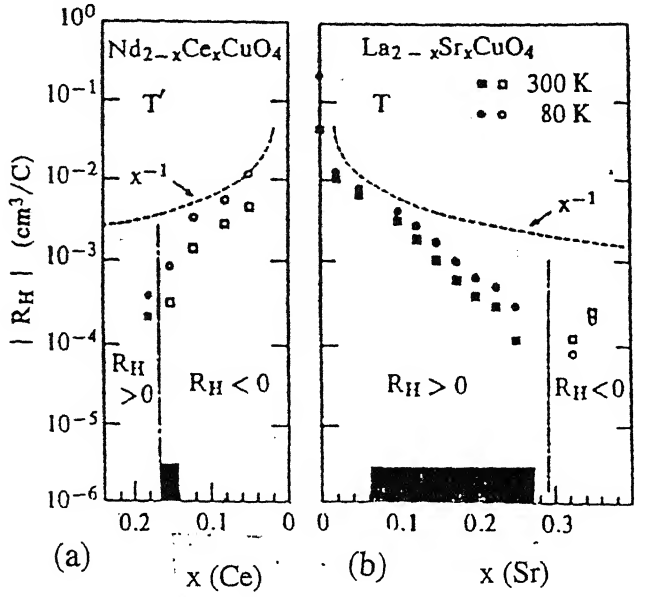

gure 1.3: R_H vs. doping level in (a) electron-doped, (b) hole-doped systems. Figure taken om Reference 29.

rface from photo-emission [25] and positron-annihilation [26] experiments, and the effective ass determined from the magnetic susceptibility [27] and the Drude component of optical nductivity [28] are consistent with each other. On the one hand, the transport properties, e resistivity and Hall effect, can be interpreted only in terms of a doped Mott-insulator, ther than a standard Fermi liquid. How to reconcile these two apparently contradictory pects is the main challenge to theory.

The temperature dependence of resistivity in several families of high-T_c superconductors ow the following general features — it increases linearly over a wide range of temperature, is quite small when extrapolated to absolute zero of temperature. In conventional metals e temperature dependence of resistivity can be divided into two distinct regimes. In the gh temperature regime, calculation of resistivity shows $\rho = A + BT$ for $T > 0.2\Theta_D$, where $_D$ is the Debye temperature. At low temperatures one gets, ρT^5, for $T \ll 0.2\Theta_D$. Extension the linear temperature dependence of ρ for Bi-Sr-Ca-Cu-O down to 10K suggests that some echanism other than electron-phonon collision is at work.

The behaviour of the Hall constant is even more peculiar. Figure 1.3 shows R_H changes

with composition in electron and hole doped superconductors. The signs of Hall coefficient indicates that in the La-system the carriers are holes and in Nd-system they are electrons. This observation is consistent with a doped Mott-Hubbard picture. The magnitude of R_H has a $\frac{1}{x}$ dependence, but deviates from this at higher doping concentrations [29]. The most interesting point is the change in R_H-sign at a critical concentration of doping where superconductivity disappears and usual metallic behaviour shows up. The region of 'anomalous' Hall constant coincides with the regime of linear temperature resistivity, as well as with linear temperature dependence of R_H^{-1} [30].

The angle-resolved photoemission experiment is a useful tool to study the energy spectrum of electrons. From the energy and angular dependence of emitted electrons one can, in principle, recover the spectral function $A(\vec{k},\omega)$. First in Bi-Sr-Ca-Cu-O [25], then in Y-Ba-Cu-O [31] compounds a well-defined Fermi surface has been found in good agreement with local density functional calculations. This Fermi surface is large as required by the Luttinger theorem. The more subtle question is the precise shape of the spectral function which can check the Fermi liquid theory in a quantitative way. Unfortunately, the present precision does not allow one to make unambiguous conclusions. The main puzzle comes from the comparison with transport measurements. As mentioned above, they are consistent with a Mott-Hubbard picture, *ie.*, the charge carrier concentration is x instead of $1-x$, where x is the doping concentration. In other words, the Fermi surface, even if it exists, should be a 'small' one corresponding to these 'pockets'.

1.3.3 Magnetic properties

From neutron scattering studies on La_2CuO_4 it was concluded that the system undergoes a three-dimensional antiferromagnetic transition at the Néel temperature T_N, at about 200K. The staggered order parameter has a characteristic temperature dependence of a 3D transition. This transition was first discovered by Vaknin *et al.* [32] in their powder diffrac-

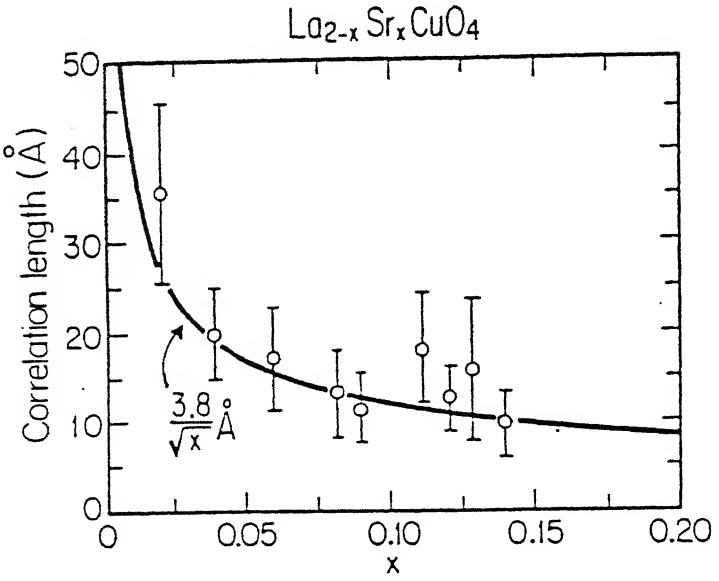

gure 1.4: Correlation length vs. doping concentration for $La_{2-x}Sr_xCuO_4$. The solid curve calculation of the mean spacing between the holes. Figure taken from Reference 38.

on study. It was found that the 3D transition temperature is extremely sensitive to oxygen ncentration [33]. Although the maximum possible T_N may be $\sim$ 300K, a small change in ygen concentration can reduce T_N drastically. Vaknin *et al.* [32] also found that in the nit $T \rightarrow 0$ the ordered moment is $0.5 \pm 0.15\mu_B$, considerably smaller than the saturation lue for Cu^{+2}, which is $\sim 1\mu_B$.

Y-Ba-Cu-O systems show striking similarities with lanthanum $La_{2-x}Sr_xCuO_4$ system. he first evidence of magnetic ordering in Y-Ba-Cu-O came from muon spin rotation (μSR) periments by Nishida *et al.* [34]. Soon after that superlattice reflections indicative of) long-range antiferromagnetic order (AFLRO) were observed by Tranquada *et al.* [35] in utron powder diffraction measurements. The spin structure which was deduced from the ak intensities was later corroborated by several groups [36, 37].

Addition of holes in the CuO_2 planes has drastic effects on the magnetic properties. ortly after the discovery of high-T_c cuprates, samples of $La_{2-x}M_xCuO_4$ with M=Ca^{+2},

Ba^{+2}, or Sr^{+2} were studied with a wide range of probes including bulk susceptibility, NMR, NQR, neutron scattering. As already mentioned, neutron diffraction on powder samples showed that Néel state disappeared before the appearance of superconducting phase upon doping.

Availability of large single superconducting crystals has made it possible to pursue the study of magnetic scattering into the superconducting phase. The main results of the neutron scattering experiments on these systems are as follows. 2D AF fluctuations are still observed in the doped and the superconducting samples, but with a much shorter in-plane correlation length, which turns out to be essentially temperature independent. As shown in Figure 1.4, the correlation length ξ decreases from $\sim$ 35Åto only 8Åas the Sr concentration x increases. The solid line, $3.8/\sqrt{x}$Å, is the average separation between the O^- holes in the CuO_2 planes. Within rather large experimental uncertainties ξ agrees with this distance quite well. The scattering is strongly inelastic, as in pure La_2CuO_4. The integrated inelastic intensity is comparable to that in La_2CuO_4, implying that there are still sizeable moments on the Cu atoms in the superconducting phase [38].

Experiments on large single-crystals of $YBa_2Cu_3O_{6+\delta}$ in the superconducting phase by Shirane and coworkers [38] have revealed that magnetic fluctuations are present in these crystals also. The crystals were found to be orthorhombic so that the possibility of included oxygen-deficient tetragonal AF phases was discounted. The intensities of these fluctuations disappeared rapidly near room temperature.

1.3.4 Models for the CuO_2 planes

As discussed above, the transport and magnetic properties suggest that these cuprate materials are Mott-Hubbard insulators. Very soon after the discovery of high-T_c superconductors, P. W. Anderson [39] suggested that one should start from a Mott insulator, because superconductivity occurs near metal-insulator transition. Moreover, he proposed that the

-band Hubbard model given by the Hamiltonian,

$$H = -t \sum_{\langle ij \rangle \sigma} (a^{\dagger}_{i\sigma} a_{j\sigma} + a^{\dagger}_{j\sigma} a_{i\sigma}) + U \sum_{i} n_{i\uparrow} n_{i\downarrow}, \tag{1.1}$$

ere $a^{\dagger}_{i\sigma}(a_{i\sigma})$ is the creation(annihilation) operator for spin σ fermions (electrons or holes) site i, $n_{i\sigma} = a^{\dagger}_{i\sigma} a_{i\sigma}$ is the number operator, t is the nearest-neighbour (NN) hopping and is the on-site Coulomb repulsion, can bring out the essential physics. Also, this would ow us to describe superconductivity and magnetism in a unified fashion so far as the same ctrons are responsible for both phenomena. This suggestion is supported by the fact that ıny of the magnetic properties of the high-T_c cuprates can be understood within a quantum isenberg antiferromagnet (QHAF), to which the Hubbard model can be mapped in the ong-coupling limit ($U \gg t$). Spin-wave theory on a $S = \frac{1}{2}$ QHAF predicts that due to antum fluctuations the ordered moment in the AF phase in 2D should be $\sim 0.6\mu_B$, which in close agreement with Vaknin's measurement. The temperature variation of the spin-spin rrelation length in these materials agrees well with the calculated value from a 2D QHAF. ıe temperature evolution of constant energy scans in neutron-scattering measurements e in agreement with theoretical results obtained using dynamic structure factor given by ıakravarty, Halperin and Nelson [40] and Tyc, Halperin and Chakravarty [41]. The energy pendencies of the integrated intensities of constant energy scans at different temperatures e also in agreement with the results obtained from the dynamic structure factor proposed Chakravarty, Halperin and Nelson [40].

Many electron spectroscopy experiments suggest that the high-T_c cuprate materials are arge-transfer insulators rather than Mott-Hubbard insulators. For example, in resonant tended photoelectron spectroscopy in $Bi_2Sr_2CaCu_2O_8$ [42] the spectrum displays a high ıergy satellite located approximately at -12.0 eV along with the main valence-band region hich has a width of roughly 4 eV. The enhancement of the intensity of the satellite at 74 eV, which is the Cu3p$\rightarrow$Cu3d threshold, identifies this peak with a $Cu3d^9 \rightarrow Cu3d^8$

transition [42]. Similar Cu3d^8 final state energies have been obtained in $YBa_2Cu_3O_{6+\delta}$ and $La_{2-x}Sr_xCuO_4$ [43, 44]. In $Nd_{2-x}Ce_xCuO_4$ this energy is -13.3 eV [45]. Since the Cu3d^8 peak is below the main valence-band region, this implies that the Coulomb repulsion energy on the Cu sites (U_d) is large compared to the charge transfer energy Δ between Cu3d and O2p orbitals. This supports a CTI scenario.

Core electron X-ray emission spectroscopy (XPS) provides additional information on the size of the local Coulomb correlations [46]. XPS at the Cu2p threshold has been performed on $La_{2-x}Sr_xCuO_4$ [47, 43, 48], on $YBa_2Cu_3O_{6+\delta}$, [47, 43, 49] and on $Bi_2Sr_2CaCu_2O_8$ [50]. Cu2p$_{3/2}$ core XPS shows a double-peak structure in all investigations. In $La_{2-x}Sr_xCuO_4$, the 933 eV peak has been attributed to a Cu2p$_{3/2}$3d$^{10}\underline{\text{L}}$ final state, where Cu2p$_{3/2}$ denotes the core hole and $\underline{\text{L}}$ is a ligand hole on the surrounding oxygen sites. The satellite at 941 eV comprises of a Cu2p$_{3/2}$3d^9 final configuration [43, 48, 47, 49, 50]. A Cu2p$_{3/2}$3d^9 satellite at an energy larger than that of the charge-transfer state Cu2p$_{3/2}$3d$^{10}\underline{\text{L}}$ implies that the Coulomb repulsion U_{cd} between the Cu2p$_{3/2}$ core hole and Cu3d^9 valence-band hole is larger than the charge-transfer gap. Since the on-site repulsion U_d in 3d transition metal compounds satisfies $U_d/U_{cd} \sim 0.7$ [43], one is led to a CTI picture.

In O1s X-ray absorption spectroscopy (XAS), dipole selection rules allow only for s $\rightarrow$ p$_x$, s $\rightarrow$ p$_y$, or s $\rightarrow$ p$_z$ transitions depending on whether the incoming photon field $\vec{E}$ is oriented $\vec{E}||a$, $\vec{E}||b$, or $\vec{E}||c$ axis. For $\vec{E}||c$ a 'prepeak' is observed in insulating La_2CuO_4 and Nd_2CuO_4 at E$_p$ = 530.2 eV and E$_p$ = 529.1 eV respectively. The corresponding O1s thresholds are at E$_t$ = 528.5 eV and E$_t$ = 528.6 eV. This feature is intrinsic to the CuO_2 planes since it is absent in XAS on Nd_2O_3 [51]. The prepeak is identified with the Cu3d^{10} upper Hubbard band [52, 53, 54]. Since the initial state is approximately $|\psi_i\rangle = \alpha\,|\,\text{Cu3d}^9\rangle + \beta\,|\,\text{Cu3d}^{10}\underline{\text{L}}\rangle$, the prepeak intensity is a measure of the copper-oxygen hybridisation in the upper Hubbard band [52, 54]. In insulating La_2CuO_4 this quantity is approximately $|\beta|^2 > 0.1$ [52]. These spectra are clear evidence in favour of a CTI picture for the parent compounds and cannot

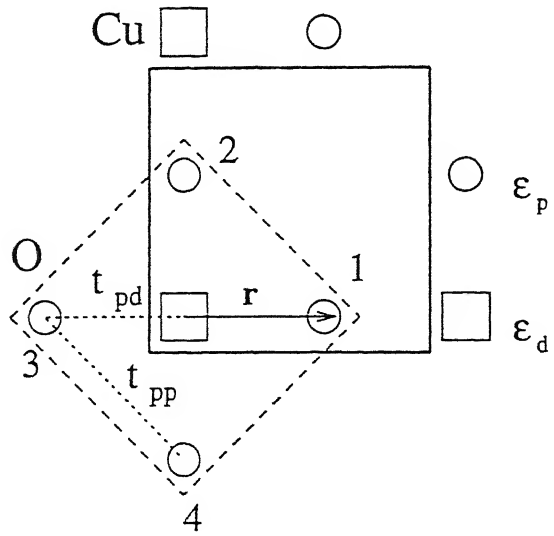

gure 1.5: Basis (solid line bounded square) and CuO_4 plaquette (dashed line bounded uare) of the CuO_2 plane of the three-band Hubbard model. The squares and the circles ark the Cu $3d_{x^2-y^2}$ and O positions, at energies ϵ_d and ϵ_p, respectively. The $2p_x$ and $2p_y$ bitals are located at 1,3 and 2,4, t_{pd}^{ij} denotes the transfer integral between copper and ygen and t_{pp}^{ij} the direct oxygen-oxygen hopping. The lattice spacing $a = 2 \mid r \mid$.

explained in terms of a LDA band structure [46].

Since these and other electron spectroscopy experiments (a comprehensive review of e topic is given in Reference [46]) support the CTI picture for the parent compounds of gh-T_c cuprates, many authors [55, 56] propose the three-band Hubbard model, which takes)th O2p and Cu3d orbitals explicitly into account, as the minimal model for describing the ıysical properties of the CuO_2 planes in these materials. The three-band Hubbard model described by the following Hamiltonian. A diagram of a portion of the CuO_2 plane it presents is shown in Figure 1.5 (adapted from Reference [46]).

$$
\begin{aligned}
H &= -t_{pd}^{ij} \sum_{\langle i,j\rangle;\sigma} (p_{i\sigma}^{\dagger} d_{j\sigma} + \text{h.c.}) - t_{pp}^{ij} \sum_{\langle l,m\rangle;\sigma} (p_{l\sigma}^{\dagger} p_{m\sigma} + \text{h.c.}) \\
&\quad + \epsilon_p \sum_{i\sigma} p_{i\sigma}^{\dagger} p_{i\sigma} + \epsilon_d \sum_{i\sigma} d_{i\sigma}^{\dagger} d_{i\sigma} \\
&\quad + U_d \sum_i n_{i\uparrow}^d n_{i\downarrow}^d + U_p \sum_i n_{i\uparrow}^p n_{i\downarrow}^p + U_{pd} \sum_{\langle i,j\rangle} n_i^p n_i^d, \qquad (1.2)
\end{aligned}
$$

where $p(p^{\dagger})$ and $d(d^{\dagger})$ are the annihilation(creation) operators for holes on the O and Cu sites, $\langle i,j\rangle$ are nearest neighbour (NN) Cu and O sites and $\langle l,m\rangle$ are two neighbouring O sites; n's are the respective number densities. t_{pd} is the hopping term between neighbouring Cu $3d$ and O $2p$ orbitals and t_{pp} is the hopping matrix element between two NN O $2p$ orbitals. ϵ_d and ϵ_p are the on-site energies of a hole sitting on Cu $3d$ or O $2p$ orbital. U_d and U_p are the Coulomb repulsion terms on the Cu and O sites respectively. U_{pd} is the repulsion between charges on the neighbouring Cu and O sites. σ is the spin index. $\Delta \equiv \epsilon_p - \epsilon_d$ is the charge-transfer gap. In the hole picture Δ is positive. The orbital symmetries of the type $d_{x^2-y^2}$ and $p_{x,y}$ imply additional phase factors for the hopping integrals t_{pd}^{ij} and t_{pp}^{ij}

$$
\begin{aligned}
t_{pd}^{0j} &= \phi^j t_{pd}, \quad \phi^1 = \phi^2 = -1, \quad \phi^3 = \phi^4 = 1, \\
t_{pp}^{ij} &= \psi^{ij} t_{pp}, \quad \psi^{12} = \psi^{34} = -1, \quad \psi^{23} = \psi^{41} = 1,
\end{aligned}
$$

where 0 labels the central copper, and 1,2,3,4 the four oxygen sites on the plaquette.

It has been argued by some researchers that the three-band Hubbard model can be reduced to an effective one-band model in order to describe the low-energy physics of the CuO_2 planes when only the spin degrees of freedom are important. But there is no consensus, rather the issue is very much controversial.

1.4 Impurity-doped cuprates

As we have already discussed, neutron scattering experiments indicate that 2D AF fluctuations are present in the superconducting state, but with a much altered magnetic

ıamics from the AF state in the parent compound. A question of fundamental importance ıow doping affects the electronic states of Cu^{+2}. Whether the electron in the $Cu^{+2}3d_{x^2-y^2}$ ţibonding state remains localised in the highly doped samples, or it gets delocalised. The ıfirmation of one of these possibilities was thought to be useful [57]. The particularly evant issues are the connection between magnetism and superconductivity, the validity of rious models based on localised moment, itinerant magnetism *etc.*

One of the techniques used from the very early days of superconductivity to study ese aspects has been substitution of Cu by impurities. This ability to dope the Cu-site the high-T_c superconductors with transition or sp elements offers an important means study these materials. Understanding of the effects of impurities on superconductivity ıd normal-state properties is crucial for elucidation of mechanism of superconductivity. ıe relevant aspects in substitution studies are to what degree magnetic and nonmagnetic ›pants affect superconductivity, and how dopants with different electronic structures alter e normal-state transport and magnetic properties.

Gang Xiao *et al.* [58, 57] of the Johns Hopkins University and Keimer *et al.* [4] have ›ne various measurements on high-T_c cuprates doped with static impurities. Xiao *et al.* ıve done extensive susceptibility measurements on impurity-doped lanthanum cuprates. eimer *et al.* have done neutron scattering experiments on this system. The substitutional ıpurities include both magnetic, such as, Fe, Ni; and nonmagnetic, such as, Zn, Al, Ga, Co; ıes. Later Mahajan *et al.* [2] and Walstedt *et al.* [59] have done various NMR experiments ı Zn-doped Y-Ba-Cu-O system. Impurity substitution studies in 1-2-3 systems is a little icky as there are two different kinds of Cu sites – in planes and in chains and one has to be reful about which copper site the impurity is going into. Various observations suggest that e divalent impurities like Zn^{+2} go into the planes, whereas, trivalent impurities, like Fe^{+3}, l^{+3} and Ga^{+3} go into the chains. There is no such complications in lanthanum cuprate as ıere are only planar copper sites.

1.4.1 Effects of impurities

All these experiments show that these impurities have four main effects on these compounds. Firstly, nonmagnetic impurities, like Zn, reduce the Néel temperature in the AF phase of these materials. Although they are less efficient in destroying AF order than mobile holes, nevertheless they are detrimental to AFLRO. Keimer *et al.* [4] measure the Néel temperature of $La_{2-x}Sr_xCu_{1-y}Zn_yO_4$ single-crystals by SQUID magnetometry. They find that T_N goes down approximately linearly with increasing Zn concentration y and the $T_N(y)$ curve for the crystals extrapolate to zero at $y \sim 0.26$, *ie.*, 26% of Zn doping completely kills AFLRO in this system.

Secondly, of these impurities, those which substitute Cu in the CuO_2 planes have drastic effect on T_c of these materials. Measurements of Xiao *et al.* [58] show that in $La_{2-x}Sr_xCu_{1-y}A_yO_4$ (A=Zn, Al, Ga, Fe, Ni, Co) T_c varies smoothly and monotonically with y. Above a critical doping level y_c, T_c reduces to zero. In lanthanum cuprates Fe suppresses T_c most efficiently, with the smallest y_c of 1.8%, and Ni has the largest y_c of 4.2%. In contrast, Zn is the most efficient in reducing T_c in Y-Ba-Cu-O. In $YBa_2Cu_3O_7$, replacement of 3% of the Cu by Zn is sufficient to reduce the T_c from 90K to about 60K. 10% of Zn doping destroys superconductivity completely. Al and Ga are much less disruptive of superconductivity in this material. This supports the site assignments stated earlier. The relative effectiveness of Zn in destroying superconductivity can be attributed to Zn-substitution on the planar sites, where it is believed that superconductivity resides. Whereas, Al and Ga, substituting Cu in the chains, have very little effect on T_c .

Thirdly, all these static impurities have very interesting magnetic effects in high-T_c cuprates. In conventional superconductors magnetic impurities are most destructive of superconductivity due to their pair-breaking effect. Nonmagnetic impurities have very little effects on superconductivity. But, as we have seen, in $YBa_2Cu_3O_7$, nonmagnetic Zn is most detrimental to superconductivity. Even in lanthanum cuprate, the largest y_c differs from the

allest y_c only by a factor of 2. One of the immediate questions is how the effect of dopant elated to its magnetic characteristics.

In order to study the relation between superconductivity and magnetic nature of the pant, Xiao *et al.* [58] measured the magnetic susceptibility (χ) with a SQUID magneneter. Interestingly, they found that irrespective of the magnetic nature of the dopant, T) shows a Curie-Weiss behaviour ($1/T$) indicative of a localised moment. All the data ıld be well-described by the relation

$$\chi(T) = \chi_0 + \frac{Np_{eff}^2\mu_B^2}{3k_B(T-\theta)}, \tag{1.3}$$

ıere χ_0 represents the background susceptibility which does not change appreciably with ping, N is the doping content and p_{eff} is the effective moment of a dopant. In their alysis, Xiao *et al.* assumed that the local moment resides on the dopant site. As will be scussed later, this is not quite correct. What is surprising about their observation is that the nonmagnetic dopants, that cannot carry a moment by their atomic structures, induce similar moment $\sim 1.2\mu_B$. Fe carries a large moment of $5\mu_B$. So, judging by their effects, the dopants at the Cu site are magnetic in nature.

Nonmagnetic dopants such as Zn^{+2}, Ga^{+3}, Al^{+3} have inert full-shell structure ($3d^{10}$ and ^{6}). Their main role is to remove the spin of $Cu^{+2}3d^9$ ($S = \frac{1}{2}$). As stated already, every nmagnetic dopant induces a moment of $1.2\mu_B$ irrespective of its electronic structure. Such nmagnetic dopants do not, in general, induce moments in conventional metals. The apparance of induced moment indicates localised nature of the d state in the superconducting $_{2-x}Sr_xCuO_4$. This moment, Xiao *et al.* argues, is nothing but the Cu^{+2} moment, which concealed from susceptibility measurement due to moment compensation in the dynamic ' state. A nonmagnetic dopant breaks the compensation and creates a net spin of $S = \frac{1}{2}$ nerating an effective moment $p_{eff} = g\sqrt{s(s+1)} = 1.9\mu_B$. The experimental p_{eff} value is ıse to $1.2\mu_B$, a 35% reduction from the theoretically expected value. This, it is believed, is

due to Cu3d$_{x^2-y^2}$–O2p hybridisation. But, as we will shortly see, this picture of an AF plus a spin-hole is rather simplistic in view of the recent NMR experiments in Y-Ba-Cu-O [2].

Another important observation that Xiao *et al.* make is that the extent of suppression of superconductivity has little relation with the valence of a dopant. For example, Zn^{+2} and Ni^{+2}, having the same valence, differ a great deal in their y_c values. On the other hand, Zn^{+2} and Al^{+3}, Ga^{+3}, Co^{+3} having different valence states, have similar y_c values. One can expect that the divalent impurities will not affect carrier concentration, whereas, trivalent ones will reduce carrier concentration with increasing doping. However, since y_c is small in every system and insensitive to the dopant valence state, argues Xiao *et al.* , suppression of T_c cannot be predominantly attributed to any change in carrier concentration.

Recently Walstedt *et al.* [59] have done Cu^{63}(2)-NMR studies and Mahajan *et al.* [2] have done Y^{89}-NMR studies on Zn-doped Y-Ba-Cu-O. Walstedt *et al.* find a predominant T^{-1} temperature dependence in the Cu(2) NMR linewidth. They have explained this observation from spin-exchange scattering of carriers from localised moments associated with Zn impurities in the CuO_2 planes. In their Y^{89}-NMR measurements on $YBa_2(Cu_{1-y}Zn_y)_3O_{6+\delta}$, Mahajan *et al.* find two satellite peaks along with the main Y^{89} peak. Comparing this with their numerical calculations, and comparing the Curie-like temperature dependence of the frequency shifts of the satellite lines with susceptibility data, they conclude that the Zn-induced local moments reside on NN Cu orbitals. This is a very significant conclusion as it makes the picture of the Zn-induced local moment as an AF with a spin-hole and the moment residing on the dopant site untenable, and calls for a more detailed microscopic understanding of the whole phenomenon. Since the frequency-shift of the main Y-line in their experiment is independent of T, they conclude that there is no change in carrier concentration in Zn-doped Y-Ba-Cu-O.

One aspect the researchers are not in consensus about is the mechanism for reduction in T_c . Since it is seen that all the dopants, whether magnetic or nonmagnetic, give rise

local moments in the CuO_2 planes and the Fe-doped $La_{2-x}Sr_xCuO_4$ system with the hest moment has the lowest y_c, whereas, the Ni-doped system with the smallest moment ; the highest y_c, Xiao *et al.* [58] believes that an Abrikosov-Gorkov (AG) pair-breaking chanism is responsible for reduction in T_c . Walstedt *et al.* [59], on the other hand, believe ıt a pair-breaking mechanism cannot explain the observed reduction in T_c . Comparing ; measured T^{-1} temperature dependent Cu(2) NMR linewidth with a calculation based RKKY-like spin-density oscillations in the CuO_2 planes driven by exchange between the)bile carriers and localised moments associated with Zn-sites, they find that the reduction T_c from the AG formula should be of the order of a tenth of a Kelvin – orders of magnitude ıaller than the observed value ($\sim$ 100K). They go on to argue that this suggests a d-wave iring in the cuprate superconductors, in which case, a strong potential scatterer like Zn n cause pair-breaking effects. Mahajan *et al.* [2] from their analysis of Y-NMR linewidths nclude that the reduction in T_c can be $\sim$ 100K from an AG theory. They believe that alstedt *et al.* reached the opposite conclusion mainly as their $\chi_c(= C_m/T)$, the Curie rm in the susceptibility in the doped systems is larger. In a recent magnetoconductance periment on single crystals of $YBa_2(Cu_{1-0.01y}Zn_{0.01y})_3O_{6+\delta}$ for y=1 and 3.5, Axnäs *et al.* 0] have found that phase-breaking scattering rate increases strongly with Zn concentration, dicating that Zn causes pair-breaking in this material. Williams *et al.* [61] from their Y-MR measurements on $Y(Ba_{1-x}La_x)_2(Cu_{1-y}Zn_y)_4O_8$ find that magnetic pair-breaking by .e induced local moments can fully explain the rapid depression in T_c with Zn substitution La-free overdoped (high hole concentration) samples. However, as the samples become ore underdoped, magnetic pair-breaking becomes increasingly unable to account for the)served decline in T_c . They believe that this occurs predominantly via a reducing pairing teraction.

Finally, the temperature dependence of the in-plane resistivity (ρ_{ab}) of Zn-doped cuprate ıperconductors shows some interesting behaviour. Fukuzumi *et al.* [62] measured the

temperature variation of ρ_{ab} in $YBa_2(Cu_{1-y}Zn_y)_3O_{6+\delta}$ and $La_{2-x}Sr_xCu_{1-y}Zn_yO_4$ over a wide range of Zn content and doped hole density. Interestingly, Zn substitution makes marked difference between underdoped and overdoped samples in these experiments. In underdoped $YBa_2(Cu_{1-y}Zn_y)_3O_{6.63}$ with Zn content ranging up to $y = 0.04$ they find that T_c is rapidly reduced and the compound becomes insulating after the superconductivity disappears. A large residual resistivity ρ_0 adds to the T-dependent component. Superconductor-insulator (SI) transition occurs at $\rho_0 \sim 400\mu\Omega cm$. This value corresponds to the 2D resistance of $\sim 6.8K\Omega/CuO_2$ plane and is near the universal value $h/4e^2 \sim 6.4K\Omega/CuO_2$ plane. In $La_{2-x}Sr_xCu_{1-y}Zn_yO_4$ for $x = 0.10$ and 0.15, the SI transition takes place near the universal 2D resistance. The highly doped superconducting compounds show a contrasting behaviour. The $x = 0.20$ $La_{2-x}Sr_xCu_{1-y}Zn_yO_4$ sample remains metallic even after the superconductivity disappears and the residual resistivity is smaller than the critical value observed for $x =$ 0.10 and 0.15 by a factor of 4. This shows that the underdoped compound is intrinsically insulating. Suppression of superconductivity drives it into an insulating state.

1.5 Outline of the thesis

In order to develop an understanding of the effects of nonmagnetic impurities in the CuO_2 planes we study the effects of such impurities on a Mott-Hubbard AF. We find that each nonmagnetic impurity gives rise to a defect state within the Hubbard gap. This state is localised mainly on the four sites neighbouring the impurity and produces a local moment [63]. We also study effects of nonmagnetic impurities in a Hubbard model with only short-range order and find that defect states are formed in this case also. These nonmagnetic impurities give rise to a logarithmically diverging correction to the magnon energy in the long-wavelength limit in a 2D system. In an anisotropic 3D (layered) AF, this divergence is cut off by the interlayer hopping. We calculate the reduction in Néel temperature due to thermal excitation of spin waves and find that T_N goes down with increasing Zn concentration

ıccordance with observations of Keimer *et al.* [4] in their neutron-scattering experiment

.

Additional holes put in a system with static nonmagnetic impurities will go into the ect state as that is the lowest energy state available for a hole. So in presence of holes the al moment will be lost. But thermal and quantum fluctuations can transfer some spectral ght of the hole in the upper Hubbard band so that part of the moment can be regained. present a quantitative estimate of how the moment is recovered with temperature and ə to quantum fluctuations.

Defect states in a one-band Hubbard model cannot explain how local moments are med in systems with added holes and at low temperatures, how the observed moment smaller than the theoretically expected value and why all nonmagnetic impurities, irre- ɛctive of their structural details, give rise to the same moment. We attempt to explain ɛse by studying the effects of nonmagnetic impurities in a CTI described by a three-band ıbbard model. In this case each impurity produces two defect states. The upper defect ıte, formed slightly below the upper Hubbard band, has amplitude mainly on the four ighbouring Cu sites and remains occupied by electrons even in the presence of added holes the system. So the moment formed in this system is robust with respect to hole doping.

We have studied the effects of magnetic impurities in a Mott-Hubbard AF. We present ɣeral formalisms representing different situations. In the case impurity spin (S') equal the host spin (S) represented by modified hoppings around the impurity site, we find momentum-independent renormalisation of the long-wavelength magnon mode energies. the high-energy end of the spectrum, a magnon mode is split-off from the band and is ə one localised at the impurity site. Its energy is modified because of different effective upling (J') between the impurity spin and the neighbouring ones. We develop a formalism represent magnetic impurities by a spin-dependent potential on the impurity site as a tural extension of the formalism developed for nonmagnetic impurities. In this case, within

a T-matrix formalism, unlike the nonmagnetic impurity case, we find no defect states within the Hubbard gap, rather, one impurity state is formed for each spin. These impurity states are localised on the impurity site and the local moment in this case is because of difference in $\uparrow$- and $\downarrow$-spin densities on the impurity site. We also develop a formalism to represent magnetic impurities by putting multiple orbitals on the impurity site. We explicitly show that the Goldstone mode is preserved in presence of impurities. We also study the effects of these impurities on the electronic spectral properties of the system. Via a scaling study within a numerical HF scheme we, find a linear reduction in the magnon velocity in the long wavelength limit with increasing doping concentration which shows a logarithmic divergence in the limit of large system size.

hapter 2

tatic Nonmagnetic Impurities in a Iott-Hubbard Antiferromagnet

The motivation for studying the effects of static impurities in a Mott-Hubbard AF has en discussed in detail in the previous chapter. In this chapter we present our formalism treating nonmagnetic impurities in a Mott-Hubbard AF. The same formalism will be ed when we discuss nonmagnetic impurities in a magnetic system with short-range order hapter 3) and in a CTI (Chapter 6).

In the first section of this chapter we briefly review the Hartree-Fock (HF) mean-field IF) treatment of the Hubbard model at half-filling. In the subsequent sections we introduce e impurity and study its effects on the electronic properties of the system. Effects on the agnetic properties will be discussed in Chapter 4.

.1 HF treatment of the Hubbard model

The quantum AF state of the Mott-Hubbard insulator has been studied in great detail thin a HF-plus-fluctuations approach by Singh and Tešanović [3]. Within HF approx- ıation the Hubbard model on a square lattice, described by the Hamiltonian given by quation 1.1, has been represented in the AF state in the two-sublattice basis as,

$$H^{\sigma}_{\mathrm{HF}}(\vec{k}) = \begin{bmatrix} -\sigma\Delta & \epsilon_{\vec{k}} \\ \epsilon_{\vec{k}} & \sigma\Delta \end{bmatrix} \tag{2.1}$$

where $\sigma = \pm 1$ for $\uparrow$- and $\downarrow$-spins, $\epsilon_{\vec{k}} = -2t[\cos(k_x a)+\cos(k_y a)]$ is the free-particle band energy for a 2D square lattice and Δ is the gap parameter. The eigenvalues of the Hamiltonian yield the quasiparticle energies

$$E^{\sigma}_{\vec{k}} = \pm(\Delta^2 + \epsilon_{\vec{k}})^{1/2}. \tag{2.2}$$

The plus(minus) sign is associated with $\vec{k}$ states lying inside(outside) the magnetic Brillouin zone (MBZ). This shows that there are two bands for both $\uparrow$- and $\downarrow$- spins. At the half-filled level, the lower Hubbard bands (LHB) for both the spins are completely occupied and the upper Hubbard bands (UHB) are completely empty. The system, therefore, is an insulator. The gap parameter is related to the sublattice magnetisation m by $2\Delta = mU$. The sublattice magnetisation is defined as the average over one sublattice of the expectation value of the z-component of the spin operator $S^i_z = a^{\dagger}_i \sigma_z a_i$, where σ_z is the z-component of the Pauli spin matrix. The quasiparticle amplitudes on the A- and B-sublattice sites are given by ${a^{\pm}_{\vec{k}\sigma}}^2 = \frac{1}{2}(1 \mp \sigma\Delta/E_{\vec{k}})$ and ${b^{\pm}_{\vec{k}\sigma}}^2 = \frac{1}{2}(1 \pm \sigma\Delta/E_{\vec{k}})$.

The sublattice magnetisation m is obtained from the difference in spin densities on a site:

$$m = \frac{2}{N}\sum_{E_{\vec{k}}<E_{\mathrm{F}}} [a_{i\uparrow}(\vec{k})^2 - a_{i\downarrow}(\vec{k})^2] = \frac{2}{N}\sum_{E_{\vec{k}}<E_{\mathrm{F}}} \frac{\Delta}{(\Delta^2 + \epsilon^2_{\vec{k}})^{1/2}}. \tag{2.3}$$

Since $2\Delta = mU$, this leads to the self-consistency condition:

$$\frac{1}{U} = \frac{1}{N}\sum_{E_{\vec{k}}<E_{\mathrm{F}}} \frac{1}{(\Delta^2 + \epsilon^2_{\vec{k}})^{1/2}}.$$

In terms of the quasiparticle amplitudes and energies, the Green's function for the system

$$g^{\sigma}(\vec{k},\omega) =< \vec{k}|\frac{1}{\omega - H_0^{\sigma}(\vec{k})}|\vec{k} >= \sum_{s=\pm} \begin{bmatrix} a^2_{\vec{k}\sigma s} & a_{\vec{k}\sigma s}b_{\vec{k}\sigma s} \\ a_{\vec{k}\sigma s}b_{\vec{k}\sigma s} & b^2_{\vec{k}\sigma s} \end{bmatrix} \frac{1}{\omega - E_{\vec{k}\sigma s} + is\eta} \tag{2.4}$$

:e s refers to the two signs $+/-$ corresponding to the upper/lower Hubbard bands.

The spin-wave mode shows up in the form of a pole in the dynamical transverse spin ;ceptibility evaluated in the Hartree-Fock AF state. The transverse susceptibility is defined terms of the spin-raising and spin-lowering operators as,

$$\chi^{-+}(\vec{r},t;\vec{r}',t') = i\theta(t-t')\langle\Psi_{\rm AF} \mid \left[S^{-}(\vec{r},t), S^{+}(\vec{r}',t')\right] \mid \Psi_{AF}\rangle. \tag{2.5}$$

ithin random phase approximation (RPA), the transverse susceptibility in the momentum ace in the sublattice basis representation is [3]

$$\chi^{-+}(\vec{Q},\Omega) = \frac{\chi^0(\vec{Q},\Omega)}{1 - U\chi^0(\vec{Q},\Omega)}. \tag{2.6}$$

ıe zeroth-order susceptibility, $\chi^0(\vec{Q},\Omega)$ is a 2×2 matrix in the sublattice basis and is given terms of the Green's function as,

$$\chi^0(\vec{Q},\Omega) = i\int_{-\infty}^{\infty}\frac{d\omega}{2\pi}\frac{1}{N}\sum_{\vec{k}} G^{\uparrow}(\vec{k},\omega)G^{\downarrow}(\vec{k}-\vec{Q},\omega-\Omega). \tag{2.7}$$

ıe RPA susceptibility matrix can be expanded in terms of the eigenvalues $\lambda(\vec{Q},\Omega)$ and the ;envectors $\mid \Phi_\lambda(\vec{Q},\Omega)\rangle$ of the $\chi^0(\vec{Q},\Omega)$ matrix as,

$$\chi^{-+}(\vec{Q},\Omega) = \sum_{\lambda}\frac{\lambda(\vec{Q},\Omega)}{1 - U\lambda(\vec{Q},\Omega)} \mid \Phi_\lambda(\vec{Q},\omega)\rangle\langle\Phi_\lambda(\vec{Q},\Omega) \mid . \tag{2.8}$$

ence it is clear that all the information regarding the nature of these collective spin excita- ons is contained in the eigensolutions $\{\mid \Phi_\lambda(\vec{Q},\Omega)\rangle, \lambda(\vec{Q},\Omega)\}$. The eigenvectors $\mid \Phi_\lambda(\vec{Q},\Omega)\rangle$

represent the spin-wave amplitude in momentum space, while the spin-wave energies, $\Omega_{\vec{Q}}$, are given by the poles at $1-U\lambda(\vec{Q},\Omega_{\vec{Q}})=0$. The wave function of the spin-wave in state $\vec{Q}$ is given by a superposition of plane waves on the two sublattices, the superposition amplitudes being given by the eigenvector $\Phi(\vec{Q},\Omega_{\vec{Q}})$,

$$\Phi(\vec{r})=\sqrt{\frac{2}{N}}\Phi(\vec{Q},\Omega)e^{i\vec{Q}.\vec{r}}. \tag{2.9}$$

In the strong-coupling limit ($U \gg t$) $\chi^0(\vec{Q},\Omega)$ has the following form up to $O(\frac{t^2}{\Delta^3})$:

$$\chi^0(\vec{Q},\Omega)=\begin{bmatrix} \mathcal{A}-\alpha\Omega & \mathcal{B}_{\vec{Q}} \\ \mathcal{B}_{\vec{Q}} & \mathcal{A}+\alpha\Omega \end{bmatrix} \tag{2.10}$$

where $\mathcal{A}=\frac{1}{U}-\frac{t^2}{\Delta^3}$, $\alpha=\frac{1}{4}\Delta^2$ and $\mathcal{B}_{\vec{Q}}=-\frac{t^2}{\Delta^3}\gamma_{\vec{Q}}$, with $\gamma_{\vec{Q}}\equiv\frac{1}{2}[\cos(Q_x a)+\cos(Q_y a)]$ in 2D. Two eigenvalues of the χ_0^{-+} matrix are,

$$\lambda=\frac{1}{U}-\frac{t^2}{\Delta^3}1\mp\left[(\frac{\Omega}{2J})^2+\gamma_{\vec{Q}}^2\right]^{1/2}, \tag{2.11}$$

where $J=\frac{4t^2}{U}$ is the NN coupling in the equivalent Heisenberg model. Equating $1-U\lambda_{\max}=0$, where $\lambda_{\max}$ is the larger of the two eigenvalues, the spin-wave energies obtained are:

$$\Omega_{\vec{Q}}=\pm 2J(1-\gamma_{\vec{Q}}^2)^{1/2}. \tag{2.12}$$

2.2 Treatment of the impurity-doped system

We now present results of our study of a Mott-Hubbard AF doped with static, nonmagnetic impurities. We use Hubbard model to describe 3d holes in the CuO_2 planes. Zn^{+2}, that replaces Cu^{+2}, has a filled $3d^{10}$ configuration. We model zinc-type dopants by high impurity potential (V) on the dopant sites, to ensure the absence of any 3d hole density on these sites.

The Hamiltonian of the system in presence of impurity is

$$H = -t \sum_{\langle ij \rangle \sigma} (a^{\dagger}_{i\sigma} a_{j\sigma} + \text{h.c.}) + U \sum_{i} n_{i\uparrow} n_{i\downarrow} + V \sum_{I,\sigma} a^{\dagger}_{I\sigma} a_{I\sigma}, \tag{2.13}$$

ere the sum over I goes over the impurity sites. We start with the HF description of the doped AF host and then treat the impurity terms perturbatively within a Green's function malism. For a single impurity the perturbation can be treated exactly in terms of the matrix formalism. There is a caveat that this procedure is not fully self-consistent as the nsity modifications introduced by the high-impurity terms are not treated self-consistently.

The Green's function for the system with a single impurity at site I can be written as,

$$G^{\sigma}_{ij}(\omega) = g^{\sigma}_{ij}(\omega) + g^{\sigma}_{iI}(\omega) V g^{\sigma}_{Ij} + g^{\sigma}_{iI}(\omega) V g^{\sigma}_{II}(\omega) V g^{\sigma}_{Ij}(\omega) + \cdots \tag{2.14}$$

nich can be summed up and written in terms of the T-matrix, $\mathrm{T}^{\sigma}(\omega) = \frac{V}{1 - V g^{\sigma}_{II}(\omega)}$ as

$$G^{\sigma}_{ij}(\omega) = g^{\sigma}_{ij}(\omega) + g^{\sigma}_{iI}(\omega) T^{\sigma}(\omega) g^{\sigma}_{Ij}(\omega). \tag{2.15}$$

formation regarding additional poles is contained in the T-matrix, and therefore, a study the local Green's function $g^{\sigma}_{II}(\omega)$ in the AF state is of interest. If, for concreteness, we nsider the impurity to be on an A-sublattice site, then we obtain,

$$g^{\sigma}_{II}(\omega) = \frac{1}{N} \sum_{\vec{k}} \frac{\omega - \sigma\Delta}{\omega^2 - E^2_{\vec{k}}} \tag{2.16}$$

plot of $g^{\uparrow}_{II}(\omega)$ vs. ω is given in Figure 2.1 and shows logarithmic divergences at energies $\sqrt{\Delta^2 + (4t)^2}$, a stronger divergence $(\omega + \Delta)^{-1/2} \ln(\omega + \Delta)$ as $\omega \to -\Delta$ from above, and a $\sqrt{\Delta - \omega} \ln(\Delta - \omega)$ dependence as $\omega \to \Delta$ from below. (See Appendix A for details). The tersection with $1/V$ yields the poles, and for large V we obtain an impurity state at energy $= V - \Delta$ (V relative to the lower band at energy $-\Delta$), and a defect state inside the

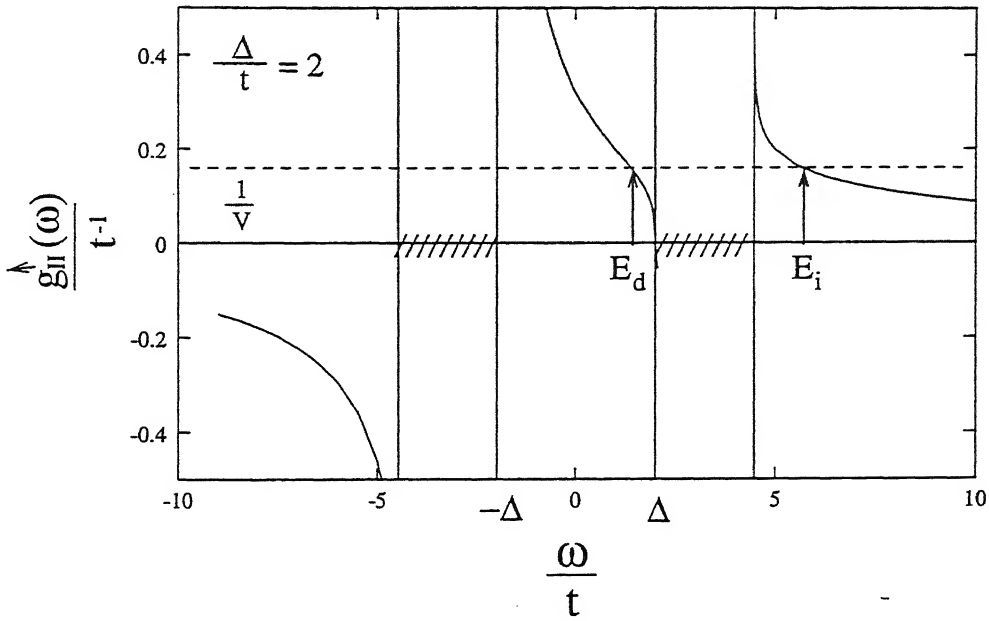

Figure 2.1: Plot of $g_{II}^{\uparrow}(\omega)$ and $1/V$.

Hubbard gap close to the upper band edge.

The energy spectra for the two spins in presence of impurity are shown in figure 2.2 In semiconductor terminology, such states in the gap arising from impurities are called *deep traps*, and for large V and two similar bands, occur near the mid-gap position. To reflect the asymptotic convergence of the trap energy to some fixed position near mid-gap as $V \to \infty$, the concept of pinning has been introduced — large differences in atomic energies influence the trap energies only weakly [65]. However, in the AF, while the two Hubbard bands are identical, the two-sublattice structure is responsible for pinning the defect states to the band edges.

The energy separation $\eta \equiv \Delta - E_{\rm d}$, of the defect state at energy $E_{\rm d}$, from the lower edge of the upper Hubbard band is approximately given by $\sqrt{\eta}\ln\eta \sim 1/V$, so that η vanishes essentially as $(1/V)^2$ as $V \to \infty$. (For details, see Appendix A).

For the sake of completeness, we show a plot of $g_{II}^{\downarrow}(\omega)$ and $1/V$ in Figure 2.3 and find that for $\downarrow$-spin there is only an impurity state and no defect state.

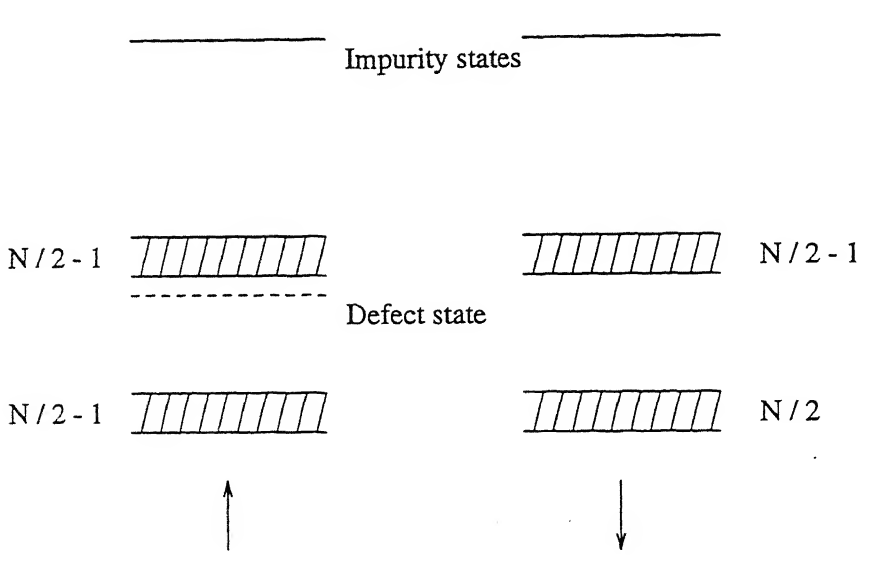

Figure 2.2: Energy spectra for the two spins for an impurity on an A-sublattice site.

Both the impurity state and the defect state, lying as they do outside the AF band, are calised. From Equation 2.15 the change in the Green's function,

$$\delta G_{ij}(\omega) = G_{ij}(\omega) - g_{ij}(\omega), \tag{2.17}$$

ıe to impurity scattering can be written, for energies outside the band and very close to .e defect state energy, E_d, as:

$$\delta G_{ij}(\omega \sim E_d) = \frac{g_{iI}(E_d)\left[-\frac{\partial g_{II}(\omega)}{\partial \omega}|_{\omega=E_d}\right]^{-1} g_{Ij}(E_d)}{\omega - E_d + i\eta} \tag{2.18}$$

here $g_{II}(\omega)$ has been Taylor-expanded near E_d, and we have used $1 - V g_{II}(E_d) = 0$ which :termines E_d. The above equation can be rewritten in the following form, yielding the :fect state Green's function in terms of $\phi_d^i \equiv g_{iI}(E_d)/\sqrt{-\partial g_{II}(\omega)/\partial\omega|_{E_d}}$, which gives the nplitudes for the defect state,

$$\delta G_{ij}(\omega \sim E_d) = \frac{\phi_d^i \phi_d^j}{\omega - E_d + i\eta}. \tag{2.19}$$

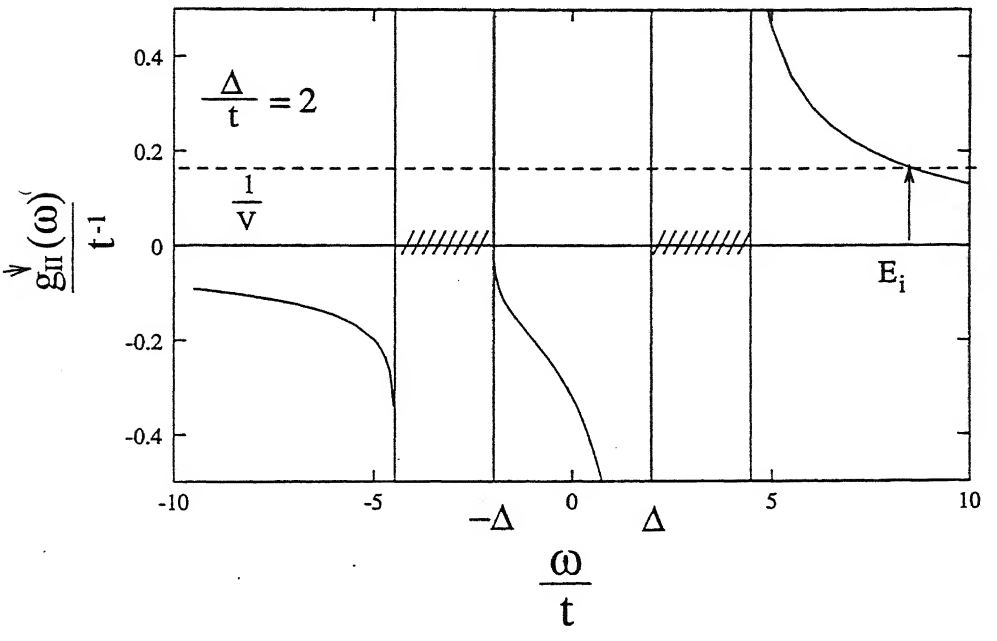

Figure 2.3: Plot of $g_{II}^{\downarrow}(\omega)$ and $1/V$.

The impurity state Green's function can be written in an exactly parallel manner, yielding the impurity state wave function, ϕ_i^i. Impurity state wave function is essentially localised on the impurity site in the strong-coupling limit and for large V. Continuing with the defect state properties, in the limit $V \to \infty$ in the strong-coupling limit, ϕ_d^i has vanishing amplitude on all A-sublattice sites, and on the B-sublattice sites, as mentioned above, it is given by $\phi_d(\vec{r}) \sim \sum_k \epsilon_k^{-1} \exp(i\vec{k}.\vec{r})$, where $\vec{r} \equiv \vec{r}_i - \vec{r}_I$. (For details see Appendix B). At large distances, the long-wavelength modes contribute predominantly, and this yields a power-law fall-off, $\phi_d(\vec{r}) \sim (\sin k_x^c x/x).(\sin k_y^c y/y)$, where k_x^c and k_x^c are the short-wavelength cut-offs in k_x and k_y respectively.

The defect state density for different values of η (or equivalently different V's) for a fixed Δ $(= 5)$ around the impurity site is shown in Figures 2.4, 2.5 and 2.6. We observe

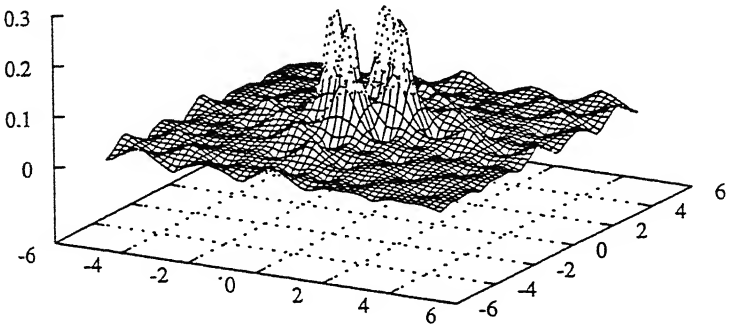

Figure 2.4: Defect state density for $\eta = 0.05$.

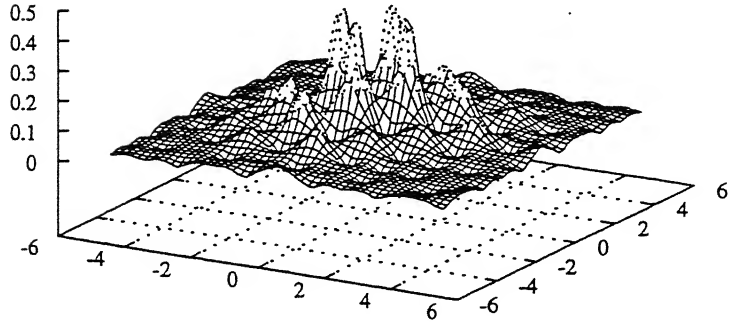

Figure 2.5: Defect state density for $\eta = 0.01$.

that as η decreases *i.e.*, V increases, the defect state has increasingly greater amplitudes on sites away from the impurity site. In other words, it is spatially more extended for larger V's.

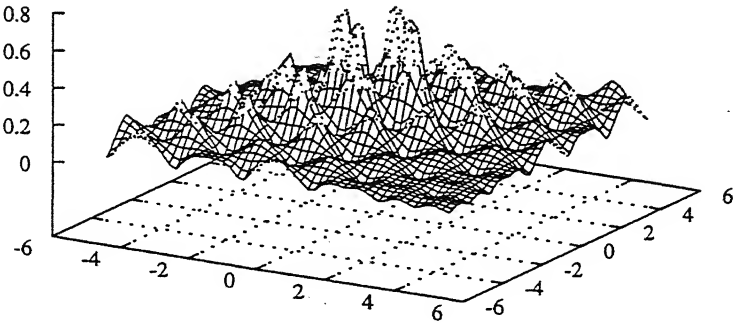

Figure 2.6: Defect state density for $\eta = 0.001$.

We believe that these defect states which are occupied with electrons and localised around the impurity sites are responsible for the presence of local moments observed in these systems. For a zinc atom sitting on an A-sublattice site, the defect state is occupied by an $\uparrow$-spin electron. In terms of electrons, the dopant site is occupied by two electrons (empty of holes), and there are $(N-1)$ $\uparrow$-spin and $\downarrow$-spin electrons in the antiferromagnetic band states (in the upper Hubbard band). These electrons form compensated spin systems, and therefore should contribute an essentially temperature-independent (for $T \ll J$) magnetic susceptibility. The lone electron in the localised defect state behaves essentially like a free spin in the dynamical state when there is no barrier between the up and down spin states, and hence should have a Curie-type $1/T$ contribution.

Chapter 3

Static Nonmagnetic Impurities in a Spin-System with Short-Range Order

In Chapter 2 we have discussed the effects of a static, nonmagnetic impurity in an AF id seen that each impurity gives rise to a defect state, which can explain the formation of cal moments seen in the susceptibility and NMR experiments. But moments are also formed compounds without AFLRO. So a study of the effects of static impurities in magnetic stems without long-range-order is relevant. The hope is that if we find such defect states this case also, then we have a more direct way of understanding the formation of local oments in the high-T_c cuprates away from their AF phase.

In this chapter we present the results of our study of nonmagnetic impurities in a spin-stem which does not necessarily have long-range-order. As in the case of an AF, we model nonmagnetic impurity by a high on-site potential (V) on the dopant site to ensure absence any 3d hole density on this site. Our main result is that defect states are formed in this se also. The defect states, lying outside the bands, will be localised and can give rise to cal moments.

The specific model we consider is again a one-band Hubbard model. In the magnetically disordered state, characterised by short-range AF order, a completely unrestricted HF

decoupling of the Hubbard Hamiltonian gives [3]:

$$H_{HF} = \mathcal{T} - \sum_i \Psi_i^\dagger [\vec{\sigma}.\vec{\Delta}_i]\Psi_i + \sum_i \Psi_i^\dagger [\frac{Un_i}{2}1]\Psi_i \tag{3.1}$$

where $\mathcal{T}$ is the hopping term, $\Psi_i^\dagger \equiv \begin{pmatrix} a_{i\uparrow}^\dagger & a_{i\downarrow}^\dagger \end{pmatrix}$, and $\vec{\Delta}_i \equiv U\langle\Psi_i^\dagger|\frac{1}{2}\vec{\sigma}|\Psi_i\rangle$. Here $\vec{\Delta}_i$ represents the local magnetic field seen by an electron on site i due to electronic correlations. For the case of one electron per site, the (last) density term simply shifts the energy levels by $U/2$. All the $\vec{\Delta}_i$'s have the same norm, but they vary in direction, which is a signature of lack of long-range-order in the system.

3.1 Analysis of impurities in a two-site system

In order to gain some elementary understanding of the system, we first consider a two-site system as shown in Figure 3.1. On site 1 the spin is pointing along the z-direction (-↑).

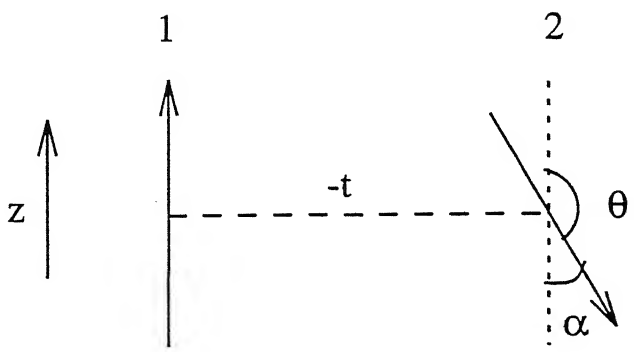

Figure 3.1: A two-site cluster.

On site 2 the spin makes an angle θ with the z-direction, *i.e.*, it is tilted at an angle $\alpha = \theta - \pi$ from a perfect AF direction. In the atomic limit ($t = 0$) the Hamiltonian $\left[\vec{\sigma}.\vec{\Delta}\right]$ for this system can be written in the two-site, two-spin basis as a 4×4 matrix,

$$H = \begin{bmatrix} -\Delta & 0 & 0 & 0 \\ 0 & \Delta & 0 & 0 \\ 0 & 0 & \Delta\cos\theta & -\Delta\sin\theta \\ 0 & 0 & -\Delta\sin\theta & -\Delta\cos\theta \end{bmatrix} \tag{3.2}$$

Diagonalising this Hamiltonian we get two sets of degenerate eigenvalues, $-\Delta$, $-\Delta$ and
Δ, $+\Delta$ with eigenvectors

$$\begin{pmatrix} 1 \\ 0 \\ 0 \\ 0 \end{pmatrix}, \begin{pmatrix} 0 \\ 0 \\ \cos\theta/2 \\ \sin\theta/2 \end{pmatrix}, \begin{pmatrix} 0 \\ 1 \\ 0 \\ 0 \end{pmatrix} \text{ and } \begin{pmatrix} 0 \\ 0 \\ \sin\theta/2 \\ -\cos\theta/2 \end{pmatrix}$$

spectively. We now treat the effect of hopping as a perturbation to these states.

We do a standard degenerate perturbation theory to first order in t. (For details see ppendix C). Once the hoppings are introduced, the states at $-\Delta$ split-off to two states at $\Delta \pm t\cos\theta/2$ and the ones at $+\Delta$ to $+\Delta \pm t\cos\theta/2$. It also tells us that the $\uparrow$-spin hole nsity of 1 on site 1 is equally distributed to the two states at $-\Delta \pm t\cos\theta/2$. If θ is not ıch different from π, we can assume that hoppings will transfer some spectral weight to the per-'band' which will essentially be same as that in a perfect AF system. So, in the strong-upling limit, distribution of $\uparrow$-spin weight of 1 on site 1 in the four states are $\frac{1}{2}(1-\frac{t^2}{\Delta^2})$, $1-\frac{t^2}{\Delta^2}$), $\frac{1}{2}\frac{t^2}{\Delta^2}$ and $\frac{1}{2}\frac{t^2}{\Delta^2}$ respectively in $-\Delta - t\cos\theta/2$, $-\Delta + t\cos\theta/2$, $+\Delta - t\cos\theta/2$ and $\Delta + t\cos\theta/2$ to first order in perturbation theory. It is easy to see that to next order e energies in the upper and lower 'bands' are shifted by constant amounts, $+\frac{t^2}{2\Delta}$ and $-\frac{t^2}{2\Delta}$ spectively, independent of θ.

From our analysis of static nonmagnetic impurities in a Mott-Hubbard AF in Chapter 2 know that if we place an impurity on site 1 we will have additional states within the 'gap' ıen $g^{\sigma}_{11}(\omega) = \frac{1}{V}$ for some ω within the 'gap'. In the limit $V \to \infty$ this gives,

$$\frac{\frac{1}{2}(1-\frac{t^2}{\Delta^2})}{\omega-(-\Delta-\frac{t^2}{2\Delta}-t\cos\theta/2)}+\frac{\frac{1}{2}(1-\frac{t^2}{\Delta^2})}{\omega-(-\Delta-\frac{t^2}{2\Delta}+t\cos\theta/2)}+$$
$$\frac{\frac{1}{2}\frac{t^2}{\Delta^2}}{\omega-(\Delta+\frac{t^2}{2\Delta}-t\cos\theta/2)}+\frac{\frac{1}{2}\frac{t^2}{\Delta^2}}{\omega-(\Delta+\frac{t^2}{2\Delta}+t\cos\theta/2)}=0 \tag{3.3}$$

For a perfect AF arrangement, *i.e.*, $\theta=\pi$, this reduces to

$$\frac{1-\frac{t^2}{\Delta^2}}{\omega+\Delta+\frac{t^2}{2\Delta}}+\frac{\frac{t^2}{\Delta^2}}{\omega-\Delta-\frac{t^2}{2\Delta}}=0 \tag{3.4}$$

For ω's within the 'gap', *i.e.*, between $-\Delta$ and $+\Delta$, the first term is always positive and the second term is always negative. In the strong-coupling limit, the numerator of the first term is close to one and that of the second term is close to zero. So, for the second term to cancel the first one its denominator also has to be small. In other words, the position of the defect state will be close to $+\Delta$. In fact, from Equation 3.4 we get,

$$E_d=\Delta-\frac{3}{2}\frac{t^2}{\Delta} \tag{3.5}$$

Following a similar line of reasoning one can see that for some θ close to but not exactly equal to π, the defect state will be close to and slightly below the state at $\Delta+\frac{t^2}{2\Delta}-t\cos\theta/2$ (Figure 3.2). So for with increasing α's the position of the defect state will be lowered.

3.2 Exact eigenstates analysis of impurities in a five-site cluster

With this elementary understanding of the effect of impurities in a spin-system which does not have a perfect AF order, we proceed to present our analysis of nonmagnetic impurities in a five site cluster of Hubbard model, within an exact eigenstates analysis. The system we consider is shown in Figure 3.3.

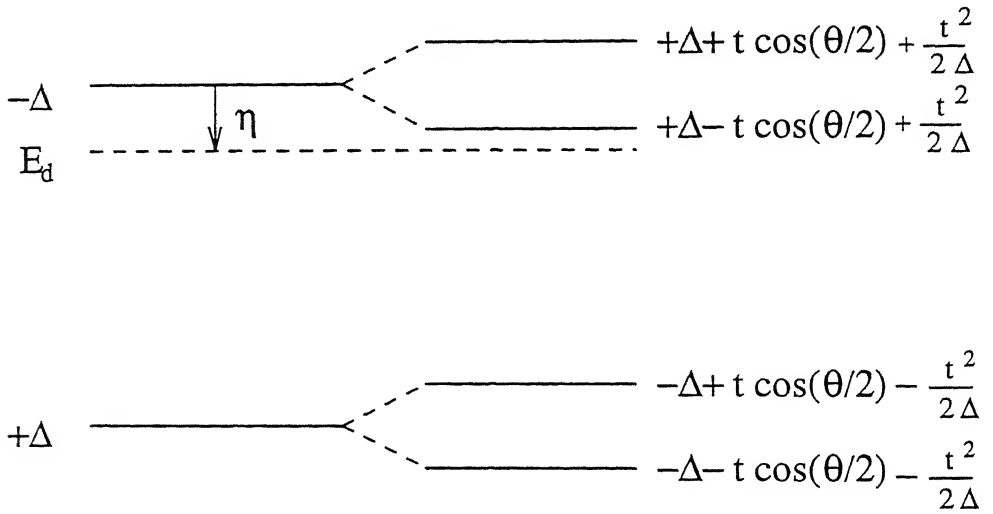

Figure 3.2: Position of the defect state in a two-site cluster.

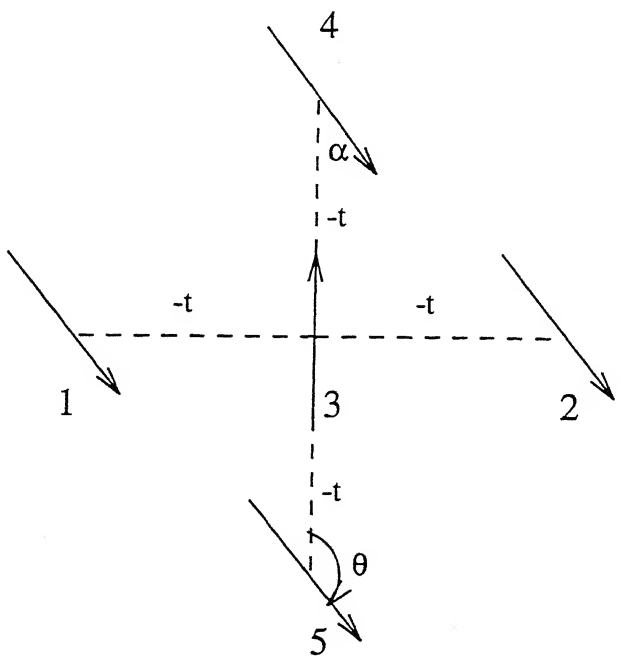

Figure 3.3: A five-site cluster.

We assume that on the central site the spin is pointing 'up'. On the four neighbouring sites the spins are tilted at an angle α with respect to a perfect AF arrangement, *i.e.*, they make angles $\theta = \pi - \alpha$ with the z-direction. In the magnetically disordered state, characterised by short-range order, that we are talking about, α is a measure of the inverse correlation length of the system, in fact, $\alpha \sim \pi\xi^{-1}$ [66]. We now find the position of the defect state as a function of α or the inverse correlation length.

In the site-plus-two-spin basis, the Hamiltonian matrix for the system is a 10×10 matrix as shown in Appendix D.

The energy-scale in the problem is set by taking $t = 1$. We take $\Delta = 4.0$ and $V = 15$. Again, if a nonmagnetic impurity is put on site 3, the position of the defect state will be given by that ω for which $G^{\sigma}_{33}(\omega) = 1/V$. So, the task is to calculate $G^{\sigma}_{33}(\omega)$ from the eigenvalues and eigenvectors of H for some chosen θ and to find that value of ω for which $G^{\sigma}_{33}(\omega) = 1/V$. By the construction of $[H]$, the $\uparrow$-spin amplitude on the central site for the n-th energy state is given by $\psi_n(5)$, where $[\psi]$'s are the eigenvectors of $[H]$. That for the $\downarrow$-spin is given by $\psi_n(6)$. So, the local Green's functions on site 3 are given by,

$$G^{\uparrow}_{33}(\omega) = \sum_n \frac{\psi_n(5)^2}{\omega - \lambda_n} \tag{3.6}$$

$$G^{\downarrow}_{33}(\omega) = \sum_n \frac{\psi_n(6)^2}{\omega - \lambda_n} \tag{3.7}$$

λ_n being the n-th eigenvalue of the Hamiltonian. It turns out that for ω within the 'gap', the $\downarrow$-spin Green's function is negative so that $G^{\downarrow}_{33}(\omega)$ can never be equal to $1/V$ for positive V. We solve Equation 3.6 for ω to see if there are any states in the gap.

We find that with increasing α the five states in the upper 'band' spreads out in energy. But there is always a value of ω below the lowest of them which satisfies Equation 3.6. So irrespective of the range of order in the system, we always have a defect state within the 'gap'. Figure 3.4 shows η, the position of the defect state from Δ as function of inverse

relation length α of the system.

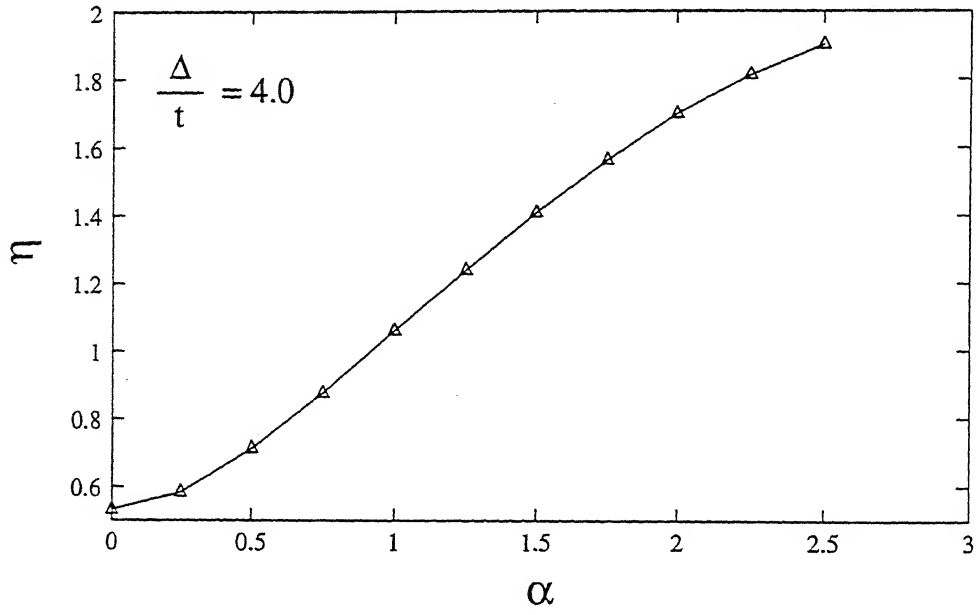

Figure 3.4: Position of the defect state with changing α.

The reason why η increases with α can be understood as follows. As we have discussed Chapter 2, the two sublattice structure with unequal distribution of the two kinds of spin ensities on them is responsible for the defect state to be formed near the band edge. With ıcreasing α the difference in densities of the two spin species will be lowered and hence the efect state will be formed more and more near the mid-gap position.

Chapter 4

Impurity-Scattering of Spin-Waves in a Doped Mott-Hubbard Antiferromagnet

In this chapter we extend our T-matrix analysis to examine impurity scattering of spin waves within the Hubbard-model representation of an antiferromagnetic insulator doped with static, non-magnetic impurities. The transverse spin-fluctuation propagator has been obtained within the Random Phase Approximation (RPA), and impurity-scattering-induced correction to spin-wave energy of long-wavelength modes has been obtained to first order in doping concentration x. In agreement with earlier results [5], we find a logarithmically divergent reduction in the spin-wave energy of long-wavelength modes in two dimensions. We also extend this analysis to a layered Mott-Hubbard system and show that the impurity-scattering-induced softening of spin-wave energies has a direct bearing on the almost linear reduction of the Néel temperature $T_{\rm N}$ with x as seen from neutron-scattering studies [4].

At the RPA level the transverse spin-fluctuation propagator for the doped system is given by $[\chi^{-+}(\Omega)] = [\chi^0(\Omega)]/\mathbf{1} - U[\chi^0(\Omega)]$, where $[\chi^0(\Omega)]$ is the bare, antiparallel-spin particle-hole propagator, and the pole $\mathbf{1} - U[\chi^0(\Omega)] = 0$ yields the spin-wave energies. We have obtained the correction to spin-wave energies perturbatively in terms of $[\delta\chi^0] \equiv [\chi^0] - [\chi^0_{\rm host}]$, the

:turbation introduced due to impurity terms in the host antiferromagnet. $[\delta\chi^0]$ has been ıluated, in turn, in terms of the modification δG^σ to the one-particle Green's function tained within the T-matrix analysis.

.1 Spin-wave spectral properties of a doped 2D antiferromagnet

In this section we focus on the spin-wave spectral properties of a doped, two-mensional AF. In order to obtain the impurity-induced perturbation $[\delta\chi^0(\Omega)]_{ij} = \int \frac{d\Omega'}{2\pi}\left[G^\uparrow_{ij}(\Omega')G^\downarrow_{ji}(\Omega'-\Omega) - g^\uparrow_{ij}(\Omega')g^\downarrow_{ji}(\Omega'-\Omega)\right]$, mentioned earlier, we consider first the lo-l density modifications caused by the high impurity potential.

For simplicity we consider the host antiferromagnet in the strong coupling limit ($U \gg t$). this limit, to order (t^2/Δ^2), the hole and particle densities on sites of the two sublattices and B have values $1 - t^2/\Delta^2$ and t^2/Δ^2. Suppose on A sublattice sites, the spin-$\uparrow$ and ›in-$\downarrow$ hole densities (coming from the lower Hubbard band) have values $1-t^2/\Delta^2$ and t^2/Δ^2 spectively. If now on a site $I \in A$, an impurity is placed with a high impurity potential $' \to \infty$), the small local spin-$\downarrow$ hole density (t^2/Δ^2) is displaced, mainly to the four nearest eighbour (NN) sites. This can also be seen by explicitly evaluating the correction to spin-$\downarrow$ ›le density on the NN sites from the Green's function in Equation 2.17. If J labels the NN tes and $\vec{\delta} \equiv \vec{r}_J - \vec{r}_I$, then for $\delta n^\downarrow_J = -i\int \frac{d\omega}{2\pi}\delta G^\downarrow_{JJ}(\omega)$, we obtain, using Equation 2.17 and ›urier transforming the host Green's functions,

$$\begin{aligned}\delta n^\downarrow_J &= \frac{1}{N^2}\sum_{\vec{k},\vec{k}'}\left(\frac{\epsilon_{\vec{k}}}{2\Delta}\right)\left(-\frac{\epsilon_{\vec{k}'}}{2\Delta}\right)\frac{1}{E^\ominus_{\vec{k}} - E^\oplus_{\vec{k}'}}\left(\frac{-1}{\frac{1}{N}\sum_{\vec{k}''}\frac{1}{E^\ominus_{\vec{k}}-E^\oplus_{\vec{k}''}}}\right)e^{i(\vec{k}-\vec{k}').\vec{\delta}} \\ &= \frac{1}{N}\sum_{\vec{Q}}\gamma_{\vec{Q}}e^{i\vec{Q}.\vec{\delta}}.\frac{t^2}{\Delta^2} = \frac{1}{4}\frac{t^2}{\Delta^2} \qquad (4.1)\end{aligned}$$

he two host Green's function terms in Equation 2.17 contribute the two $\epsilon_{\vec{k}}/2\Delta$ factors, being

off-diagonal in the two-sublattice basis. In the $V \to \infty$ limit the denominator $1 - V g^{\sigma}_{II}(\omega)$ has been approximated by $-V g^{\sigma}_{II}(\omega)$, as the host Green's function is nonvanishing for ω lying within the bands. Also we have used $\sum_{\vec{k}} \epsilon_{\vec{k}} \epsilon_{\vec{k}-\vec{Q}} = \gamma_{\vec{Q}} = (\cos Q_x + \cos Q_y)/2$. Here the frequency integral has been performed by replacing with a contour integral over the upper half plane so as to pick poles which correspond to holes in the lower Hubbard band, and only terms up to order t^2/Δ^2 have been retained. This correction to spin-$\downarrow$ hole density on NN sites can be equivalently considered in terms of a correction to the local spin-$\downarrow$ spectral function in the lower Hubbard band. In the same manner we obtain the correction to the local spin-$\uparrow$ spectral function in the upper Hubbard band, yielding an identical correction to the spin-$\uparrow$ particle density on NN sites, again due to displacement from the impurity site. We are now in a position to evaluate the correction $[\delta\chi^0(\Omega)]_{ij} = [\chi^0(\Omega)]_{ij} - [\chi^0_{\text{host}}(\Omega)]_{ij}$, to the bare, antiparallel-spin particle-hole propagator. From the correction to one-particle Green's function given in Equation 2.17, we obtain:

$$[\delta\chi^0(\Omega)]_{ij} = i \int \frac{d\omega}{2\pi} \left[g^{\uparrow}_{ij}(\omega) \delta G^{\downarrow}_{ji}(\omega - \Omega) + \delta G^{\uparrow}_{ij}(\omega) g^{\downarrow}_{ji}(\omega - \Omega) + \delta G^{\uparrow}_{ij}(\omega) \delta G^{\downarrow}_{ji}(\omega - \Omega) \right] \quad (4.2)$$

Now, in the $V \to \infty$ limit, all extended-state wave functions have a vanishing amplitude on the impurity site. The site-localised impurity states are at infinite energy and therefore do not contribute to the particle-hole process. Therefore $[\chi^0(\Omega)]_{ij}$ must vanish if $i/j = I$, i.e. the i-th row and the j-th column of the $[\chi^0]$ matrix are completely zero. This directly leads to the result given below, which can also be obtained from Equation 7.4 by substituting $\delta G^{\sigma}_{ij} = -g^{\sigma}_{ij}$ for $i/j = I$, which similarly follows from $G^{\sigma}_{ij} = 0$ for $i/j = I$,

$$[\delta\chi^0(\Omega)]_{ij} = -[\chi^0_{\text{host}}(\Omega)]_{ij} \qquad (i/j = I) \quad (4.3)$$

For $i/j = I$, we have thus obtained the correction $[\delta\chi^0(\Omega)]_{ij}$ in terms of the corresponding matrix elements for the host antiferromagnet. The undoped (host) antiferromagnet

s been studied earlier in detail, in both the strong and intermediate coupling regimes 67]. Here we consider the strong coupling limit which is the simplest to deal with ana- tically. Translational invariance holds only within the two-sublattice basis, and therefore $^0_{\rm host}(\Omega)]_{ij} = (1/N)\sum_{\vec{Q}}[\chi^0_{\rm host}(\vec{Q},\Omega)]e^{i\vec{Q}.(\vec{r}_i-\vec{r}_j)}$. where $[\chi^0_{\rm host}(\vec{Q},\Omega)]$ is a 2×2 matrix in the o-sublattice basis, and is given by Equation 2.10.

Lastly, we consider the diagonal matrix elements $[\delta\chi^0(\Omega)]_{JJ}$ on the NN sites. From our rlier discussion of the displacement of particle and hole densities by the strong impurity otential, a straightforward calculation utilizing the corrections to spectral functions yields $\chi^0(\Omega)]_{JJ} = t^2/4\Delta^3$. The various matrix elements of the correction $[\delta\chi^0(\Omega)]$ to the bare, ntiparallel-spin particle-hole propagator are summarised below:

$$\begin{aligned}
[\delta\chi^0(\Omega)]_{II} &= -\frac{1}{U} + \frac{t^2}{\Delta^3}\left(1+\frac{\Omega}{2J}\right)\\
[\delta\chi^0(\Omega)]_{IJ} &= \frac{1}{4}\frac{t^2}{\Delta^3}\\
[\delta\chi^0(\Omega)]_{JJ} &= \frac{1}{4}\frac{t^2}{\Delta^3}
\end{aligned} \tag{4.4}$$

We now turn to transverse spin-fluctuation modes in the doped system and study the npurity-scattering induced renormalisation of spin-wave energy. As mentioned earlier, we btain corrections to spin-wave energy perturbatively by treating $[\delta\chi^0(\Omega)] \equiv [\chi^0(\Omega)] - \chi^0_{\rm host}(\Omega)]$ as the perturbation matrix, and determining corrections to eigenvalues of $[\chi^0_{\rm host}(\Omega)]$. he eigenvalues and eigenvectors of $[\chi^0_{\rm host}(\Omega)]$ can be labeled by wave-vector $\vec{Q}$, and obtained n terms of the eigensolutions of the 2×2 matrix $[\chi^0_{\rm host}(\vec{Q},\Omega)]$. If $|Q\rangle \equiv (\alpha_{\vec{Q}}\ \ \beta_{\vec{Q}})$ represents he eigenvector of $[\chi^0_{\rm host}(\vec{Q},\Omega)]$, so that $\alpha_{\vec{Q}}$ and $\beta_{\vec{Q}}$ are spin-wave amplitudes on A- and B- ublattice sites respectively, then the eigensolutions $\{\lambda^{(0)}_Q, |Q\rangle\}$ of $[\chi^0_{\rm host}(\Omega)]$, to second order n $(\Omega/2J)$ and Q, are given by:

$$\lambda^{(0)}_Q = \frac{1}{U} - \frac{t^2}{\Delta^3}\left(\frac{Q^2}{4} - \frac{1}{2}\left(\frac{\Omega}{2J}\right)^2\right) \tag{4.5}$$

$$\langle i|Q\rangle = \sqrt{\frac{2}{N}}\begin{pmatrix}\alpha_{\vec{Q}}\\ \beta_{\vec{Q}}\end{pmatrix} e^{i\vec{Q}.\vec{r}_i} = \sqrt{\frac{1}{N}}\begin{pmatrix}\sqrt{1-\frac{\Omega}{2\tilde{J}}}\\ -\sqrt{1+\frac{\Omega}{2\tilde{J}}}\end{pmatrix} e^{i\vec{Q}.\vec{r}_i} \tag{4.6}$$

Before proceeding with the perturbation theory we introduce a transformation which renders the perturbation theory convergent, and therefore easier to implement. This transformation pertains to the freedom in choosing the local matrix element $[\chi^0(\Omega)]_{II}$ arbitrarily. Since the impurity site I is completely decoupled from all other sites in the $V \to \infty$ limit, eigenvalues of $[\chi^0(\Omega)]$ having extended eigenvectors would be independent of the impurity-site matrix element $[\chi^0(\Omega)]_{II}$. Therefore, except for the impurity-site localised eigenvector, all extended-state eigensolutions will remain unchanged with reselect to variation of $[\chi^0(\Omega)]_{II}$. We choose to shift $[\chi^0(\Omega)]_{II}$ up by $1/U$, so that $[\delta\chi^0(\Omega)]$ vanishes to order $1/U$, which results in a fast convergence of the perturbation theory and, as we shall see, to determine corrections to the spin-wave energy in the long-wavelength limit, we do not need to go beyond second order. We now proceed with the perturbative evaluation of correction $\delta\lambda_Q(\Omega)$ to eigenvalues of $[\chi^0_{\text{host}}(\Omega)]$ due to perturbation $[\delta\chi^0(\Omega)]$. From perturbation theory we have,

$$\delta\lambda_Q(\Omega) = \langle Q|\delta\chi^0(\Omega)|Q\rangle + \sum_{Q'} \frac{|\langle Q|\delta\chi^0(\Omega)|Q'\rangle|^2}{\lambda^{(0)}_Q - \lambda^{(0)}_{Q'}} + \cdots \tag{4.7}$$

Now, for a single impurity on site I (in A sublattice) the required matrix elements are evaluated using $[\delta\chi^0(\Omega)]$ from Equation 2.10, and the spin-wave amplitudes $\alpha_{\vec{Q}}, \beta_{\vec{Q}}$ given in Equation. 4.6. Summing over all NN sites of I and using $\gamma_{\vec{Q}} = \sum_{\vec{\delta}} e^{i\vec{Q}.\vec{\delta}}$, we obtain after substituting for the spin-wave amplitudes, and evaluating the matrix element to first order in Ω and Q:

$$\begin{aligned}\langle Q|\delta\chi^0|Q'\rangle &= \frac{1}{N}\frac{t^2}{\Delta^3}\times \\ &\left[\left(1+\frac{\Omega}{2\tilde{J}}\right)\alpha_{\vec{Q}}\alpha_{\vec{Q}'} + \beta_{\vec{Q}}\beta_{\vec{Q}'}\tilde{\gamma}_{\vec{Q}-\vec{Q}'} + \alpha_{\vec{Q}}\beta_{\vec{Q}'}\tilde{\gamma}_{\vec{Q}'} + \beta_{\vec{Q}}\alpha_{\vec{Q}'}\tilde{\gamma}_{\vec{Q}}\right] e^{-i(\vec{Q}-\vec{Q}').\vec{r}_I} \\ &= \frac{1}{N}\frac{t^2}{\Delta^3}\left[\frac{\Omega}{2J}\right] e^{-i(\vec{Q}-\vec{Q}').\vec{r}_I}.\end{aligned} \tag{4.8}$$

nce we are only interested in $O(\Omega^2, Q^2)$ corrections in $\delta\lambda_Q(\Omega)$ in order to obtain the spin-ave velocity renormalisation, we can ignore higher-order terms in $\langle Q|\delta\chi^0|Q'\rangle$ in the second der correction $\delta\lambda_Q^{(2)}(\Omega)$. For the same reason higher-order terms in the perturbation series an be dropped if we are only interested in the low-energy and long-wavelength modes. For ie first-order correction $\delta\lambda_Q^{(1)}(\Omega)$, we do need to consider $\langle Q|\delta\chi^0|Q\rangle$ up to second order in ^{2} and Q^2. We find that the order Ω^2 terms cancel exactly, so that for a single impurity on site I of the A sublattice we obtain

$$\langle Q|\delta\chi^0(\Omega)|Q\rangle = \frac{1}{N}\frac{t^2}{\Delta^3}\left[\frac{\Omega}{2J} + \frac{Q^2}{2}\right] \tag{4.9}$$

Now we extend these results for a finite impurity concentration x_A/x_B of impurities on ie A/B sublattice. For an impurity in the B sublattice Ω is replaced by $-\Omega$. If x_A and x_B re the impurity concentrations on A and B sublattices respectively, then summing over all npurity sites I, we obtain for the first and second-order corrections:

$$\delta\lambda_Q^{(1)}(\Omega) = \frac{t^2}{\Delta^3}\left[\frac{\Omega}{2J}\left(\frac{x_A - x_B}{2}\right) + \left(\frac{Q^2}{2}\right)\left(\frac{x_A + x_B}{2}\right)\right] \tag{4.10}$$

$$\delta\lambda_Q^{(2)}(\Omega) = \sum_{Q'\neq Q}\left(\frac{1}{N}\frac{t^2}{\Delta^3}\right)^2 \sum_{I\in A/B}\sum_{I'\in A/B} \frac{\left(\pm\frac{\Omega}{2J}\right)\left(\pm\frac{\Omega}{2J}\right)}{\lambda_Q^{(0)} - \lambda_{Q'}^{(0)}} e^{-i(\vec{Q}-\vec{Q}').(\vec{r}_I - \vec{r}_{I'})} \tag{4.11}$$

If we now perform configuration averaging with $\langle\frac{1}{N}e^{-i(\vec{Q}-\vec{Q}').(\vec{r}_I-\vec{r}_{I'})}\rangle = x_A/x_B\ \delta_{II'}$ (since $) \neq Q'$), so that terms in the product $\langle Q|\delta\chi^0|Q'\rangle\langle Q'|\delta\chi^0|Q\rangle$ pair-up with the same impurity ite, then the configuration-averaged second-order correction $\langle\delta\lambda_Q^{(2)}\rangle$ is obtained as:

$$\langle\delta\lambda_Q^{(2)}\rangle = \left(\frac{t^2}{\Delta^3}\right)^2\left(\frac{\Omega}{2J}\right)^2\left(\frac{x_A + x_B}{2}\right)\frac{1}{N}\sum_{Q'}\frac{1}{\lambda_Q^{(0)} - \lambda_{Q'}^{(0)}} \tag{4.12}$$

n the symmetric case when $x_A = x_B = x$, the $O(\Omega)$ term in $\langle\delta\lambda_Q^{(1)}\rangle$ drops out, and substitut-ng for $\lambda_Q^{(0)} - \lambda_{Q'}^{(0)}$ from Equation 4.5 in Equation 4.12, we obtain the following expressions for

the first- and second-order corrections, and therefore, up to second order, for the eigenvalue $\lambda_Q(\Omega)$ we have:

$$\langle \delta\lambda_Q^{(1)} \rangle = \frac{t^2}{\Delta^3}\left[\frac{Q^2}{2}\right] \; x \tag{4.13}$$

$$\langle \delta\lambda_Q^{(2)} \rangle = \frac{t^2}{\Delta^3}\left[\left(\frac{\Omega}{2J}\right)^2\right]\frac{1}{N}\sum_{Q'\neq Q}\frac{4}{Q'^2-Q^2} \; x \tag{4.14}$$

$$\lambda_Q(\Omega) = \frac{1}{U} - \frac{t^2}{\Delta^3}\left[\frac{Q^2}{4}(1-2x) - \frac{1}{2}\left(\frac{\Omega}{2J}\right)^2\left(1+8x\frac{1}{N}\sum_{Q'}\frac{1}{Q'^2-Q^2}\right)\right] \tag{4.15}$$

The spin-wave energy Ω_Q can now be obtained from the pole $1 - U\lambda_Q(\Omega_Q) = 0$. To first order in impurity concentration x, this yields for the spin-wave energy Ω_Q of long-wavelength modes,

$$\begin{aligned}\Omega_Q &= \sqrt{2}JQ\left[1 - x - 4x\,\frac{1}{N}\sum_{Q'}\frac{1}{Q'^2-Q^2}\right] \\ &= \sqrt{2}JQ\left[1 - x - 4x\left(\frac{1}{\pi}\ln\frac{Q_c}{Q} + \frac{i}{2}\right)\right]\end{aligned} \tag{4.16}$$

where Q_c is an upper momentum cutoff of order 1. Thus in two dimensions there is a logarithmic singularity as $Q \to 0$, indicating a logarithmically divergent reduction to the spin-wave velocity. Impurity scattering also introduces an imaginary part in the spin-wave energy leading to a damping of the spin-wave modes.

4.2 Spin-wave spectral properties of a doped layered antiferromagnet

We now extend our analysis of impurity scattering of spin waves to a layered antiferromagnet. All high-T_c cuprates show 3D antiferromagnetic long-range order (AFLRO) below the Néel temperature, due partly to the very small effective interlayer coupling be-

veen copper-oxide planes arising from the orthorhombic distortion. The small in-plane and it-of-plane anisotropies which lead to anisotropy gaps in the spin-wave spectrum also contribute to the finite Néel temperature [68]. In doped cuprates wherein impurities like Zn place the planar Cu sites, T_N is found to decrease almost linearly with increasing impurity oncentration [4]. We have therefore examined effects of impurity scattering of spin waves on agnetic dynamics due to thermal excitation of spin waves in the doped system, aiming at quantitative understanding of reduction of Néel temperature with impurity concentration.

If r denotes the ratio of the interplanar and planar hopping strengths, then the free-article energy for the layered system gets modified to $\epsilon_{\vec{k}} = -2t[\cos k_x + \cos k_y + r \cos k_z]$. gain retaining terms up to order (t^2/Δ^3) in the bare antiparallel-spin particle-hole propagator, we have [3]

$$[\chi^0_{\rm host}(\vec{Q},\Omega)] = \frac{1}{U}\mathbf{1} - \frac{t^2}{\Delta^3}(1+r^2/2)\begin{bmatrix} 1+\frac{\Omega}{2\tilde{J}} & \tilde{\gamma}_{\vec{Q}} \\ \tilde{\gamma}_{\vec{Q}} & 1-\frac{\Omega}{2\tilde{J}} \end{bmatrix} \tag{4.17}$$

here the spin-wave energy scale $\tilde{J}$ is related to the planar exchange energy $J = 4t^2/U$ by $= J(1+r^2/2)$, and $\tilde{\gamma}_{\vec{Q}} = (\cos Q_x + \cos Q_y + r^2 \cos Q_z)/(2+r^2)$. The spin-wave energy has he same form $\Omega_Q = 2\tilde{J}\sqrt{1-\tilde{\gamma}^2_{\vec{Q}}}$. For high-$T_c$ cuprates $r \ll 1$, so that for long-wavelength lanar modes we have $\tilde{\gamma}^2_{\vec{Q}} \approx 1 - Q_p^2/2 - r^2(1-\cos Q_z)$, where $Q_p \equiv \sqrt{Q_x^2+Q_y^2}$ is the planar omentum. The zeroth-order eigenvalue in Equation 4.5 therefore gets modified to:

$$\lambda^{(0)}_Q(\Omega) = \frac{1}{U} - \frac{t^2}{\Delta^3}(1+r^2/2)\left(\frac{Q_p^2}{4} - \frac{1}{2}\left(\frac{\Omega}{2J}\right)^2 + \frac{r^2}{2}(1-\cos Q_z)\right) \tag{4.18}$$

nd up to second order in $\Omega/2J$, Q_p and r the spin-wave amplitudes remain unchanged as iven in Equation 4.6. The impurity-induced perturbation $[\delta\chi^0(\Omega)]$ to the antiparallel-spin, article-hole propagator can be evaluated using the analysis presented before, and the matrix lements given in Equation 4.4 are modified to:

$$
\begin{aligned}
[\delta\chi^0(\Omega)]_{II} &= -\frac{1}{U} + \frac{t^2}{\Delta^3}(1+r^2/2)\left(1+\frac{\Omega}{2J}\right) \\
[\delta\chi^0(\Omega)]_{IJ} &= [\delta\chi^0(\Omega)]_{JJ} = \frac{1}{4}\frac{t^2}{\Delta^3} \\
[\delta\chi^0(\Omega)]_{IK} &= [\delta\chi^0(\Omega)]_{KK} = \frac{1}{4}\frac{t^2}{\Delta^3}r^2
\end{aligned}
\tag{4.19}
$$

where J and K are respectively the in-plane and out-of-plane NN sites of I. As expected, the out-of-plane couplings are reduced by a factor of r^2. Perturbative corrections to eigenvalues of $[\chi^0_{\rm host}(\Omega)]$ can now be calculated as before using these matrix elements of the perturbation matrix $[\delta\chi^0(\Omega)]$. For a single impurity on the A sublattice, in terms of the unchanged spin-wave amplitudes $(\alpha_{\vec{Q}}\ \ \beta_{\vec{Q}})$ given in Equation 4.6, we obtain for the matrix element between spin-wave states $|Q\rangle$ and $|Q'\rangle$,

$$
\begin{aligned}
\langle Q|\delta\chi^0|Q'\rangle = \frac{1}{N}\frac{t^2}{\Delta^3}(1+r^2/2)\times \\
\left[\left(1+\frac{\Omega}{2J}\right)\alpha_{\vec{Q}}\alpha_{\vec{Q}'} + \beta_{\vec{Q}}\beta_{\vec{Q}'}\tilde{\gamma}_{\vec{Q}-\vec{Q}'} + \alpha_{\vec{Q}}\beta_{\vec{Q}'}\tilde{\gamma}_{\vec{Q}'} + \beta_{\vec{Q}}\alpha_{\vec{Q}'}\tilde{\gamma}_{\vec{Q}}\right] e^{-i(\vec{Q}-\vec{Q}').\vec{r}_I},
\end{aligned}
\tag{4.20}
$$

which has the same form as Equation 4.8, however, in terms of $\tilde{\gamma}_{\vec{Q}}$ defined earlier. For $\vec{Q}' \neq \vec{Q}$ we need to evaluate this matrix element to first order only, and substituting the spin-wave amplitudes we obtain the same result as in Equation 4.8 except for the additional factor of $(1+r^2/2)$. For the first order correction we do need to evaluate the matrix element $\langle Q|\delta\chi^0|Q\rangle$ to second order in Ω, Q_p, r as before, and we obtain

$$
\langle Q|\delta\chi^0|Q\rangle = \frac{1}{N}\frac{t^2}{\Delta^3}(1+r^2/2)\left[\frac{\Omega}{2J} + \frac{Q_p^2}{2} + r^2(1-\cos Q_z)\right].
\tag{4.21}
$$

Now for a finite impurity concentration x in the symmetric case ($x_A = x_B = x$), with impurities randomly distributed on sites of the two sublattices, summing over all impurity sites as before and performing the configuration average, we obtain for the first- and second-order corrections:

$$\langle \delta\lambda_Q^{(1)} \rangle = \frac{t^2}{\Delta^3}(1+r^2/2)\left[\frac{Q_p^2}{2} + r^2(1-\cos Q_z)\right] \quad x. \tag{4.22}$$

$$\langle \delta\lambda_Q^{(2)} \rangle = \frac{t^2}{\Delta^3}(1+r^2/2)\left(\frac{\Omega}{2J}\right)^2 \frac{1}{N}\sum_{\vec{Q}'\neq\vec{Q}} \frac{4}{({Q'_p}^2 - Q_p^2) + 2r^2(\cos Q_z - \cos Q'_z)} \quad x. \tag{4.23}$$

'herefore up to second-order in perturbation theory, where terms up to $O(\Omega^2, Q_p^2, r^2)$ have een retained, the corrected eigenvalue is given by:

$$\lambda_Q(\Omega) = \frac{1}{U} - \frac{t^2}{\Delta^3}(1+r^2/2)\times \left[\left(\tfrac{Q_p^2}{4} + \tfrac{r^2}{2}(1-\cos Q_z)\right)(1-2x) - \tfrac{1}{2}\left(\tfrac{\Omega}{2J}\right)^2 (1+8x\ S_r(Q_p,Q_z))\right], \tag{4.24}$$

here $S_r(Q_p,Q_z)$ denotes the sum $(1/N)\sum_{\vec{Q}'}[({Q'_p}^2 - Q_p^2) + 2r^2(\cos Q_z - \cos Q'_z)]^{-1}$. The)in-wave energy Ω_Q is now given by the solution of $1 - U\lambda_Q(\Omega)=0$, and in terms of the)in-wave energy $\Omega_Q^0 = \sqrt{2}J[Q_p^2+2r^2(1-\cos Q_z)]^{1/2}$ for the undoped layered antiferromagnet, e obtain:

$$\Omega_Q = \Omega_Q^0[1 - x - 4x\ S_r(Q_p,Q_z)]. \tag{4.25}$$

We now examine the impurity-scattering-induced renormalisation of spin-wave energy)r the layered system. We show that the interlayer hopping term acts to cutoff the loga- .thmic divergence observed earlier in two dimensions. For this purpose we study the sum $_r(Q_p,Q_z)$ in different limits. Replacing the sum over $\vec{Q}'$ by integrals over Q'_z and Q'_p, and ıcluding a factor of 2 to account for the identical contribution from the corners of the $\vec{Q}'_p$ rillouin zone, we obtain:

$$S_r(Q_p,Q_z) \;=\; 2\int_{-\pi}^{\pi}\frac{dQ'_z}{2\pi}\int_0^{Q_c}\frac{Q'_p dQ'_p}{2\pi}\frac{1}{({Q'_p}^2 - Q_p^2) + 2r^2(\cos Q_z - \cos Q'_z)}$$

$$\approx \frac{1}{2\pi}\int_{-\pi}^{\pi}\frac{dQ_z'}{2\pi}\ln\left(\frac{Q_c^2}{2r^2(\cos Q_z-\cos Q_z')-Q_p^2}\right), \tag{4.26}$$

where Q_c is a planar-momentum cutoff of order 1. Since we are interested in the temperature regime $kT \ll J$ and predominantly long-wavelength spin-wave modes with energy $JQ_p \leq kT$ are thermally excited, therefore we are really interested only in long-wavelength modes with $Q_p \ll 1$. Consequently the cutoff Q_c is typically much larger than Q_p and r, and therefore an additive 1 in the argument of the logarithm in the above equation has been dropped. We now examine $S(Q_p, Q_z)$ in two limiting cases with respect to the planar momentum Q_p and the hopping ratio r.

(a) $Q_p \gg r$: In this limit the r^2 term can be dropped and the integral simply yields $S_r(Q_p, Q_z) \approx (1/2\pi)[\ln(Q_c^2/Q_p^2) + i\pi]$, so that the planar momentum itself acts as the cutoff, just as for the planar system, and the spin-wave energy reduction goes as $\ln(Q_c/Q_p)$.

(b) $Q_p \ll r$: In this limit the Q_p term can be dropped in the integral and in the limit $Q_z \to 0$, we obtain $S_r(Q_p, Q_z \to 0) = (1/2\pi)\ln(Q_c^2/r^2)$. The logarithmic divergence observed for the two dimensional system as the planar momentum goes to zero is therefore removed by the interlayer hopping term as expected, and the spin-wave energy reduction goes as $\ln(Q_c/r)$ in this limit. We can therefore write the renormalized spin-wave energy as,

$$\begin{aligned}\Omega_Q &\simeq \Omega_Q^0\left(1-\alpha x\ln\frac{Q_c}{Q_p}\right) \quad (Q_p \gg r)\\ \Omega_Q &\simeq \Omega_Q^0\left(1-\alpha x\ln\frac{Q_c}{r}\right) \quad (r \gg Q_p).\end{aligned} \tag{4.27}$$

We have neglected the non-singular correction, and α is a constant of order unity which has a value $4/\pi$ in the two limits considered.

.3 Reduction in Néel temperature

We now turn to the magnetic dynamics in a doped layered antiferromagnet and examine ects of impurity scattering of spin waves on reduction in sublattice magnetisation due to ermal excitation of spin waves. Qualitatively, the softening of spin waves due to impurity attering causes an enhancement in their thermal excitation at finite temperature, which ads to a greater thermal reduction in sublattice magnetisation, and hence a lowering of the éel temperature. Using the expression for the renormalized spin-wave energy, we obtain the duction in sublattice magnetisation with temperature within the linear spin-wave theory. xtrapolation of this to the temperature where the sublattice magnetisation vanishes yields quantitative estimate of the Néel temperature. This estimate ignores the temperature gion where critical fluctuations are important. From spin-wave theory the reduction in iblattice magnetisation at a temperature T is given by,

$$\begin{aligned} -\delta M(T) &= \frac{1}{N}\sum_{\vec{Q}} \frac{2J}{\Omega_Q} \frac{2}{e^{\beta\Omega_Q}-1} \\ &= 2\int_{-\pi}^{\pi} \frac{dQ_z}{2\pi} \int_0^{Q_c} \frac{Q_p dQ_p}{2\pi} \frac{2J}{\Omega_Q} \frac{2}{e^{\beta\Omega_Q}-1}, \end{aligned} \tag{4.28}$$

here the spin-wave energy can be written as: $\Omega_Q = \Omega_Q^0[1 - \alpha x \ln(Q_c/(Q_p, r)_{\max})]$. Now, the spin-wave-energy expression the impurity scattering term is $\ln(Q_c/r)$ for $Q_p < r$. owever, we can approximate this term as $\ln(Q_c/r)$ in the whole range of the Q_p integral. his is because thermal excitation of short-wavelength spin-wave modes ($Q_p \sim Q_c \sim 1$) suppressed at low temperatures ($kT \ll J$). Therefore only long wavelength modes are edominantly excited, so that Q_p is closer to r than to 1. Hence the weak logarithmic pendence over Q_p can be neglected in the first approximation. Thus within the q_p integral, e can approximate the spin-wave energy expression as $\Omega_Q = \Omega_Q^0[1-\alpha x \ln(Q_c/r)]$, so that the ipurity-scattering-induced renormalisation is seen effectively as a momentum independent normalisation of the spin-wave energy scale.

The finite-temperature reduction in sublattice magnetisation arising from thermal excitation of spin waves in the undoped layered antiferromagnet has been studied earlier [69], and the integrals over Q_p and Q_z have been evaluated in various temperature regimes. For $kT \gg 2Jr$, which is about 20K for La_2CuO_4 [68], an essentially linear falloff of sublattice magnetisation with temperature was obtained: $-\delta M^0(T) \sim (kT/J)\ln(kT/Jr)$. Incorporating the renormalisation due to impurity scattering, and neglecting the weak logarithmic temperature dependence, we obtain to first order in x:

$$-\delta M(T) \sim \frac{kT}{J} \ln \frac{1}{r} \left(1 + \alpha x \ln \frac{1}{r}\right) \tag{4.29}$$

Now a quantitative estimate for the Néel temperature can be obtained by extrapolating this linear fall-off to the temperature axis which yields the temperature at which the sublattice magnetisation vanishes. Taking the zero-temperature magnetisation as 1.0 (neglecting quantum spin fluctuations which reduce $M(0)$ from 1 to nearly 0.6), we obtain the Néel temperature for the doped antiferromagnet by setting $-\delta M(T_N) = 1$,

$$T_N(x) \sim T_N(0) \left(1 - \alpha x \ln \frac{1}{r}\right) \tag{4.30}$$

where $T_N(0) = J/\ln(1/r)$ provides a quantitative estimate of the Néel temperature for the undoped layered antiferromagnet. In La_2CuO_4 the ratio r of interlayer and planar hopping terms is $\sim 6 \times 10^{-3}$ [68] so that the $\ln(1/r)$ term is about 5. This indicates, upon extrapolation, that the Néel temperature vanishes at impurity concentration of roughly 20%, which agrees well with experiments. It must be mentioned that in La_2CuO_4 there are in-plane and out-of-plane anisotropies as well which lead to anisotropy gaps in the spin-wave spectrum. Anisotropy gap by itself also provides a cutoff in the logarithmic singularity in two dimensions. Therefore a more realistic study for La_2CuO_4 must incorporate both the interlayer hopping and the anisotropy gap Δ_a. For the undoped system the magnetic

namics involving both these has been studied [68], and roughly $\sqrt{r^2 + (\Delta_a/2J)^2}$ is seen to place r as the effective cutoff. Since in La_2CuO_4 both r and $\Delta_a/2J$ are of the same order $\sim 6 \times 10^{-3}$), the falloff of T_N with x will be nearly same as in Equation 4.30.

Chapter 5

Local Moment in Presence of Added Holes

We now consider doping additional holes into an impurity-doped Mott-Hubbard AF. We consider the simplest case where one hole is added in presence of a single impurity. The defect state being the lowest in energy for the holes, the hole will go into this localised state. So in presence of the hole the local moment will be lost. But fluctuations – both thermal and quantum – can transfer some of the spectral weight of the trapped hole to the UHB. In other words, now there will be some spectral weight of the electrons in the defect state, ensuring that part of the moment is recovered. In this Chapter we present an estimate of how the spectral weight of a trapped hole is transfered to UHB and at least part of the local moment survives even in presence of added holes.

In order to calculate the recovery of moment due to thermal fluctuations, we use a numerical Hartree-Fock calculation on a finite-sized lattice. We begin the Chapter by giving a brief outline of our numerical studies on a finite sized Hubbard model in the first section. The later sections give estimates of the recovered moment.

1 Numerical HF studies on a finite-sized Hubbard model

In this section we present the general scheme for numerical HF studies on a finite-sized ıbbard model. The model is again described by the Hamiltonian

$$H = -\sum_{\langle ij\rangle,\sigma}(a^{\dagger}_{i\sigma}a_{j\sigma} + \text{h.c.}) + U\sum_{i} n_{i\uparrow}n_{i\downarrow}, \tag{5.1}$$

.d the technique we use is the same as in Reference [70].

In the HF approximation relevant to symmetry breaking along the z-direction only, the teraction terms can be written as, $U\langle n_{i\uparrow}\rangle n_{i\downarrow} + U\langle n_{i\downarrow}\rangle n_{i\uparrow}$, so that the on-site energy of spin $\equiv -\sigma$ hole on the i-th site is $U\langle n_{i\sigma}\rangle$. In the site basis, matrix elements of the Hamiltonian r spin σ are given by, $\langle i \mid H_\sigma \mid i\rangle = U\langle n_{i\bar{\sigma}}\rangle$ and $\langle i \mid H_\sigma \mid j\rangle = -t$ where i and j are NN ;es. Choice of an initial configuration of spin $\bar{\sigma}$ densities on the lattice gives the starting amiltonian matrix H_σ which is diagonalised to give the eigensolutions $E_{l\sigma}, \phi_{l\sigma}$. From these .e spin densities are evaluated using $\langle n_{i\sigma}\rangle = \sum_{E_{l\sigma}<E_F}(\phi^{i}_{l\sigma})^2$. Now $H_{\bar{\sigma}}$ is formed from these ;nsities and diagonalised, which, in turn, yields $\langle n_{i\bar{\sigma}}\rangle$. The procedure is continued till lf-consistency is achieved. The impurity is modeled, as before, by putting a high on-site ɔtential V on the impurity site for both the spins.

In our model the energy scale is set by t, and we take $U/t = 8$ and $V/t = 15$. We take 10×10 system with periodic boundary conditions. In the pure case there are two bands, ıch containing 50 states, for both $\uparrow$- and $\downarrow$-spins. For each impurity there is one hole less ɔmpared to the half-filled case. So with a single impurity on an A-sublattice site there are) $\uparrow$- and 50 $\downarrow$-spin holes. HF calculation in this case gives rise to a defect state and an ıpurity state for the $\uparrow$-spin and only an impurity state for the $\downarrow$-spin just as we saw in hapter 2. Now there are 49 states in the LHB for the $\uparrow$-spins and the 50th state is the ɛfect state. This defect state, since it is occupied by electrons, we have argued, can give

rise to local moment.

5.2 Recovery of moment due to thermal fluctuations

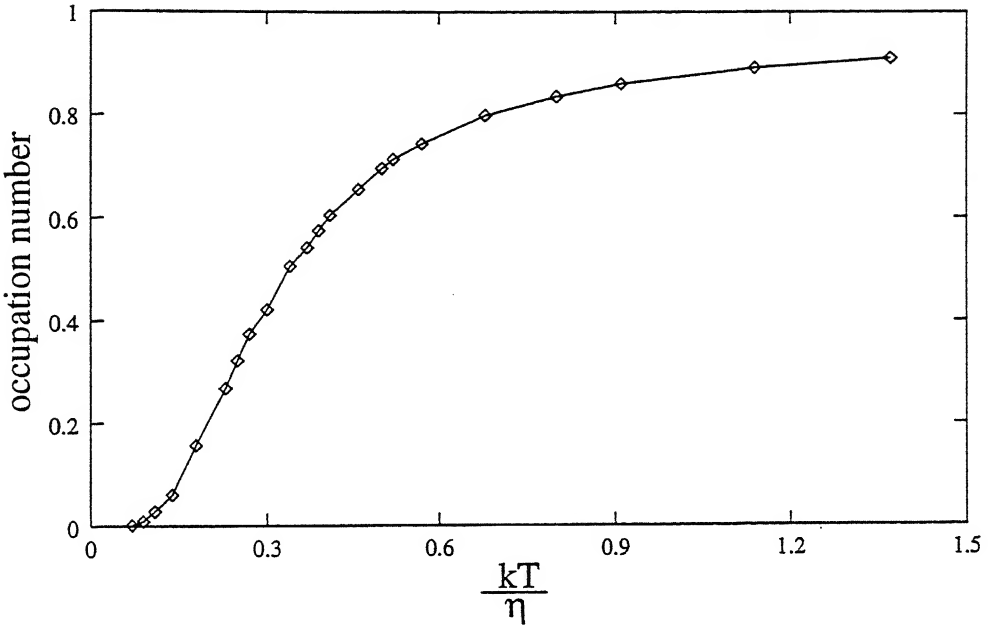

Figure 5.1: Occupation number of electrons in the defect state.

If an ↑-spin hole is now added, it will go in the defect state. In this section we study how the spectral weight of the hole is transfered to the UHB with increasing temperature. We consider a 10×10 Hubbard model with a single impurity as discussed in the previous section. The energy difference between the defect state and the UHB, denoted by η, is found to be $0.189t$ for the set of parameters chosen. At zero temperature, the density of electrons in the defect state is zero. To calculate the density of electrons in this state with increasing temperature, we find out the Fermi energy, μ, of the system at different temperatures. This is done by equating $\sum_i \frac{1}{1+e^{(\epsilon_i-\mu)/kT}}$, where ϵ_i's are the energy eigenvalues of the ↑-spins, to the total number of ↑-spin holes in the system,*i.e.*, 50. The Fermi factor $\frac{1}{1+e^{(E_d-\mu)/kT}}$ then gives the occupation number of holes in the defect state. So the number of electrons in the defect

ce is simply $1 - \frac{1}{1+e^{(E_d-\mu)/kT}}$, which is also a measure of the local moment, the variation which is shown in Figure 5.1. Since the only temperature scale in the system, as far as rmal excitation of holes to the UHB is concerned, is set by η, we plot the occupation nber as a function of $\frac{kT}{\eta}$. As expected, the occupation number of the electrons in the ect state is small at low temperatures as a small fraction of the defect state hole is excited the UHB. Then it grows with increasing temperature and saturates at higher $\frac{kT}{\eta}$. It is lieved that the one-band Hubbard model in the intermediate-coupling ($U \sim$ free-particle ndwidth) regime can represent the CuO_2 planes in the high-T_c cuprates. If the parameters have taken are realistic, ($t = 1$ eV and $U = 8$ eV) then a temperature of 100K corresponds $\frac{kT}{\eta} = 0.04$ and we find that even at this temperature the local moment present in the fect state is quite small.

.3 Recovery of moment due to quantum fluctuations

Due to interaction of the holes with the symmetry-restoring spin waves, part of the fect state spectral-weight will be transfered to the UHB. So, beyond mean-field, at the in-fluctuation level, part of the local moment can be recovered in presence of added holes en at zero temperature. For analytical simplicity we consider the case when impurity otential V is not too large so that the defect state wave function is essentially localised the four NN's of the impurity site. For a single impurity on an A-sublattice site, we are terested in processes like:

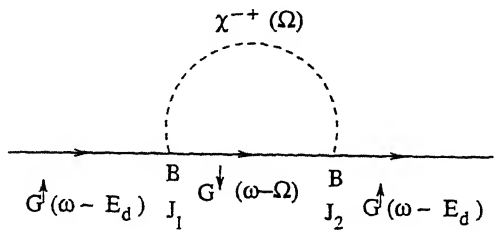

where $G^{\uparrow}(E_d)$'s are the local Green's functions on the NN sites to the impurity, J_1 and J_2 are two NN's of the impurity site residing on the B-sublattice. The self-energy correction due to such interaction of the quasiparticles with the spin waves and the resulting transfer of the spectral-weight to the UHB has been calculated in detail for a pure AF [3]. We proceed along similar lines here. In the sublattice basis and momentum space, the self-energy correction due to the process is

$$\Sigma(\vec{k},\omega) = \frac{1}{N}\sum_{\vec{Q}} \int \frac{d\Omega}{2\pi i} U^2 \chi^{-+}(\vec{Q},\Omega) G^{\downarrow}(\vec{k}-\vec{Q},\omega-\Omega), \tag{5.2}$$

where it is understood that the corresponding elements of the two matrices, χ and $G^{\downarrow}$ are to be multiplied. We note that $G^{\downarrow}(\vec{k}-\vec{Q},\omega-\Omega)$ has to be in the upper band as all the lower band $\downarrow$-spin states are occupied. The χ^{-+} matrix has the following form in the strong-coupling limit [3]:

$$\chi^{-+}(\vec{Q},\Omega) = -\frac{1}{2}\begin{bmatrix} 1-\frac{\Omega}{2J} & -\gamma_{\vec{Q}} \\ -\gamma_{\vec{Q}} & 1+\frac{\Omega}{2J} \end{bmatrix} \frac{1}{\sqrt{1-\gamma_{\vec{Q}}^2}} \left[\frac{1}{\Omega-\Omega_{\vec{Q}}+i\eta} - \frac{1}{\Omega+\Omega_{\vec{Q}}-i\eta}\right], \tag{5.3}$$

where $\Omega_{\vec{Q}}$'s are the spin-wave energies. Now picking up the appropriate matrix elements, replacing the Ω-integral by a contour integral and taking residues at the spin-wave poles we have,

$$\Sigma_{BB}(\vec{k},\omega) = -\frac{U^2}{2}\frac{1}{N}\sum_{\vec{Q}} \left(1+\frac{\Omega_{\vec{Q}}}{2J}\right) \frac{1}{\sqrt{1-\gamma_{\vec{Q}}^2}} \frac{t^2/\Delta^2}{\omega-\Omega_{\vec{Q}}-E^{\oplus}_{\vec{k}-\vec{Q}}+i\delta}. \tag{5.4}$$

As the $\downarrow$-spin Green's function is in the upper band, only one of the spin wave poles, which has a negative imaginary part, contributes in the contour integral. It has been assumed that the spin wave amplitude on the sites neighbouring the impurity remain essentially unchanged in presence of impurities. So for two particular NN sites J_1 and J_2,

$$\Sigma_{J_1,J_2}(\omega) = -\frac{U^2}{2}\frac{1}{N}\sum_{\vec{k}}\frac{1}{N}\sum_{\vec{Q}}\left(1+\frac{\Omega_{\vec{Q}}}{2J}\right)\frac{1}{\sqrt{1-\gamma_{\vec{Q}}^2}}\frac{t^2/\Delta^2}{\omega-\Omega_{\vec{Q}}-E^{\oplus}_{\vec{k}-\vec{Q}}+i\delta}e^{i\vec{k}.(\vec{r}_{J_1}-\vec{r}_{J_2})}. \quad (5.5)$$

In the strong-coupling limit taking $E^{\oplus}_{\vec{k}-\vec{Q}} \sim \Delta$, so that there is no k-dependence, and ing the $\vec{k}$-sum yields,

$$\Sigma(\omega) = -\frac{U^2}{2}\frac{1}{N}\sum_{\vec{Q}}\left(1+\frac{\Omega_{\vec{Q}}}{2J}\right)\frac{1}{\sqrt{1-\gamma_{\vec{Q}}^2}}\frac{t^2/\Delta^2}{\omega-\Omega_{\vec{Q}}-\Delta+i\delta}\delta(\vec{r}_{J_1}-\vec{r}_{J_2}). \quad (5.6)$$

iis shows that the self-energy due to interaction of the quasiparticles with spin-waves is agonal in position space.

The defect state weight of 1 is equally distributed on the 4 NN sites of the impurity. So, corporating the self-energy correction due to interaction with spin waves, the local defect ate Green's function, denoted by $\mathcal{G}$ is modified by

$$\delta\mathcal{G}^{\uparrow}_{JJ}(\omega \sim E_d) = \frac{1/4}{\omega-E_d-i\delta}\Sigma(\omega)\frac{1/4}{\omega-E_d-i\delta}. \quad (5.7)$$

dding contributions from all the four nearest neighbours, the portion of the spectral-weight ansfered to the UHB is

$$4\times\int_{\omega>E_F}\frac{d\omega}{2\pi}2Im\mathcal{G}^{\uparrow}_{JJ}(\omega\sim E_d). \quad (5.8)$$

straightforward integration gives this to be $\frac{1}{2}\frac{t^2}{\eta^2}\frac{1}{N}\sum_{\vec{Q}}\left(1+\frac{\Omega_{\vec{Q}}}{2J}\right)\frac{1}{\sqrt{1-\gamma_{\vec{Q}}^2}}$.

This is correct only in the limit of small V, when the assumptions that $\eta \gg \frac{t^2}{\Delta}$ and that ıe defect state is localised only on the four NN's of the impurity are valid (see Appendix B). lso, the first-order perturbative calculation we have done is meaningful only in the limit small $\frac{t^2}{\eta^2}$. At this stage we cannot perform the Q-sum as we do not have an analytical cpression for the spin-wave energy in presence of impurities over the entire Q-range.

Chapter 6

Static Nonmagnetic Impurities in a Charge-Transfer Insulator

It has already been discussed that electron spectroscopy experiments suggest that the parent compounds of the high-T_c superconductors are CTI's rather than MH insulators. This itself makes the study of static impurities in a CTI interesting. Otherwise, in view of the experiments on static, nonmagnetic-impurity-doped systems, although some of their properties have been understood within a one-band model, as discussed in the previous chapters, others require a more detailed picture like the three-band model for their understanding.

In the one-band Hubbard model in hole picture, the defect state is formed slightly below the upper Hubbard band (UHB), in the Hubbard gap. This being the lowest unoccupied state for the holes, the first added hole goes into this state and the moment is lost. Due to thermal excitation of the hole from the defect state to the UHB at temperatures comparable to the energy difference between the two, and also due to quantum fluctuations, part of the moment can be regained as discussed in Chapter 5. But how, for any kind of nonmagnetic impurity, a moment of $\sim 1.2\mu_B$ per impurity is obtained irrespective of the doping level even at low temperature, and why this moment is $\sim$ 35% less than the theoretically expected value [58] – these questions cannot be answered within a one-band model.

In this chapter we consider the full three-band Hubbard model description of the Cu 3d
:s in the copper-oxide planes in the insulating state and present a self-consistent numerical
study of the system. In the first section we discuss our results for the undoped system.
:he next section a study of the impurity-doped system is presented.

1 Pure system

We consider the three-band Hubbard Hamiltonian given by Equation 1.2 for 3d holes
:he CuO_2 planes. In this section we shall be talking about a half-filled system when we
're exactly one hole per copper site.

For all our calculations we take $t_{pd} = 1.3$ eV, $U_p = 0$ eV, $U_{pd} = 0$ eV, and $\epsilon_p = 3.0$ eV
l $\epsilon_d = 0$ eV so that the bare charge-transfer gap $\Delta = 3.0$ eV, and do a numerical HF
:ulation on a a 10×10 CuO_2 lattice using periodic boundary conditions in both x- and
irections. A more detailed discussion on the choice of the values of parameters is given
:he section on doped system. The numerical HF scheme is same as that for a one-band
bbard model discussed in Chapter 5 the only difference being that now we have to take
e of oxygen and copper sites separately. For AF symmetry breaking along the z-direction
y, the interaction terms can again be written as $U\langle n_{i\uparrow}\rangle n_{i\downarrow} + U\langle n_{i\downarrow}\rangle n_{i\uparrow}$. In the site basis,
trix elements of the Hamiltonian for spin σ are given by, $\langle i \mid H_\sigma \mid i\rangle = \epsilon_d + U_d\langle n_{i\bar{\sigma}}\rangle$ if i is
:u site and $\langle i \mid H_\sigma \mid i\rangle = \epsilon_p + U_p\langle n_{i\bar{\sigma}}\rangle$ if i is an oxygen site. $\langle i \mid H_\sigma \mid j\rangle = \pm t_{pd}$ if i and j
NN Cu and O sites and $\langle l \mid H_\sigma \mid m\rangle = \pm t_{pp}$ if l and m are two NN O sites. After this,
numerical calculation proceeds exactly as before till self-consistency is achieved.

Exact numerical (Quantum Monte Carlo) calculations reveal that the three-band Hub-
:d model with a finite positive U_d possesses an AF ground-state [71]. In order to study the
gnetic behavior of the system with changing U_d we have calculated the sublattice mag-
isation as a function of U_d. Figure 6.1 shows the variation of sublattice magnetisation as
unction of U_d for different values of t_{pp}. For $t_{pp} = 0$ the system goes into an AF state

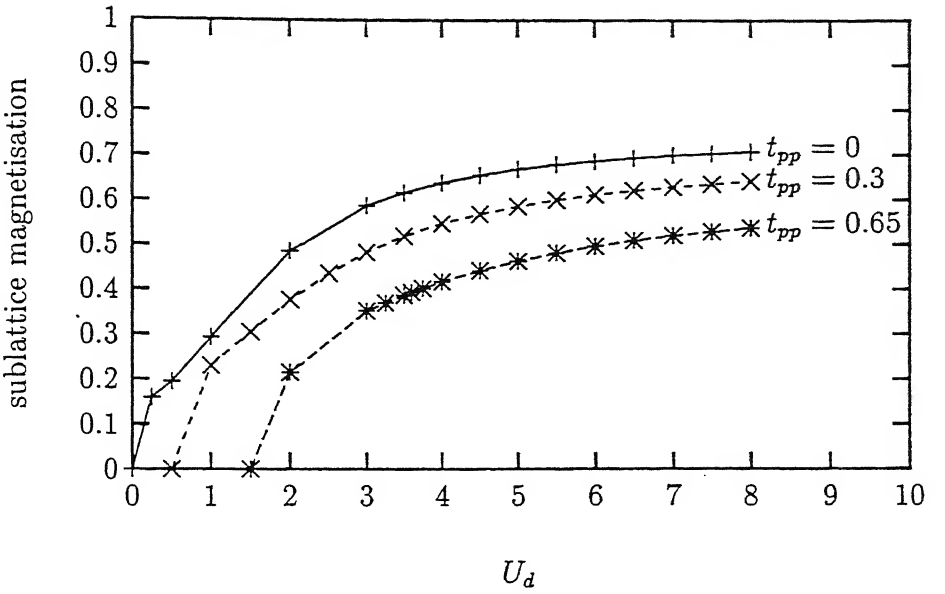

Figure 6.1: Sublattice magnetisation vs. U_d for different t_{pp} (all energies in eV).

for any finite positive U_d. This is because of nesting of the Fermi surface. When $t_{pp} \neq 0$ the system loses its nesting property and a critical value of U_d is required for the system to become antiferromagnetic. This critical value of U_d increases with t_{pp}.

A study of the energy spectrum of the system shows that for large values of U_d ($U_d \gg \Delta$) the system is a CTI. For an $L \times L$ CuO_2 lattice, having L^2 Cu and $2L^2$ O sites, the first $L^2/2$ states form the LHB. The oxygen 2p band in the middle has $2L^2$ states and the UHB has another $L^2/2$ states. The 2p band is further split into three sub-bands similar to Zhang-Rice singlet-triplet splitting. The singlet sub-band lies below the bare oxygen energy, there are a group of non-bonding (NB) states at the bare oxygen energy ϵ_p and the triplet sub-band lies above these NB states. For $U_d < \Delta$ but above the critical value so that the system is an AF, the UHB goes below the oxygen band. The charge-gap is maintained and the system is a MH insulator. Below the critical value of U_d when the sublattice magnetisation vanishes, the charge-gap also disappears and the system becomes a d-type metal. There are no singlet-triplet splitting in the oxygen band in these cases (Figure 6.2). The situation in

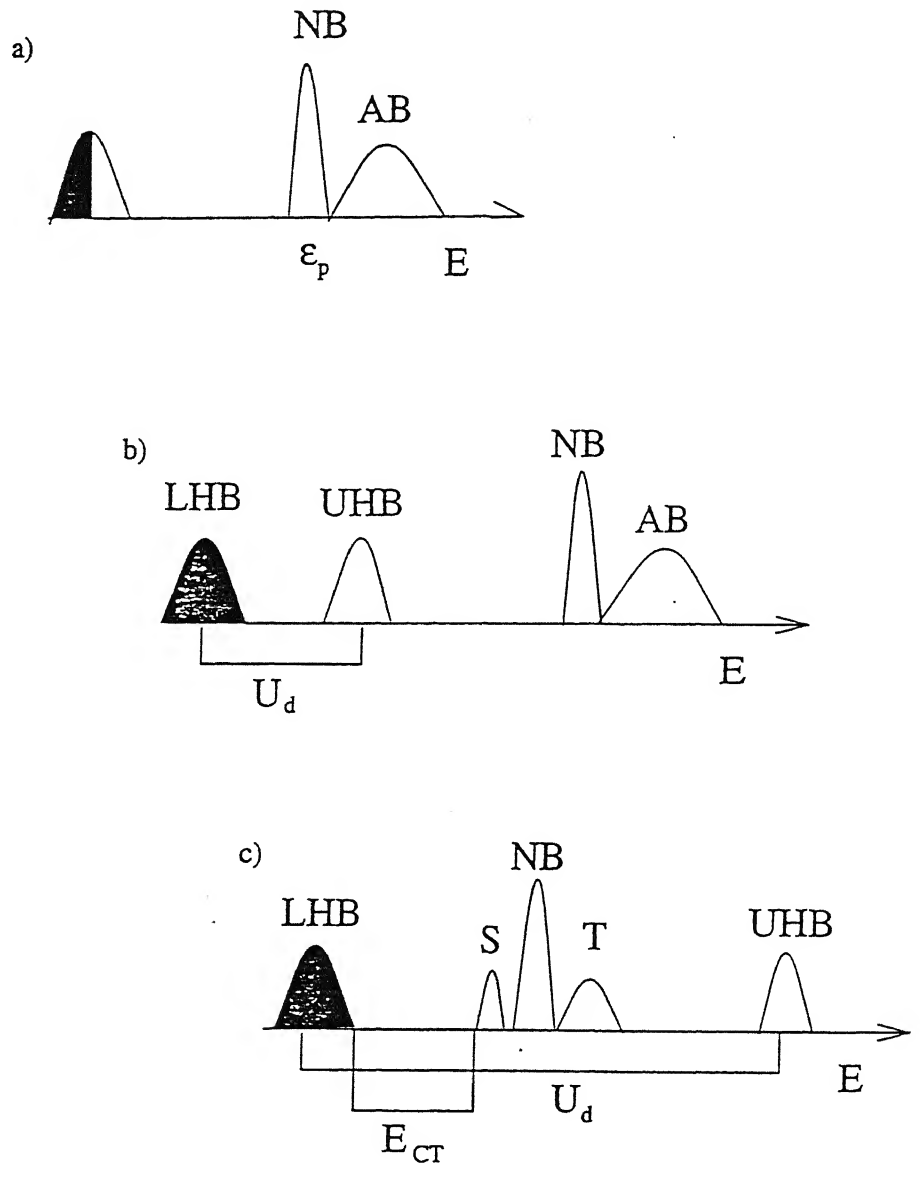

ure 6.2: Single-particle energy-bands for the three-band Hubbard model in the hole pic-
e: (a) metal, (b) Mott-Hubbard insulator, (c) charge-transfer insulator with a singlet-
let splitting. Shaded regions denote the occupied states. [N](A)B=[non](anti)bonding,
singlet, T=triplet, E_{CT} = renormalised charge-transfer gap.

intermediate range of values of U_d is more complicated because the UHB and the oxygen band are strongly mixed.

In the one-band Hubbard model and its strong-coupling analogue, the Heisenberg model, the nature of spin excitations has been studied extensively. It is well known that in these systems the spin-wave spectrum is gapless with the existence of a Goldstone mode and the dispersion for the long-wavelength spin-wave modes is linear in the momentum Q. As already discussed, the spin-wave modes are obtained from the poles of the time-ordered transverse spin propagator $\langle T[S^-(i,t), S^+(j,t')]\rangle$ which, in the random phase approximation, has the form $[\chi^{-+}(\Omega)] = \frac{[\chi^0(\Omega)]}{1-U_d[\chi^0(\Omega)]}$. The matrix elements of $[\chi^0(\Omega)]$, the bare antiparallel-spin particle-hole propagator, are given by,

$$[\chi^0(\Omega)]_{ij} = i\int_{-\infty}^{\infty}\frac{d\omega}{2\pi}g_{ij}^{\uparrow}(\omega)g_{ji}^{\downarrow}(\omega-\Omega), \tag{6.1}$$

where g's are the Green's functions in the AF state. In terms of the eigensolutions E_l, ϕ_l in the self-consistent state, $\chi^0(\Omega)$ has the form:

$$[\chi^0(\Omega)]_{ij} = \sum_{E_{l\uparrow}>E_F}^{E_{m\downarrow}<E_F}\frac{\phi_{l\uparrow}^i\phi_{l\uparrow}^j\phi_{m\downarrow}^i\phi_{m\downarrow}^j}{E_{l\uparrow}-E_{m\downarrow}-\Omega} + \sum_{E_{l\uparrow}<E_F}^{E_{m\downarrow}>E_F}\frac{\phi_{l\uparrow}^i\phi_{l\uparrow}^j\phi_{m\downarrow}^i\phi_{m\downarrow}^j}{E_{m\downarrow}-E_{l\uparrow}+\Omega}. \tag{6.2}$$

Since only the Cu spins form AF order, spin-waves will have amplitude only on the Cu sites, and so we calculate $[\chi^0(\Omega)]_{ij}$ connecting only the Cu sites. In Equation 6.2 the site indices i and j thus run only through the Cu sites, but the eigenvalue indices l and m run through all three bands.

All information regarding the nature of the spin-wave excitations is again contained in the eigensolutions of $[\chi^0(\Omega)]$, as the full RPA susceptibility can be expanded in terms of the eigenvalues $\lambda(\Omega)$ and the eigenvectors $|\,\phi_\lambda(\Omega)\rangle$ of $[\chi^0(\Omega)]$ as:

$$[\chi^{-+}(\Omega)] = \sum_{\lambda}\frac{|\,\phi_\lambda(\Omega)\rangle\langle\phi_\lambda(\Omega)\,|}{1-U_d\lambda(\Omega)}. \tag{6.3}$$

e spin-wave energies are obtained from the pole $1 - U_d\lambda(\Omega) = 0$ in the RPA spin suscep-
lity, and the eigenvector yields the spin-wave amplitude.

In the three-band model, as in the one-band model, the largest eigenvalue $\lambda_{\max}(\Omega = 0)$ the $[\chi^0(\Omega)]$ matrix for $\Omega = 0$ is found to be exactly equal to $\frac{1}{U_d}$, confirming that the n-wave excitations are gapless. Nature of spin-wave modes can be studied by obtaining angles of rotation θ_i of local spin vectors from the spin-wave amplitudes ϕ_i and the local gnetisation S_z^i using [3]:

$$\theta_i = \sin^{-1} \frac{\phi_\lambda^i}{S_z^i}. \tag{6.4}$$

e $\Omega_0 = 0$ mode corresponds to a spin-wave excitation which has equal amplitudes on sites and rotates all the spins by equal angles and is identified as the Goldstone mode. us, as in the one-band model, the spin-wave excitation in a three-band model is gapless l there exists a Goldstone mode as one one would expect in a system with continuous n-rotational symmetry.

2 Impurity-doped system

We have studied the problem of static nonmagnetic impurities doped in the three-band bbard model. As in the one-band case, we model the impurities by a high on-site repulsive ential V to restrict the Cu 3d holes from occupying that site. The Hamiltonian for the urity-doped system is,

$$H = H_{\text{pure}} + V \sum_{I,\sigma} a_{I\sigma}^\dagger a_{I\sigma}, \tag{6.5}$$

ere H_{pure} is the Hamiltonian for the pure system given by Equation 1.2, and I runs over impurity sites.

The values of most of the parameters of the model are related to electron spectroscopy

and are obtained from comparison with the results of these experiments. Different kinds of theoretical techniques give slightly different sets of values. But a generally acceptable set of values is [46] $t_{pd} = 1.3$ eV, $t_{pp} = 0.65$ eV, $U_d = 8.8$ eV, $U_p = 0$ eV, $U_{pd} = 0$ eV, $\Delta = 3.0$ eV. In this section we work with this set of values of the parameters. The pure system at half-filling is a CTI with this set of parameters.

Starting from the pure system at half-filling one Cu 3d hole is removed for each added impurity. For each impurity, depending on the sublattice of its substitution, a self-consistent solution of this Hamiltonian shows that in the spectrum of one particular spin there are three states outside the bands and for the other there is one outside. Consider an impurity on an A-sublattice site (having majority of $\uparrow$-spin holes) in an $L \times L$ system. In the $\uparrow$-spin spectrum there are $(L^2/2 - 1)$ states in the LHB. One state goes out to the impurity state which is the highest in energy ($\sim V$). The oxygen band and the UHB have $(2L^2 - 1)$ and $(L^2/2 - 1)$ states respectively, one state from each coming down to form two defect states. The $L^2/2$-th and the $2L^2$-th states are the two defect states. In the spectrum for the $\downarrow$-spin hole, the LHB and the oxygen band remain unaffected. The UHB has $(L^2/2 - 1)$ states, one state going to the impurity state. The situation is simply reversed if the impurity is placed on a B-sublattice site. The energy-spectra for the two spins for a single impurity on an A-sublattice site is shown in Figure 6.3.

Coming to the nature of these states, we find that the impurity state is essentially site-localised on the impurity site, whereas the lower defect state, coming out of the oxygen band, has amplitude mainly on the oxygen sites around the impurity, and the upper defect state has amplitude mainly on the four Cu sites neighbouring the impurity. In this respect the upper defect state is similar to the defect state in a one-band model. This state, when occupied by electrons, creates a local moment residing predominantly on the four Cu sites neighbouring the impurity. With only a nonmagnetic impurity on an A-sublattice and no

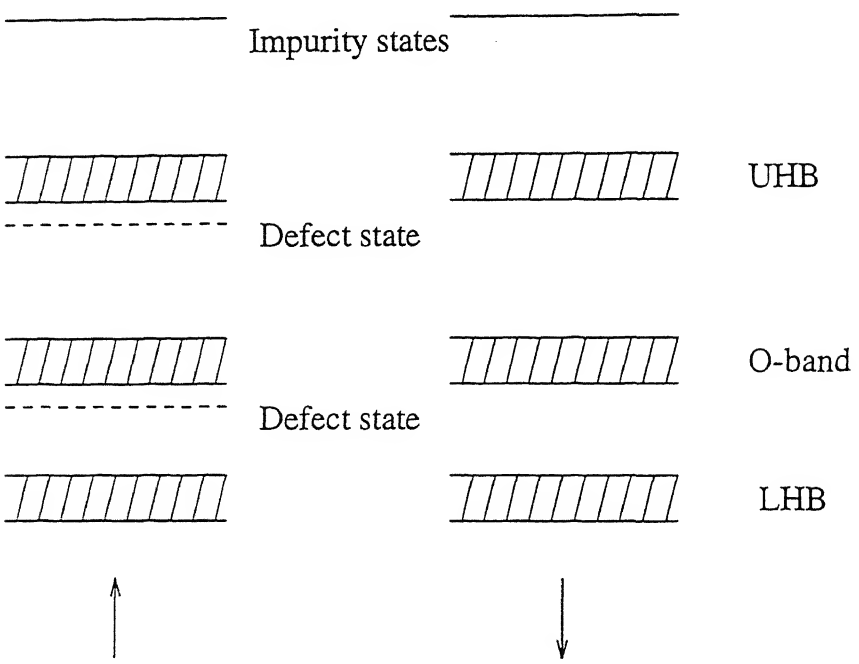

igure 6.3: Energy-spectra for the two spins for a single impurity on an A-sublattice site.

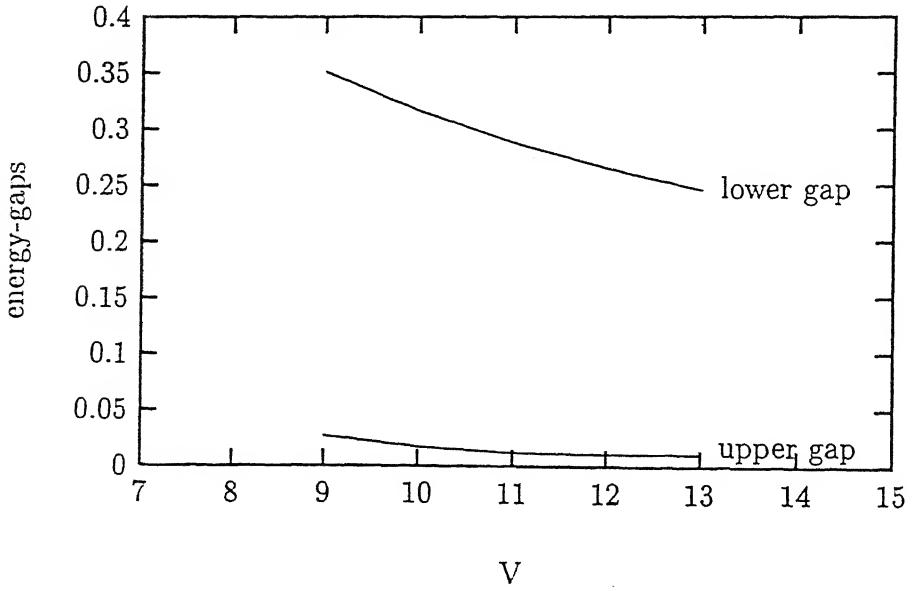

Figure 6.4: Variation of the two energy gaps with V.

extra added hole, the system has $(L^2/2 - 1)$ $\uparrow$-spin and $L^2/2$ $\downarrow$-spin holes. So the LHB is completely filled and all the other states are empty of holes. The lower defect state being the lowest unoccupied state for the holes, the first added $\uparrow$-spin hole goes into this state and subsequent holes go into the oxygen band. So even at finite concentration of hole doping the upper defect state remains occupied by electrons. Thus unlike in one-band model, the local moment in three-band model is robust with respect to hole doping. In Figure 6.4 we show the variations of the two energy gaps — between lower defect-state and oxygen band and the upper defect-state and the UHB. It is interesting to note that although the lower gap varies considerably, the upper gap is relatively insensitive to the variation of V.

The magnitude of the local moment is proportional to the density of the defect state on the copper sites. We find that the total density of the upper defect state on the copper sites is less than 1, and that for a larger value of t_{pd} the reduction is larger. In our calculations, for $t_{pd} = 1.3$ eV about 21% of the defect state density goes out to the oxygen sites, whereas for $t_{pd} = 0.75$ eV, only 7% of the density goes out. This supports the view that part of the local moment is transferred to the oxygen sites because of Cu-O hybridisation, which leads to the observed moment being less than the theoretically expected value. Figure 6.5 and Figure 6.6 show total density of the upper defect state on Cu sites for $t_{pd} = 1.3$ eV and 0.75 eV respectively.

The density is larger for smaller t_{pd} but is interestingly found to be essentially constant over the range of V studied in our calculations. This leads to the significant conclusion that the defect-state-induced moment is more or less independent of the details of the nonmagnetic impurity within our model of the impurity potential term and leads to an understanding of the observation that independent of their detailed electronic nature, all nonmagnetic impurities, Zn^{+2}, Al^{+3}, Ga^{+3}, give moments of same magnitude.

We have also studied the nature of spin-wave excitations in the impurity-doped system. We find that the gapless Goldstone mode associated with spontaneous symmetry-breaking in

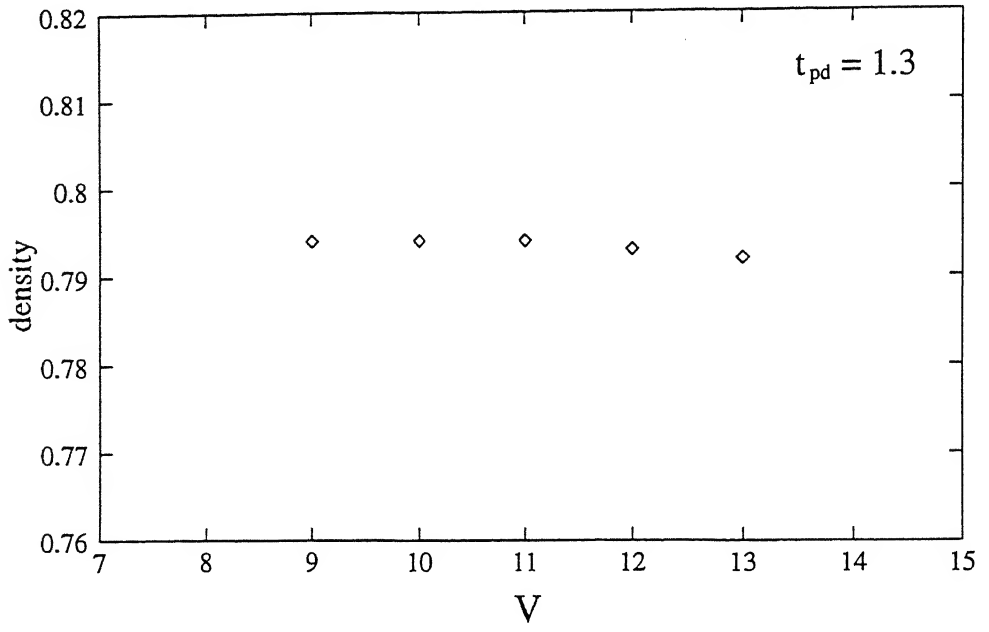

Figure 6.5: Upper defect state density on Cu sites for $t_{pd} = 1.3$ eV.

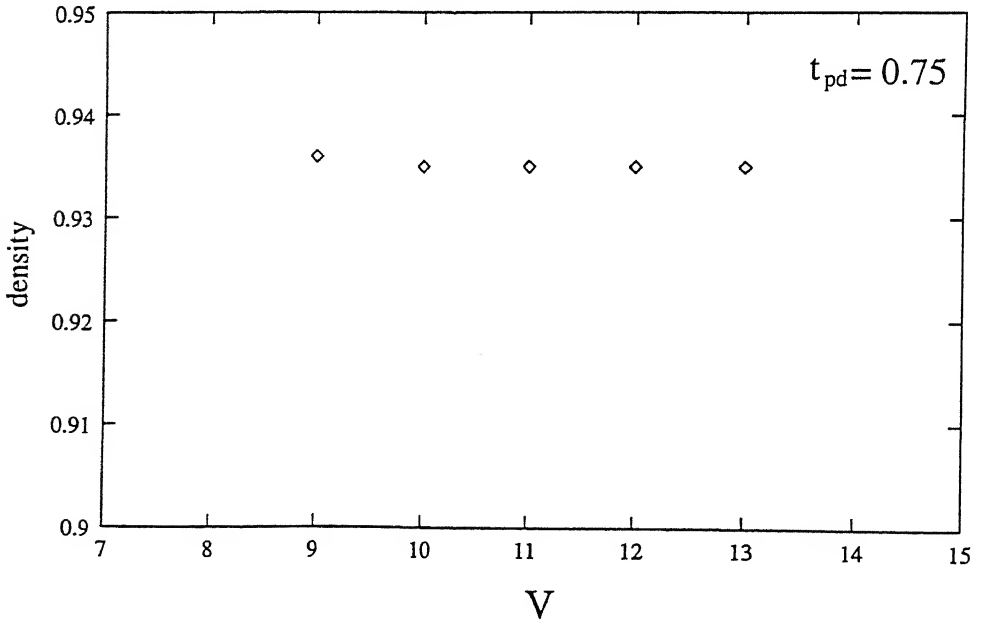

Figure 6.6: Upper defect state density on Cu sites for $t_{pd} = 0.75$ eV.

the AF ground state is preserved in presence of impurities and even when the concentration of impurities on the two sublattices are not equal. This is because the continuous spin-rotational symmetry of the Hamiltonian, which is broken in the AF ground state, is still preserved. Wan *et. al.* [5] have obtained two modes of spin-wave excitation in case of unequal concentration of impurities on the two sublattices. We believe that the gapless mode in our calculation corresponds to their acoustic mode.

hapter 7

tatic Magnetic Impurities in a Iott-Hubbard Antiferromagnet

The effects of nonmagnetic impurities on a Mott-Hubbard AF was studied in Chapters 2 l 4. The problem of magnetic impurities in an AF has been studied within a Heisenberg del by Wan *et al.* [5]. But to our knowledge, no such study of magnetic impurities a Mott-Hubbard AF exists. In this chapter we develop several formalisms, representing 'erent situations, to treat magnetic impurities in a Mott-Hubbard AF.

In the first section we look at the problem of a single-orbital magnetic impurity in a gle-orbital Hubbard model. The impurity is represented by a modified hopping between impurity-orbital and its nearest neighbours, and its effects on the magnon-spectrum is died both within a perturbative and an exact-eigenstates analysis. In the second section extend the spin-independent potential used in the case of a nonmagnetic impurity to pin-dependent potential for a magnetic impurity and study its effects on the electronic ctra and spin-wave properties. In the last section we study the effects of higher-spin purities on a spin 1/2 AF by multiple-orbital representation of the impurity site. We dy their effects on electronic properties and on magnon properties through a numerical study on a finite-sized system.

7.1 Single-orbital magnetic impurity

In this section we consider a single-orbital magnetic impurity in an AF host which is described by the Hubbard model on a square lattice with one orbital per site at half filling. The host Hamiltonian is again given by:

$$H_0 = -t \sum_{\langle ij \rangle \sigma} (a^\dagger_{i\sigma} a_{j\sigma} + a^\dagger_{j\sigma} a_{i\sigma}) + U \sum_i n_{i\uparrow} n_{i\downarrow}. \tag{7.1}$$

where t is the NN hopping strength and U the on-site Coulomb repulsion.

We model the single-orbital impurity by taking the hopping term t' between the impurity orbital and its NN orbitals to be different from the NN hopping terms t in the host system. The Hamiltonian with such an impurity can be written as below, where the sum is over all the impurity sites I and their nearest neighbours J, and $\delta t = t' - t$.

$$H = H_0 + \delta t \sum_{\langle IJ \rangle \sigma} (a^\dagger_{I\sigma} a_{J\sigma} + a^\dagger_{J\sigma} a_{I\sigma}) \tag{7.2}$$

In the strong-coupling limit the Mott-Hubbard AF with $\mathcal{N}$-orbitals per site maps onto an $S = \mathcal{N}/2$ quantum Heisenberg AF with NN coupling $J = \frac{4t^2}{U}$. So the present situation represents an $S' = 1/2$ impurity in an $S = 1/2$ host AF with modified couplings $J' = \frac{4t'^2}{U}$ between impurity-spin and its NN's. We treat the host AF in the HF approximation as discussed in Section 2.1, and treat the effects of magnetic impurities on this HF state.

7.1.1 Perturbative Expansion

We first consider the perturbative technique which is exactly similar to the one used in the case of a nonmagnetic impurity discussed in Chapter 4. The idea is to calculate the correction $[\delta\chi^0]$ to the $[\chi^0]$ matrix in powers of $\delta t/t$, from that to calculate the correction to the eigenvalues of $[\chi^0]$ perturbatively and hence to calculate the renormalised magnon energies.

Diagrams which contribute to $[\delta\chi^0_{II}]$ and $[\delta\chi^0_{IJ}]$ to first order in δt are shown in Figure 7.1, where the continuous lines represent the host Green's functions and the dashed lines are the

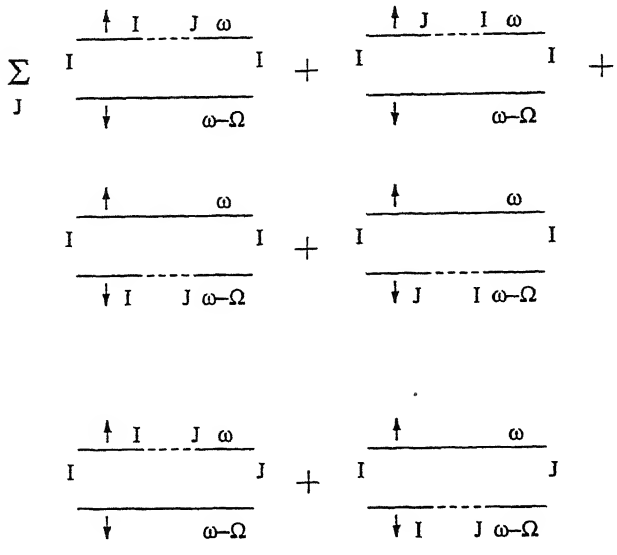

Figure 7.1:

hopping perturbations δt between the impurity site I and the nearest neighbour J. The upper and lower lines are respectively the $\uparrow$-spin and $\downarrow$-spin propagators with frequencies ω and $\omega - \Omega$.

We now discuss the evaluation of the matrix-elements of the $[\delta\chi^0(\Omega)]$ matrix in the strong-coupling limit wherein, as before, terms only upto order t^2/Δ^3 are retained. The first term in $\delta\chi^0_{IJ}$ is given by the expression,

$$i\int \frac{d\omega}{2\pi}\left[\frac{1}{\omega-\Delta^- - i\eta}.\delta t.\frac{1}{\omega-\Delta^+ + i\eta}\right]\left[\frac{-t/2\Delta}{\omega-\Omega-\Delta^- - i\eta}+\frac{t/2\Delta}{\omega-\Omega-\Delta^+ + i\eta}\right], \qquad (7.3)$$

where we have taken terms upto $O(1)$ in the local Green's function and upto $O(t/\Delta)$ in the NN Green's function, and $E^{\pm}_{\vec{k}} \equiv \Delta^{\pm} \equiv \pm\Delta$. The integral can be easily evaluated using contour-integral method. Adding equal contributions from the two diagrams we have, $[\delta\chi^0]_{IJ} = -\frac{1}{2}\frac{\delta t}{t}\frac{t^2}{\Delta^3}$.

To calculate $[\delta\chi^0_{II}]$ we consider δG, the perturbation-induced correction to the Green's

function. As discussed in Section 4.1

$$[\delta\chi^0(\Omega)]_{ij} = i\int (d\omega/2\pi)\left[\delta G^{\uparrow}_{ij}(\omega)g^{\downarrow}_{ji}(\omega-\Omega) + g^{\uparrow}_{ij}(\omega)\delta G^{\downarrow}_{ji}(\omega-\Omega)\right] \tag{7.4}$$

Since χ^0 is the antiparallel-spin, particle-hole propagator, we need to examine the change in spectral weights of Green's functions in the lower and upper Hubbard bands. Therefore we consider first the correction to the local spin-up Green's function to first order in hopping perturbation, $\delta G^{\uparrow}_{II} = 2\sum_J g^{\uparrow}_{II}\delta t g^{\uparrow}_{JI}$, where the sum is over all z nearest neighbours. We take the impurity site I to be on the A sublattice. In the strong-coupling limit, again substituting the appropriate expressions upto order t/Δ for host Green's function matrix elements, we obtain:

$$\delta G^{\uparrow}_{II} = 2z\frac{1}{\omega-\Delta^- - i\eta}.\delta t.\left[\frac{-t/2\Delta}{\omega-\Delta^- - i\eta} + \frac{t/2\Delta}{\omega-\Delta^+ + i\eta}\right] \tag{7.5}$$

Now the change in spectral weight in the lower Hubbard band is obtained by integrating the imaginary part of the Green's function over the lower Hubbard band. Contribution comes only from the particle-hole possibility, the second-order pole at Δ^- yielding no contribution, and we obtain:

$$-i\int_{\ominus}\frac{d\omega}{2\pi}\delta G^{\uparrow}_{II}(\omega) = -2z\frac{\delta t}{t}\left(\frac{t}{2\Delta}\right)^2. \tag{7.6}$$

From this change in the spectral weight it is straightforward to obtain the correction $\delta\chi^0_{II}$ to the particle-hole propagator. Since the $\downarrow$-spin spectral-weight in the upper-band is 1 to leading order, these give the correction $[\delta\chi^0]_{II} = -\frac{z}{2}\frac{\delta t}{t}\frac{t^2}{\Delta^3}$. A similar calculation gives $[\delta\chi^0]_{JJ} = -\frac{1}{2}\frac{\delta t}{t}\frac{t^2}{\Delta^3}$. So, upto $O(\frac{t^2}{\Delta^3})$, the relevant matrix elements of the $[\delta\chi^0]$ matrix are:

$$[\delta\chi^0]_{II} = -\frac{z}{2}\frac{\delta t}{t}\frac{t^2}{\Delta^3}; \quad [\delta\chi^0]_{IJ} = [\delta\chi^0]_{JI} = [\delta\chi^0]_{JJ} = -\frac{1}{2}\frac{\delta t}{t}\frac{t^2}{\Delta^3}. \tag{7.7}$$

dentical result is obtained if the impurity is placed on the B-sublattice.

As we have already discussed in Section 4.1, in the long-wavelength limit, the eigensolutions of the $[\chi^0]$ matrix are:

$$\lambda_Q^0 = \frac{1}{U} - \frac{t^2}{\Delta^3}\left(\frac{Q^2}{4} - \frac{1}{2}\left(\frac{\Omega}{2J}\right)^2\right) \tag{7.8}$$

$$\langle i \mid Q\rangle = \sqrt{\frac{2}{N}}\begin{pmatrix}\alpha_Q\\ \beta_Q\end{pmatrix} e^{i\vec{Q}.\vec{r_i}} = \sqrt{\frac{1}{N}}\begin{pmatrix}\sqrt{1-\frac{\Omega}{2J}}\\ -\sqrt{1+\frac{\Omega}{2J}}\end{pmatrix} e^{i\vec{Q}.\vec{r_i}} \tag{7.9}$$

The first order correction to the eigenvalue is given by

$$\delta\lambda^1 = \langle Q \mid [\delta\chi^0] \mid Q\rangle = \frac{1}{N}\left(\alpha_{\vec{Q}}^2\delta\chi_{II}^0 + \alpha_{\vec{Q}}\beta_{\vec{Q}}z\gamma_{\vec{Q}}\delta\chi_{IJ}^0 + \beta_{\vec{Q}}\alpha_{\vec{Q}}z\gamma_{\vec{Q}}\delta\chi_{JI}^0 + \beta_{\vec{Q}}^2 z\delta\chi_{JJ}^0\right). \tag{7.10}$$

If the concentration of impurities on the A- and B-sublattices are x_A and x_B respectively, then summing over the contribution from all impurities, we have,

$$\langle\delta\lambda^1\rangle = -(x_A + x_B)z\frac{\delta t}{t}\frac{t^2}{\Delta^3}\left[\frac{1}{2}\left(\frac{\Omega}{2J}\right)^2 + \frac{Q^2}{4}\right]. \tag{7.11}$$

The renormalised magnon energy is now obtained from the solution of the equation $1 - U(\lambda^0 + \delta\lambda^1) = 0$, and upto first order in the total impurity concentration $2x = x_A + x_B$, we obtain:

$$\Omega_Q = \Omega_Q^0\left(1 + 2z.x.\frac{\delta t}{t}\right) \tag{7.12}$$

where $\Omega_Q^0 = \sqrt{2}JQ$ is the magnon energy for the two-dimensional host antiferromagnet in the long-wavelength limit. The result agrees exactly with the calculations on the Heisenberg model [5] in that there are no singular corrections to the magnon energy in the case $S' = S$, and the correction is proportional to $\delta t/t = (1/2)\delta J/J$. In Reference [5] the magnon energy in the long-wavelength limit was obtained as: $e_Q(x) = e_Q(0)[1 + 2x(j-1)/j)]$, where $j \equiv J'/J$.

7.1.2 Exact-eigenstates analysis

In the exact eigenstates method, we do a numerical HF study on a finite-sized Hubbard model as discussed in Chapter 5. For the case $S' = S = \frac{1}{2}$ which we consider here, the magnetic impurities are represented by a modified local hopping term, *i.e.*, $\langle i \mid H \mid j \rangle = t$ if none of i and j is the impurity site, but $= t'$ if one of them is the impurity site and the other is a NN. Once the self-consistent AF state is obtained, the eigensolutions are used to construct the $[\chi^0(\Omega)]$ matrix as discussed in Chapter 6 and the magnon modes are obtained from the the eigensolutions of the $[\chi^0]$ matrix. The energy Ω_n on the n-th magnon mode is obtained by solving, $1 - U\lambda_n(\Omega_n) = 0$ for the appropriate (n-th from the top) eigenvalue $\lambda_n(\Omega)$. The root of the equation, $\lambda_n(\Omega_n) = 1/U$ is determined by obtaining $\lambda_n(\Omega)$ for closely spaced values of Ω on both sides of the root, and finally linearly interpolating between them. Suppose $(\lambda_n^1, \Omega_n^1)$ and $(\lambda_n^2, \Omega_n^2)$ are two sets of values for two energies very close to, and on either side of the root, then the root Ω_n is determined from,

$$\lambda(\Omega_n) = \frac{1}{U} = \lambda_n^1 + \frac{\lambda_n^2 - \lambda_n^1}{\Omega_n^2 - \Omega_n^1}(\Omega_n - \Omega_1) \tag{7.13}$$

Here we focus on the short wavelength (high Ω) modes. The magnon spectrum is shown in Figure 7.2 for different values of $\delta t/t$ for a 10×10 lattice with $U/t = 10$, and clearly shows that precisely one magnon state at the upper end of the spectrum is split off from the magnon-energy band. This is the short-wavelength mode corresponding to local spin deviation at the impurity site. Furthermore, it is seen that the energy difference of the split-off state from the upper end of the spectrum increases roughly in proportion to δt for small δt's. This is easily understood as making a local spin deviation on the impurity site costs an energy $\Delta\epsilon \propto (J' - J)$, *i.e.*, $\Delta\epsilon \propto \delta t/t$ to first order in $\delta t/t$. The localised nature of the split-off mode is shown in Figure 7.3 where the square of the magnon wave function for this mode is plotted on the lattice grid.

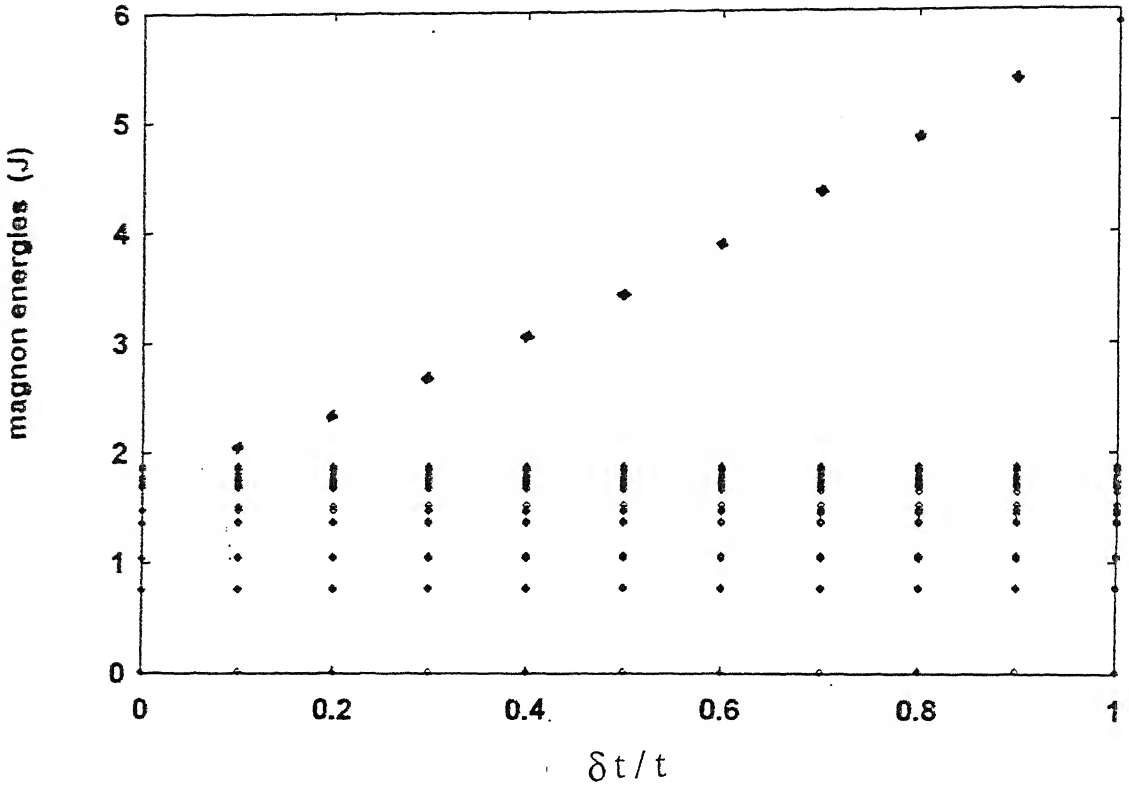

Figure 7.2: Magnon spectrum for a single-orbital magnetic impurity.

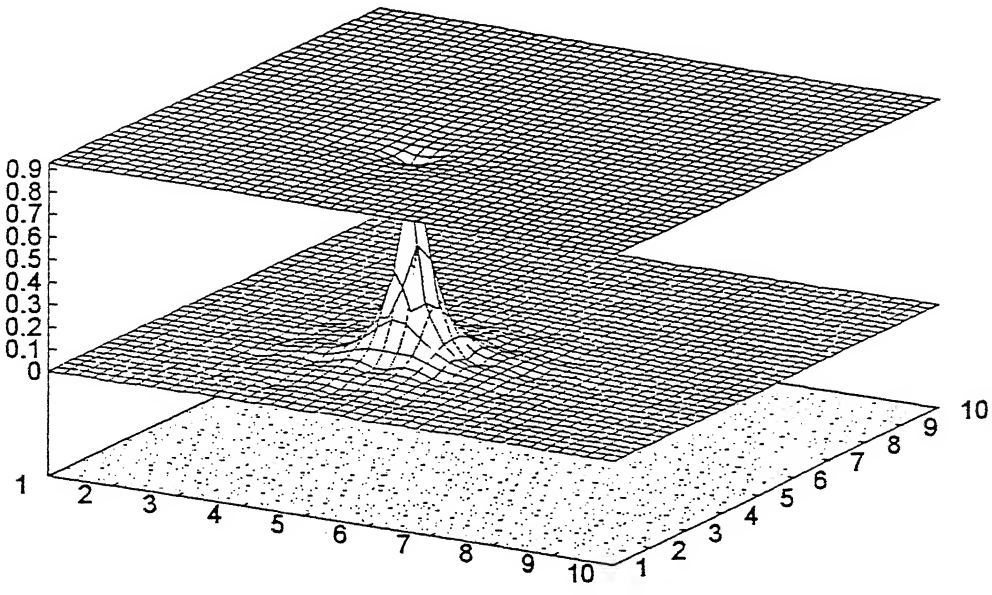

Figure 7.3: Magnon wave function (lower) and sublattice magnetisation (upper surface).

7.2 Spin-dependent impurity potential

Nonmagnetic impurities such as Zn, Al, Ga, etc. in the Mott-Hubbard AF were represented via spin-independent impurity potential term $V \sum_{I\sigma} a^{\dagger}_{I\sigma} a_{I\sigma}$ in the Hamiltonian. A natural extension for magnetic impurities is in terms of a spin-dependent impurity potential term, and we therefore consider the following impurity term in the Hamiltonian

$$H^{\rm mag}_{\rm imp} = \sum_I \Psi^{\dagger}_I [-\sigma_3 V] \Psi_I \tag{7.14}$$

where $\Psi_I = (a_{I\uparrow} \;\; a_{I\downarrow})$. A spin-independent impurity potential ϵ_0 can be included for generality, however, we shall consider the limit $V \gg \epsilon_0$, so that the potential for spin σ fermion is $V_\sigma \approx -\sigma V$. We choose V to be positive if the impurity is on an A-sublattice site, so that $V_\uparrow$ is very low and $V_\downarrow$ is very high. The sign of V is reversed for impurities on B-sublattice sites. This choice of potential ensures that the magnetisation on the impurity sites follows the host AF ordering. Such a spin-dependent impurity potential can arise from a coupling $-\vec{\sigma}.\vec{S}_{\rm imp}$

between the itinerant fermion spin σ and the static magnetic impurity spin $S_{\rm imp}$. Within a classical picture the impurity spin provides a local magnetic field at the impurity site. Since experiments on high-T_c cuprates doped with static impurities show the impurity spin to be antiferromagnetically coupled with the host spins [58], we take the local field direction to be along the local magnetisation direction ($\hat{z}$), and this yields the $-\sigma_3 V$ potential. We thus have an effective one-orbital-per-site model for the magnetic impurity in the AF host in which the spin-$\uparrow$ (-$\downarrow$) fermions feel a strong attractive (repulsive) potential at the impurity site.

The remaining analysis of this section closely follows the earlier study with nonmagnetic impurities [64]. Within a T-matrix approach the Green's function for the two spins can be written as

$$G^{\sigma}_{ij}(\omega) = g^{\sigma}_{ij}(\omega) + g^{\sigma}_{iI}(\omega)\frac{V_\sigma}{1 - V_\sigma g^{\sigma}_{II}(\omega)} g^{\sigma}_{Ij}(\omega) \tag{7.15}$$

Energies of impurity-induced states are then obtained from the singularities in the T-matrix, and are given by solutions of $g^{\sigma}_{II}(\omega) = 1/V_\sigma$. The local host Green's function in the AF state was obtained as $g^{\sigma}_{II}(\omega) = \frac{1}{N}\sum_{\vec{k}}(\omega - \sigma\Delta)/(\omega^2 - E^2_{\vec{k}})$ for $I \in$ A where $\sigma = \pm 1$ for $\uparrow$ and $\downarrow$-spins respectively [63].

A plot of $g^{\sigma}_{II}(\omega)$ vs. ω is shown in Figures 7.4 and 7.5 for the two spin cases together with $1/V_\sigma$. Intersection of $g^{\uparrow}_{II}(\omega)$ with the $-1/V$ line gives a impurity state for spin-$\uparrow$ at an energy $\sim -V$. Similarly, there is an impurity state for spin-$\downarrow$ from the intersection of $g^{\downarrow}_{II}(\omega)$ and $1/V$ at an energy $\sim V$. For large $|V|/U$, these impurity states are essentially site localised on the impurity site, and therefore decoupled from the system. Similarly when the magnetic impurity is on a B-sublattice site, again no defect states are formed in the gap, only impurity states are formed. This follows immediately from the spin-sublattice symmetry which results in $g^{\sigma}_{II}(\omega)|_{I\in B} = g^{\bar{\sigma}}_{II}(\omega)|_{I\in A}$. Also the signs of the impurity potentials for the two spins are reversed, as mentioned earlier. As a consequence the intersections with

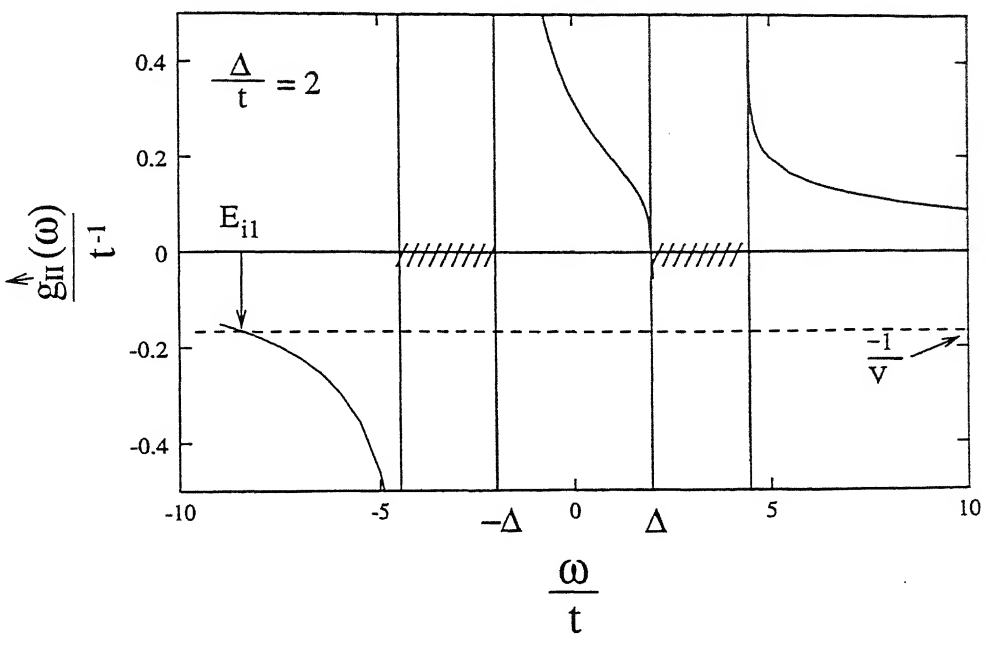

Figure 7.4: Plot of $G^{\uparrow}_{II}(\omega)$ and $-1/V$.

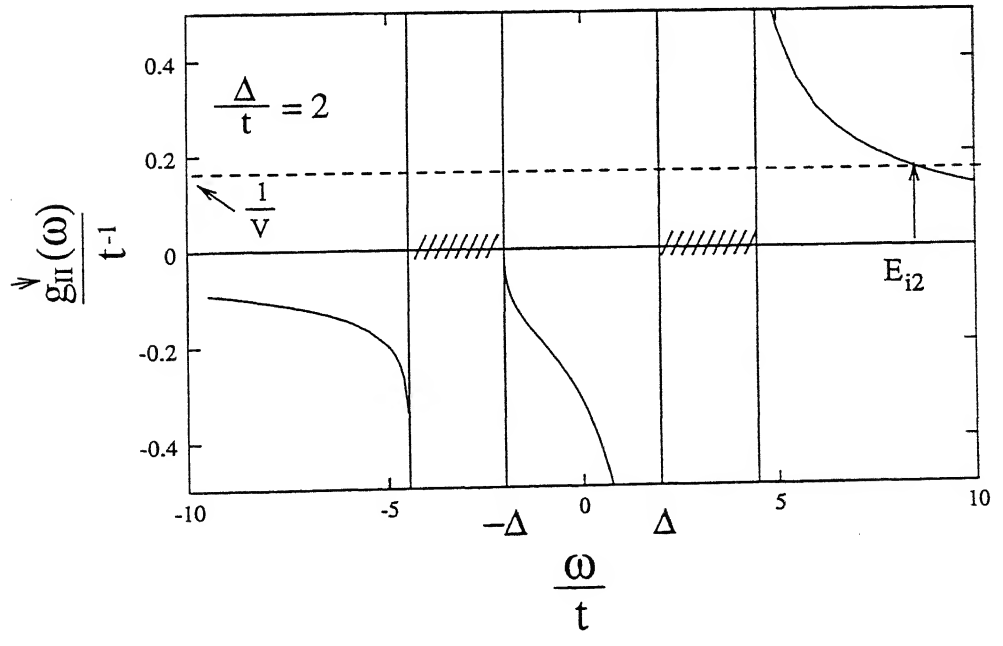

Figure 7.5: Plot of $G^{\downarrow}_{II}(\omega)$ and $1/V$.

$1/V_\sigma$ yielding the two impurity states are at the same energies.

Thus a significant difference for the magnetic impurity case, when the impurity spin is antiferromagnetically coupled to the neighbouring host spins, is that there are no defect states formed in the Hubbard gap, rather there are only impurity states formed far removed in energy from the Hubbard bands.

For magnetic-impurity doping in the AF host the fermion number is unchanged, unlike the case of nonmagnetic impurities where one fermion is removed for every added impurity. However, in the limit $V \to \infty$ the impurity site gets decoupled from the host in much the same way, so that an identical impurity-induced perturbation $[\delta\chi^0(\Omega)]$ is obtained. This is because while for the nonmagnetic impurity placed on, say, an A-sublattice site, it was the removal of one spin-$\uparrow$ fermion which reduced the minority spin-$\uparrow$ density by $t^2/4\Delta^2$ on the NN B-sublattice sites, for the magnetic impurity case, it is the strong attraction due to potential $-V$ at the impurity site which leads to this depletion.

We now turn to the renormalisation of magnon energy. In the limit of $V \to \infty$, all extended-state wave functions have vanishing amplitude on the impurity site, and the impurity-localised states at infinite energy have vanishing contribution to the particle-hole process for small (order J) energies. Therefore, $[\chi^0(\Omega)]_{ij}$ must vanish if $i/j = I$, so that,

$$[\delta\chi^0(\Omega)]_{ij} = -[\chi^0_{\rm host}(\Omega)]_{ij} \tag{7.16}$$

The only other terms in $[\delta\chi^0]$ to $O(\frac{t^2}{\Delta^3})$ are $\delta\chi^0_{JJ}$ where J's are NN to I. The small $\downarrow$-spin particle density of the order of $\frac{t^2}{\Delta^2}$ sitting on the A-sublattice site I is repelled due to high potential V to the four NN sites J, so that the change in each one of them is $\delta n^{\ominus}_{J\downarrow} = \frac{1}{4}\frac{t^2}{\Delta^2}$. Similarly the small $\uparrow$-spin hole density of $\frac{t^2}{\Delta^2}$ is also removed to the neighbouring sites so that $\delta n^{\oplus}_{J\uparrow} = \frac{1}{4}\frac{t^2}{\Delta^2}$, corresponding to the shift in $\delta n_{J\uparrow}$ to the impurity site. The situation is exactly similar to the case of nonmagnetic impurity except that we are now working in the electron picture. Proceeding as earlier (4), we have $\delta\chi^0_{JJ} = \frac{1}{4}\frac{t^2}{\Delta^3}$, and so the various matrix elements

of the correction to the bare, antiparallel-spin particle-hole propagator are as follows:

$$\left[\delta\chi^0(\Omega)\right]_{II} = -\frac{1}{U} + \frac{t^2}{\Delta^3}(1 + \frac{\Omega}{2J}) \tag{7.17}$$

$$\left[\delta\chi^0(\Omega)\right]_{IJ} = \frac{1}{4}\frac{t^2}{\Delta^3} = \left[\delta\chi^0(\Omega)\right]_{JI} = \left[\delta\chi^0(\Omega)\right]_{JJ} \tag{7.18}$$

These are identical to the case of a nonmagnetic impurity in an AF and lead to an identical result for the renormalised magnon energy. For low impurity concentrations and in the long-wavelength limit, we again have a logarithmically divergent reduction to the spin-wave energy in 2D,

$$\begin{aligned}\Omega_Q &= \sqrt{2}JQ\left[1 - x - 4x\,\frac{1}{N}\sum_{Q'}\frac{1}{Q'^2 - Q^2}\right] \\ &= \sqrt{2}JQ\left[1 - x - 4x\left(\frac{1}{\pi}\ln\frac{Q_c}{Q} + \frac{i}{2}\right)\right]\end{aligned} \tag{7.19}$$

where Q_c is an upper momentum cutoff of order 1. In two dimensions there is a logarithmic singularity as $Q \to 0$, indicating a logarithmically divergent reduction to the magnon velocity. Impurity scattering also introduces a damping of spin-wave modes.

Therefore we conclude that irrespective of whether the impurity is magnetic or nonmagnetic, if a site is decoupled from the system by putting a large on-site potential – attractive or repulsive – it acts as a 'strong' perturbation to the spin-wave excitations and leads to singular corrections to spin-wave energy in 2D. The hopping-perturbation, on the other hand, is a 'weak' perturbation for long-wavelength modes and only causes a momentum-independent shift in the spin-wave energy proportional to the impurity concentration.

7.3 Multiple-orbital representation of a magnetic impurity

We can represent higher-spin magnetic impurities ($S' > 1/2$) within the Hubbard model by incorporating multiple orbitals at the impurity site. An $S' = \frac{N}{2}$ impurity can be represented by putting N orbitals on the that site. A HF numerical study can be done on this system with the only difference that we now have an enlarged basis including the N impurity orbitals. We can reach a self-consistent state in this enlarged basis and from that calculate the magnon energies exactly as in Section 7.1. We focus on Goldstone mode, electronic feature of the magnetic impurity and magnon-energy renormalisation due to scattering off the impurities.

As the simplest approximation, we assume all the impurity orbitals to be connected to the NN's through the same hopping t, and to involve the same on-site Hubbard repulsion U as in the host system. The Hamiltonian for such a system can be written as:

$$H = -t \sum_{\langle ij\rangle\sigma}{}' (a^\dagger_{i\sigma} a_{j\sigma} + \text{h.c.}) + U \sum_i{}' n_{i\uparrow} n_{i\downarrow} - t \sum_{\langle IJ\rangle\sigma\alpha} (a^\dagger_{I\sigma\alpha} a_{J\sigma} + \text{h.c.}) + U \sum_{I\alpha} n_{I\uparrow\alpha} n_{I\downarrow\alpha}. \quad (7.20)$$

Here J are the NN sites of the impurity site I, the primes represent sums over sites except the impurity sites, and $\alpha = 1, 2, \ldots N$ denote the N orbitals at the impurity sites. Since the N impurity orbitals are independent, in the strong-coupling limit this model can be mapped onto a quantum Heisenberg model with the Hamiltonian:

$$H_{eff} = J \sum_{\langle ij\rangle}{}' \vec{S}_i . \vec{S}_j + J \sum_{\langle IJ\rangle} \vec{S}_J . (\vec{S}^1_I + \vec{S}^2_I + \cdots \vec{S}^N_I) \quad (7.21)$$

where, as before, $J = \frac{4t^2}{U}$, and $S^\alpha_I = \Psi_{I\alpha}(\vec{\sigma}/2)\Psi_{I\alpha}$ with $\alpha = 1, 2, \ldots, N$ are the impurity spin operators constructed from the fermion operators. The "impurity spin" $\vec{S_{\text{imp}}} = \vec{S}^1_I + \vec{S}^2_I + \cdots + \vec{S}^N_I$ is not exclusively a spin N/2 object. However, in the HF AF state, since all

the impurity orbitals are connected to the same set of NN's through the same hopping, they will preferably be occupied with electrons of the same spin, thus effectively projecting out possibilities of other spin configurations.

We expect the Goldstone mode in the transverse spin fluctuations to be retained even in presence of impurities as the continuous spin-rotational symmetry is preserved as is evident from the effective Heisenberg Hamiltonian in Equation 7.21. One way to understand transverse spin fluctuations in the Hubbard model is in terms of the rotation angles $\theta_i = \sin^{-1} \frac{\Phi_i}{s_i^z}$, where Φ_i and s_i^z are the magnon-mode amplitude and the local magnetisation at the site i [70]. Now, in order to treat the magnetic impurity as a single object, we simply add the magnetisations and the magnon amplitudes on all the impurity orbitals to obtain $s_I^z = \sum_{\alpha=1}^{N} s_{I\alpha}^z$ and $\phi_I = \sum_{\alpha=1}^{N} \Phi_{I\alpha}$. In our numerical HF studies we find that for $\Omega = 0$, the largest eigenvalue of the $[\chi^0(\Omega)]$-matrix is exactly equal to $\frac{1}{U}$ and the rotation angles for this mode are identical on all sites, including the impurity sites with $\theta_I = \sin^{-1} \frac{\Phi_I}{s_I^z}$, for $N = 2$, and 3, thus explicitly confirming the existence of gapless Goldstone mode.

7.3.1 Electronic features of multiple-orbital magnetic impurity

We now consider some interesting features in the electronic spectra in presence of the multiple-orbital magnetic impurities we are considering. For concreteness, we consider the impurity to be on an A-sublattice site. In the HF state in the strong-coupling limit, the $\uparrow$-spin and $\downarrow$-spin amplitudes are $1 - \frac{t^2}{\Delta^2}$ and $\frac{t^2}{\Delta^2}$ respectively on an A-sublattice site. This continues to hold even for the impurity orbitals as they are connected to four NN's through hopping t, and a density of $\frac{t^2}{4\Delta^2}$ is transferred from each one of them to each one of the NN's. However, in our numerical HF calculations we find that when $\frac{U}{t}$ is not too large there is an enhancement of local magnetisation on the impurity orbitals. For example, for three orbitals on the impurity site, (*i.e.*, $S' = 3/2$) the magnetisation is uniform for a $\frac{U}{t} = 25$, but there is an enhanced magnetisation on the impurity sites when $\frac{U}{t} = 10$. This is because the hopping

of an ↑-spin electron from one of the impurity orbitals to the NN's suppresses the hoppings of the electrons in the other impurity orbitals and this is a higher-order (in powers of $\frac{t}{U}$) effect. So the ↑-spin electrons in the impurity orbitals tend to get localised and hence get partially decoupled from the system.

Within HF approximation this enhanced magnetisation on the impurity orbitals leads to a lowered HF potential for ↑-spin electrons on these orbitals. This relatively lower HF potential can be treated as a *weak attractive* potential $V_{eff} = U(n_I^{\downarrow} - n_{host}^{\downarrow})$ for the ↑-spins on the impurity site and it is easy to see from our earlier T-matrix analysis (??) that this will lead to a localised state just below the LHB by solving the equation $1 - V_{eff} g_{II}^{\uparrow}(\omega) = 0$.

There is another mechanism in case of multiple-orbital magnetic impurities which leads to localised states on the impurity site. Since all the impurity orbitals are connected to the four NN's through the same hopping t, any localised state on the impurity site such that its amplitudes on the impurity orbitals add up to zero, *i.e.*, the hopping contributions from the different impurity orbitals cancel exactly, will be an *exact eigenstate* of the HF Hamiltonian. This is energetically made possible by lowering of the HF potential for ↑-spins at each of the impurity orbitals. So, for an N-orbital magnetic impurity, a site localised state on the impurity site with amplitudes $\phi_1, \phi_2, \ldots, \phi_N$ on the N impurity orbitals will be an exact eigenstate of the HF Hamiltonian if the following condition is satisfied:

$$\phi_1 + \phi_2 + \cdots + \phi_N = 0. \tag{7.22}$$

Actually there are two conditions involving these N quantities. One is given by Equation 7.22, and the other is the demand that the site-localised state be normalised, *i.e.*,

$$|\phi_1|^2 + |\phi_2|^2 + \cdots |\phi_N|^2 = 1. \tag{7.23}$$

For a spin 1 impurity with $N = 2$, there is a unique solution with $\phi_1 = -\phi_2 = \frac{1}{\sqrt{2}}$

satisfying these two conditions. So, for a two-orbital magnetic impurity, a site-localised state which is antisymmetric between the impurity orbitals will be an exact eigenstate. However, for $N > 2$ there are infinite possibilities for the ϕ_α's. Any suitable linear combination of these infinite possibilities will be a site-localised exact eigenstate leading to partial decoupling of the impurity site.

7.3.2 Magnon-energy renormalisation

Now we focus on magnon-energy renormalisation due to scattering off the impurities. We have seen in the case of a nonmagnetic impurity and a magnetic impurity represented by a spin-dependent potential that decoupling of a site from the system causes strong scattering of the spin waves and leads to a diverging correction to the spin-wave velocity in 2D. It will be interesting to see how the spin-wave velocity gets renormalised in this case. In their work on impurities in a Heisenberg AF, Wan *et al.* [5] found a logarithmically diverging correction to the spin-wave velocity in the long-wavelength limit in 2D for $S' \neq S$. So it is of interest to see the scaling of spin-wave velocity renormalisation due to scattering off the impurities with system size.

Spin-wave modes in a finite-sized system can be assigned wave-numbers $Q = \frac{2\pi}{L}\sqrt{n_x^2 + n_y^2}$ [70]. The first mode after the Goldstone mode corresponds to $n_x = 1$, $n_y = 0$ or equivalently $n_x = 0$ and $n_y = 1$ so that $Q = \frac{2\pi}{L}$. Similarly, the second mode corresponds to $Q = \frac{2\pi}{L}\sqrt{2}$. In Figure 7.6 we plot the spin-wave energy for these modes for a 12×12 system with two spin 1 impurities, represented by putting two orbitals on each of the impurity sites. The spin-wave energy is found to be linear in Q for small Q's even in presence of impurities.

As the spin-wave energy is proportional to the wave-vector, the spin-wave velocity v can be defined by $\Omega_Q = vQ$ in the long-wavelength limit. The spin-wave velocity has been expressed in the form $v(x) = v(0)(1 - \alpha x)$ [5], in the low-impurity-concentration limit. α has two parts and can be written as $\alpha = \alpha_0 + \alpha_L$, where α_0 is a constant independent of

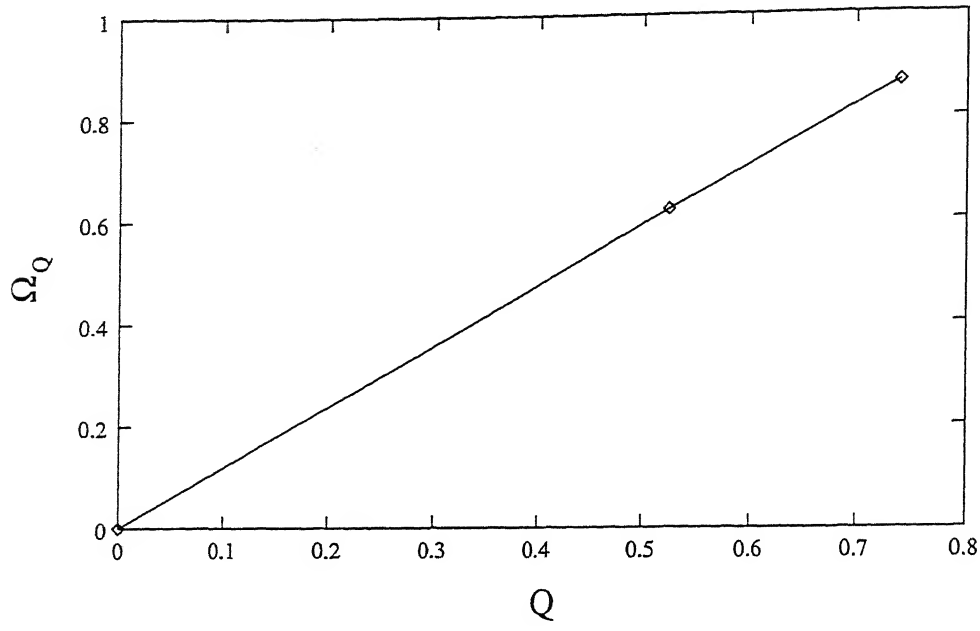

Figure 7.6: Spin-wave energy for small Q's in presence of impurities.

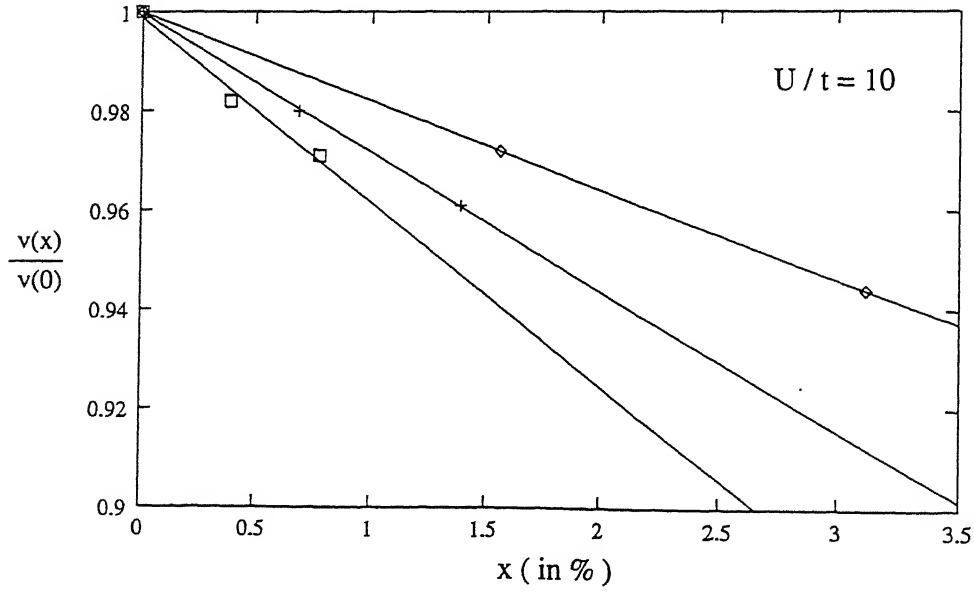

Figure 7.7: Renormalisation to the spin-wave velocity as a function of impurity concentration for different system sizes — 8×8 (diamond), 12×12 (plus) and 16×16(square). The points are the calculated values and the lines represent the best fits.

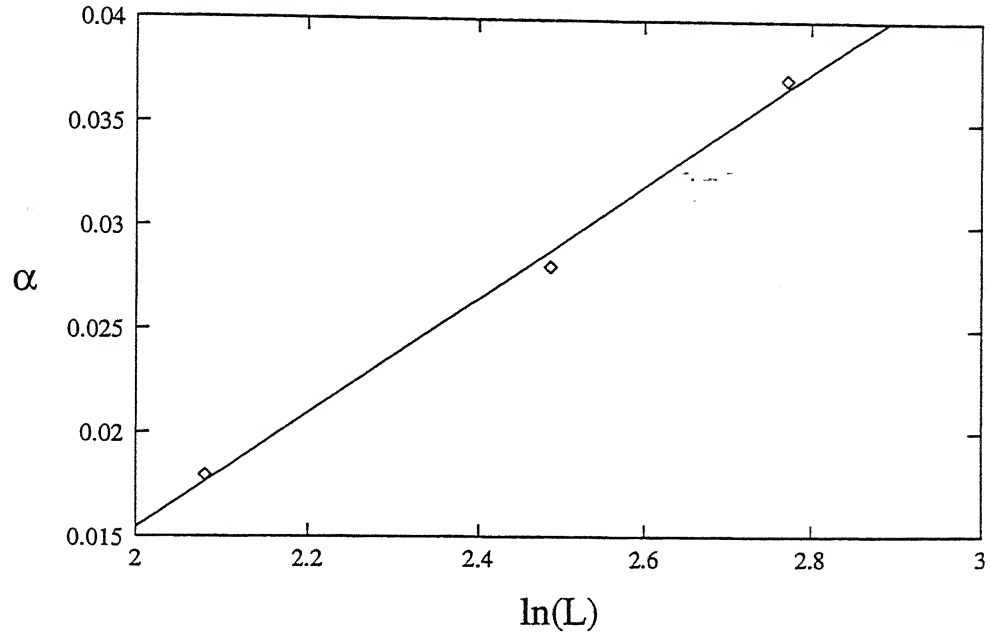

Figure 7.8: Plot of α vs. $\ln L$. The points are the calculated values and the line represents the best fit.

the system-size and α_L depends on the system-size L. If there is a logarithmic divergence in the renormalisation to the spin-wave velocity in the long-wavelength limit, then we should see an increase in the absolute value of the slope of the spin-wave-velocity-renormalisation vs. impurity concentration curve and should have $\alpha \propto \ln L$. In Figure 7.7 we show the renormalisation of spin-wave velocity with doping concentration for three different system sizes — 8×8, 12×12 and 16×16. It is clear that for the small impurity concentrations we have studied, the spin-wave velocity decreases linearly with increasing impurity concentration and the x-dependence (absolute value of the slope) increases with system size. This implies a diverging correction in the limit of large system. In Figure 7.8 we plot α, the slope of the impurity concentration vs. spin-wave velocity curve, as a function of $\ln L$ and find that the variation is linear, which signifies a log-divergence.

References

[1] G. Xiao *et al.*, Phys. Rev. Lett. **60**, 1446 (1988).

[2] A. V. Mahajan, H. Alloul, G. Collin, and J. F. Marucco, Phys. Rev. Lett. **72**, 3100 (1994).

[3] A. Singh and Z. Tešanović, Phys. Rev. B **41**, 11457 (1990).

[4] B. Keimer *et al.*, Phys. Rev. B **45**, 7430 (1992).

[5] C. C. Wan, A. B. Harris, and D. Kumar, Phys. Rev. B **48**, 1036 (1993).

[6] J. G. Bednorz and K. A. Müller, Z. Phys. B **64**, 188 (1986).

[7] D. M. Ginsberg, in *Physical properties of High-Temperature superconductors I* (World Scientific, SIngapore, 1988).

[8] Y. Tokura, in *Physics of High-temperature Sueprconductors,Proc. Toshiba Int. School of Superconductivity, Kyoto, Japan*, Vol. 106 of *Springer Series in Solid-State Sciences*, edited by S. Maekawa and M. Sato (Springer, Berlin, Heidelberg, 1992), p. 191.

[9] N. P. Ong, in *Physical Properties of High-Temperature Superconductors II*, edited by D. M. Ginsberg (World Scientific, Singapore, 1988).

[10] Y. Lu, ICTP Preprint No. IC/91/339.

[11] T. Yamashita *et al.*, Jpn. Jl. of Appl. Phys. **26**, L635 (1987).

[12] T. J. Witt, Phys. Rev. Lett. **61**, 1423 (1988).

[13] D. Esteve *et al.*, Europhys. Lett. **3**, 1237 (1987).

[14] R. H. Koch *et al.*, Appl. Phys. Lett. **51**, 200 (1987).

[15] C. E. Gough *et al.*, Nature **326**, 855 (1987).

[16] J. Niemeyer *et al.*, Z. Phys. B **67**, 155 (1987).

[17] O. S. Akhtyamov, Sov. Phys. JETP Lett. **3**, 183 (1966).

[18] B. G. Levi, Phys. Today 19 (Jan. 1996).

[19] W. L. McMillan, Phys. Rev. **167**, 331 (1968).

[20] J. Appel, Phys. Rev. Lett. **21**, 1164 (1968).

[21] P. A. Lee and N. Read, Phys. Rev. Lett. **58**, 2691 (1987).

[22] T. R. Lemberger and L. Coffey, Phys. Rev. B **38**, 7058 (1988).

[23] Y. Yeshurun and A. P. Malozemoff, Phys. Rev. Lett. **60**, 2202 (1988).

[24] P. B. Allen *et al.*, in *Physical Properties of High-Temperature Superconductors I*, edited by D. M. Ginsberg (World Scientific, Singapore, 1988).

[25] C. G. Olson *et al.*, Phys. Rev. B **42**, 381 (1990).

[26] H. Haghighi *et al.*, Phys. Rev. Lett. **67**, 382 (1991).

[27] D. C. Johnston, Phys. Rev. Lett. **62**, 957 (1989).

[28] G. Grüner, Physica C **162-164**, 8 (1989).

[29] G. Burns, *High-Temperature Superconductivity: An Introduction* (Academic Press Inc., Harcourt Brace Javanovich Publishers., Boston, San Diego, New York, London, Sedney, Tokyo, Toronto., 1992).

[30] T. R. Chien *et al.*, Phys. Rev. B **43**, 6242 (1991).

[31] J. C. Campuzano *et al.*, Phys. Rev. Lett. **64**, 2308 (1990).

[32] D. Vaknin *et al.*, Phys. Rev. Lett. **58**, 2802 (1987).

[33] K. Yamada *et al.*, Solid State Commun. **64**, 753 (1987).

[34] N. Nishida *et al.*, Jpn. Jl. Appl. Phys. **26**, L1856 (1987).

[35] J. M. Tranquada *et al.*, Phys. Rev. Lett. **60**, 156 (1988).

[36] W. Li, Phys. Rev. B **37**, 9844 (1988).

[37] P. Burlet *et al.*, Physica C **153-155**, 1115 (1988).

[38] S. K. Sinha, in *Proceedings of the I LACHTS. First Latin American Conf. on High Temperature Superconductivity, Rio De Jeneiro, Brazil, 4-6 May, 1988* (World Scientific, Singapore, 1988), pp. 202–210.

[39] P. W. Anderson, Science **235**, 1196 (1987).

[40] S. Chakravarty, B. I. Halperin, and D. R. Nelson, Phys. Rev. B **39**, 7443 (1988).

[41] S. Tyc, B. I. Halperin, and S. Chakravarty, Phys. Rev. Lett. **62**, 835 (1989).

[42] R. S. List *et al.*, Physica C **159**, 439 (1989).

[43] Z. X. Shen *et al.*, Phys. Rev. B **36**, 8414 (1987).

[44] P. Thiry *et al.*, Europhys. Lett. **5**, 55 (1988).

[45] H. Namatame *et al.*, Phys. Rev. B **41**, 7205 (1990).

[46] W. Brenig, Phys. Reports **251**, 179 (1995).

[47] A. Fujimori *et al.*, Phys. Rev. B **35**, 8814 (1987).

[48] N. Nücker *et al.*, Z. Phys. B **67**, 9 (1987).

[49] D. van der Marel, Phys. Rev. B **37**, 5136 (1988).

[50] F. Parmigiani *et al.*, Phys. Rev. B **43**, 3085 (1991).

[51] E. Pellegrin *et al.*, Phys. Rev. B **47**, 3354 (1993).

[52] H. Romberg *et al.*, Phys. Rev. B **42**, 8768 (1990).

[53] C. T. Chen *et al.*, Phys. Rev. Lett. **66**, 104 (1991).

[54] P. Kupier, Phys. Rev. B **38**, 6483 (1988).

[55] V. J. Emery, Phys. Rev. Lett. **58**, 2794 (1987).

[56] C. M. Varma, S. Schmitt-Rink, and E. Abrahams, Solid State Commun. **62**, 681 (1987).

[57] G. Xiao, M. Z. Cieplak, and C. L. Chien, Phys. Rev. B **42**, 240 (1990).

[58] G. Xiao, M. Z. Cieplak, J. Q. Xiao, and C. L. Chien, Phys. Rev. B **42**, 8752 (1990).

[59] R. E. Walstedt *et al.*, Phys. Rev. B **48**, 10646 (1993).

[60] J. Axnäs *et al.*, Phys. Rev. B **53**, R3003 (1996).

[61] G. V. M. Williams *et al.*, Phys. Rev. B **52**, R7034 (1995).

[62] Y. Fukuzumi *et al.*, Phys. Rev. Lett. **76**, 684 (1996).

[63] P. Sen, S. Basu, and A. Singh, Phys. Rev. B **50**, 10381 (1994).

[64] P. Sen and A. Singh, Phys. Rev. B **53**, 328 (1996).

[65] H. P. Hjalmarsson, P. Vogl, D. J. Wolford, and J. D. Dow, Phys. Rev. Lett. **44**, 810 (1980).

[66] A. Singh and Z. Tešanović, Phys. Rev. B **45**, 7258 (1992).

[67] A. Singh, Phys. Rev. B **48**, 6668 (1993).

[68] A. Singh and Z. Tešanović, Phys. Rev. B **43**, 11445 (1991).

[69] A. Singh *et al.*, Phys. Rev. Lett. **64**, 2571 (1990).

[70] S. Basu and A. Singh, Phys. Rev. B **53**, 6406 (1996).

[71] G. Dopf, A. Maramatsu, and W. Hanke, Europhys. Lett. **17**, 559 (1992).

[72] E. Merzbacher, *Quantum Mechanics*, 2nd ed. (John Wiley & Sons, New Yrok, Chichester, Brisbane, Toronto, 1970).

Appendix A

Local Green's function and position of the defect state

For $I \in A$,

$$\begin{aligned} g^{\uparrow}_{II}(\omega) &= \sum_{\vec{k}} \left[\frac{a^{\ominus 2}_{\uparrow}(\vec{k})}{\omega - E^{\ominus}_{\vec{k}}} + \frac{a^{\oplus 2}_{\uparrow}(\vec{k})}{\omega - E^{\oplus}_{\vec{k}}} \right] \\ &= \sum_{\vec{k}} \left[\frac{a^{\ominus 2}_{\uparrow}(\vec{k})}{\omega + E_{\vec{k}}} + \frac{a^{\oplus 2}_{\uparrow}(\vec{k})}{\omega - E_{\vec{k}}} \right] \\ &= \sum_{\vec{k}} \frac{\omega \left(a^{\ominus 2}_{\uparrow}(\vec{k}) + a^{\oplus 2}_{\uparrow}(\vec{k}) \right) - E_{\vec{k}} \left(a^{\ominus 2}_{\uparrow}(\vec{k}) - a^{\oplus 2}_{\uparrow}(\vec{k}) \right)}{\omega^2 - E^2_{\vec{k}}}. \end{aligned}$$

We have $a^{\ominus 2}_{\uparrow}(\vec{k}) + a^{\oplus 2}_{\uparrow}(\vec{k}) = 1$, and from Equation 2.3 we have $a^{\ominus 2}_{\uparrow}(\vec{k}) - a^{\oplus 2}_{\uparrow}(\vec{k}) = \frac{\Delta}{E_{\vec{k}}}$. Using these we can write,

$$g^{\uparrow}_{II}(\omega) = \sum_{\vec{k}} \frac{\omega - \Delta}{\omega^2 - E^2_{\vec{k}}}. \tag{A.1}$$

Similarly, for the down-spin Green's function, using $a^{\ominus 2}_{\downarrow}(\vec{k}) + a^{\oplus 2}_{\downarrow}(\vec{k}) = 1$, and $a^{\oplus 2}_{\downarrow}(\vec{k}) - a^{\ominus 2}_{\downarrow}(\vec{k}) = \frac{\Delta}{E_{\vec{k}}}$, we can write,

$$g_{II}^{\downarrow}(\omega) = \sum_{\bar{k}} \frac{\omega + \Delta}{\omega^2 - E_{\bar{k}}^2}. \tag{A.2}$$

These two can be combined to write,

$$g_{II}^{\sigma} = \sum_{\bar{k}} \frac{\omega - \sigma\Delta}{\omega^2 - E_{\bar{k}}^2}, \tag{A.3}$$

where $\sigma = \pm 1$ for $\uparrow$- and $\downarrow$-spins respectively.

For the $\uparrow$-spin Green's function,

$$\begin{aligned} g_{II}^{\uparrow}(\omega) &= \frac{1}{N} \sum_{\bar{k}} \frac{\omega - \Delta}{\omega^2 - E_{\bar{k}}^2} \\ &= \frac{1}{N} (\Delta - \omega) \sum_{\bar{k}} \frac{1}{\epsilon_{\bar{k}}^2 + (\Delta^2 - \omega^2)} \\ &= \frac{1}{N} (\Delta - \omega) \int \frac{\ln \epsilon \, d\epsilon}{\epsilon^2 + (\Delta^2 - \omega^2)} \end{aligned} \tag{A.4}$$

where we assume a logarithmic density of states in 2D. Evaluating the integral we have,

$$g_{II}^{\uparrow}(\omega) \sim (\Delta - \omega) \frac{\ln (\Delta^2 - \omega^2)}{\sqrt{\Delta^2 - \omega^2}}. \tag{A.5}$$

As $\omega \to \Delta$ from below, this $\to 0$ as $\sqrt{\Delta - \omega} \ln (\Delta - \omega)$.

As $\omega \to -\Delta$ from above, this blows up as $(\omega + \Delta)^{-1/2} \ln (\omega + \Delta)$.

Since a solution of the equation $g_{II}^{\uparrow}(\omega) = 1/V$ gives the position of the defect state, and the defect state is formed close to the upper Hubbard band in the limit of large V, from the first of the above relations we have,

$$\sqrt{\eta} \ln \eta \sim 1/V. \tag{A.6}$$

where η is the difference between the upper band-edge (Δ) and the defect state energy (E_d).

Appendix B

Defect state wave function

The defect state wave function on a site i is, by definition, $\phi_d^i \equiv d_{iI}^{\uparrow}(E_d)/\sqrt{-\frac{\partial g_{II}(\omega)}{\partial \omega}\,|_{\omega=E_d}}$. The denominator will give just a constant. So, up to a multiplicative constant, the defect state wave function is simply $g_{iI}^{\uparrow}(E_d)$.

As we have assumed, $I \in$ A. First we consider $i \in$A. $g_{iI}^{\uparrow}(E_d)$ is then given by the Fourier transform of $g_{AA}^{\uparrow}(\vec{k}, E_d)$.

$$g_{iI}^{\uparrow}(E_d) = \sum_{\vec{k}} \left[\frac{a_{\uparrow}^{\ominus 2}(\vec{k})}{E_d - E_{\vec{k}}^{\ominus}} + \frac{a_{\uparrow}^{\oplus 2}(\vec{k})}{E_d - E_{\vec{k}}^{\oplus}} \right] e^{i\vec{k}.\vec{r}}, \tag{B.1}$$

where $\vec{r} \equiv \vec{r}_i - \vec{r}_I$.

In the strong-coupling limit $a_{\uparrow}^{\ominus 2}(\vec{k}) = 1 - \frac{\epsilon_{\vec{k}}^2}{4\Delta^2}$ and $a_{\uparrow}^{\oplus 2}(\vec{k}) = \frac{\epsilon_{\vec{k}}^2}{4\Delta^2}$, so that

$$g_{iI}^{\uparrow}(E_d) = \sum_{\vec{k}} \left[\frac{1 - \frac{\epsilon_{\vec{k}}^2}{4\Delta^2}}{E_d - E_{\vec{k}}^{\ominus}} + \frac{\frac{\epsilon_{\vec{k}}^2}{4\Delta^2}}{E_d - E_{\vec{k}}^{\oplus}} \right] e^{i\vec{k}.\vec{r}}. \tag{B.2}$$

We have $E_d = \Delta - \eta$. With this, $\frac{1}{E_d - E_{\vec{k}}^{\ominus}} \approx \frac{1}{2\Delta}\left(1 - \frac{\epsilon_{\vec{k}}^2}{4\Delta^2}\right)$ and $\frac{1}{E_d - E_{\vec{k}}^{\oplus}} \approx \frac{-1}{\epsilon_{\vec{k}}/2\Delta}\left(1 - \frac{\eta}{\epsilon_{\vec{k}}^2/2\Delta}\right)$, if $\frac{\epsilon_{\vec{k}}^2}{2\Delta} \gg \eta$.

From these we have,

$$g^{\uparrow}_{iI}(E_d) = \frac{-1}{2\Delta}\sum_{\vec{k}}\left[\frac{\epsilon^2_{\vec{k}}}{2\Delta^2} - \frac{\eta}{\epsilon^2_{\vec{k}}/2\Delta}\right]e^{i\vec{k}.\vec{r}}. \tag{B.3}$$

As $\eta \to \frac{1}{V^2}$, in the limit $V \to \infty$, the defect state wave function on the A-sublattice sites are $O(\frac{1}{\Delta^3})$ or smaller.

For $i \in B$, the defect state wave function is given by the Fourier transform of $g^{\uparrow}_{BA}(E_d)$ and in the strong-coupling limit,

$$g^{\uparrow}_{iI}(E_d) = \sum_{\vec{k}}\left[\frac{\epsilon_{\vec{k}}/2\Delta}{E_d - E^{\ominus}_{\vec{k}}} + \frac{\epsilon_{\vec{k}}/2\Delta}{E_d - E^{\oplus}_{\vec{k}}}\right]e^{i\vec{k}.\vec{r}}. \tag{B.4}$$

Proceeding as before, we obtain,

$$g^{\uparrow}_{iI}(E_d) = \frac{-1}{2\Delta}\sum_{\vec{k}}\left[\frac{2\Delta}{\epsilon_{\vec{k}}} - \frac{\epsilon_{\vec{k}}}{2\Delta}\right]e^{i\vec{k}.\vec{r}}. \tag{B.5}$$

This shows that in the strong-coupling limit and with $V \to \infty$, the defect state has vanishing amplitude on the A-sublattice sites. Whereas, to leading order, the defect state wave function on the B-sublattice sites are given by $\phi^i_d(\vec{r}) \sim \sum_{\vec{k}} \epsilon^{-1}_{\vec{k}} e^{i\vec{k}.\vec{r}}$, up to a multiplicative constant.

On the other hand, when V is not too large so that η is not too small, we have $\frac{1}{E_d - E^{\ominus}_{\vec{k}}} = \frac{1}{\Delta - \eta + \Delta + \frac{\epsilon^2_{\vec{k}}}{2\Delta}}$. This can be written as $\frac{1}{E_d - E^{\ominus}_{\vec{k}}} \approx \frac{1}{(2\Delta - \eta)}\left(1 - \frac{\epsilon^2_{\vec{k}}}{2\Delta(2\Delta - \eta)}\right)$, if $\eta \gg \frac{\epsilon^2_{\vec{k}}}{2\Delta}$. In this limit, $\frac{1}{E_d - E^{\oplus}_{\vec{k}}} \approx \frac{-1}{\eta}\left(1 - \frac{\epsilon^2_{\vec{k}}}{2\Delta\eta}\right)$. Proceeding as before, for $i \in$ B, we have,

$$g^{\uparrow}_{iI}(E_d) \sim \sum_{\vec{k}}\left[\frac{\epsilon_{\vec{k}}}{2\Delta(2\Delta - \eta)} - \frac{\epsilon_{\vec{k}}}{2\Delta\eta}\right]e^{i\vec{k}.\vec{r}}. \tag{B.6}$$

Fourier transform of $\epsilon_{\vec{k}} \sim (\cos\vec{k}_x + \cos\vec{k}_y)$ is nonzero only when $\vec{r}$ is a vector connecting NN sites. This shows that when V is not too large, defect state will be localised only on the four NN sites.

Appendix C

Perturbation due to hopping

Here we present the corrections to the energy states of a two-site system due to hopping t. The notation we use is the same as in Reference [72]. We have four states – two at $-\Delta$ with eigenvectors $\begin{bmatrix} 1 \\ 0 \\ 0 \\ 0 \end{bmatrix}$ and $\begin{bmatrix} 0 \\ 0 \\ \cos(\theta/2) \\ \sin(\theta/2) \end{bmatrix}$ and two at $+\Delta$ with eigenvectors $\begin{bmatrix} 0 \\ 1 \\ 0 \\ 0 \end{bmatrix}$ and $\begin{bmatrix} 0 \\ 0 \\ \sin(\theta/2) \\ -\cos(\theta/2) \end{bmatrix}$.

For the states at $-\Delta$ the V-matrix will be a 2×2 one with $V_{ij} = \langle i|[t]|j\rangle$, where $|i\rangle$ and $|j\rangle$ are the eigenvectors of the Hamiltonian (Equation 3.2) with eigenvalues $-\Delta$ and $[t]$ is the hopping matrix in the two-site, two-spin basis given by,

$$[t] = \begin{bmatrix} 0 & 0 & -t & 0 \\ 0 & 0 & 0 & -t \\ -t & 0 & 0 & 0 \\ 0 & -t & 0 & 0 \end{bmatrix}. \tag{C.1}$$

A straightforward algebra gives,

$$[V] = \begin{bmatrix} 0 & -t\cos(\theta/2) \\ -t\cos(\theta/2) & 0 \end{bmatrix}. \tag{C.2}$$

The $[V]$-matrix has eigenvalues $-\Delta \pm t\cos(\theta/2)$ with normalised eigenvectors $\frac{1}{\sqrt{2}}\begin{bmatrix} 1 \\ 1 \end{bmatrix}$ and $\frac{1}{\sqrt{2}}\begin{bmatrix} 1 \\ -1 \end{bmatrix}$. This shows that the two states at $-\Delta$ are split because of the hopping to $-\Delta \pm t\cos(\theta/2)$ and the weights are equally distributed to the states at these energies.

A similar calculation shows the states at $+\Delta$ to be split to $+\Delta \pm t\cos(\theta/2)$ with weights getting equally distributed to the split-up states.

Appendix D

Hamiltonian for a five-site cluster

$$
H = \begin{bmatrix}
-\Delta\cos\theta & -\Delta\sin\theta & 0 & 0 & -t & 0 & 0 & 0 & 0 & 0 \\
-\Delta\sin\theta & \Delta\cos\theta & 0 & 0 & 0 & -t & 0 & 0 & 0 & 0 \\
0 & 0 & -\Delta\cos\theta & -\Delta\sin\theta & -t & 0 & 0 & 0 & 0 & 0 \\
0 & 0 & -\Delta\sin\theta & \Delta\cos\theta & 0 & -t & 0 & 0 & 0 & 0 \\
-t & 0 & -t & 0 & -\Delta & 0 & -t & 0 & -t & 0 \\
0 & -t & 0 & -t & 0 & \Delta & 0 & -t & 0 & -t \\
0 & 0 & 0 & 0 & -t & 0 & -\Delta\cos\theta & -\Delta\sin\theta & 0 & 0 \\
0 & 0 & 0 & 0 & 0 & -t & -\Delta\sin\theta & \Delta\cos\theta & 0 & 0 \\
0 & 0 & 0 & 0 & -t & 0 & 0 & 0 & -\Delta\cos\theta & -\Delta\sin\theta \\
0 & 0 & 0 & 0 & 0 & -t & 0 & 0 & -\Delta\sin\theta & \Delta\cos\theta
\end{bmatrix}
$$